

Technische Universität München  
Physik-Department

Study of the biokinetics of zirconium isotopes in humans  
and its relevance to internal dosimetry

Matthias Greiter

Vollständiger Abdruck der von der Fakultät für Physik  
der Technischen Universität München zur Erlangung des akademischen Grades eines  
Doktors der Naturwissenschaften  
genehmigten Dissertation.

Vorsitzender: Univ.-Prof. Dr. J. L. van Hemmen

Prüfer der Dissertation:

1. Hon.-Prof. Dr. H.G. Paretzke

2. Univ.-Prof. Dr. F. von Feilitzsch

Die Dissertation wurde am 27.09.2007 bei der Technischen Universität München  
eingereicht und durch die Fakultät für Physik am 22.04.2008 angenommen.

**Author contact information:**

Matthias Greiter  
Institute of Radiation Protection  
Helmholtz Zentrum München  
German Research Center for Environmental Health (GmbH)  
Ingolstaedter Landstrasse 1  
85764 Neuherberg  
Germany  
E-mail: [matthias.greiter@helmholtz-muenchen.de](mailto:matthias.greiter@helmholtz-muenchen.de)

# Table of contents

Abstract .....	1
List of acronyms, symbols and abbreviations .....	2
1 Aim of the study .....	3
1.1 Natural occurrence of zirconium compounds .....	3
1.2 Applications of stable zirconium .....	5
1.3 Applications of unstable isotopes of zirconium .....	5
1.4 Current biokinetic model of the International Commission on Radiological Protection (ICRP) .....	7
2 Investigations with stable isotope tracers .....	11
2.1 Double isotope technique and obtainable data .....	11
2.2 Preparation of tracer solutions .....	12
2.3 Experimental scheme .....	14
3 Measurement methods .....	16
3.1 Requirements .....	16
3.2 Mass spectrometric methods .....	16
3.2.1 Sample preparation for thermal ionisation mass spectrometry (TIMS) .....	21
3.2.2 Description of the TIMS instrument and measurement .....	24
3.2.3 Tracer concentration calculation with the isotope dilution technique .....	26
3.3 Activation analysis .....	28
3.3.1 Proton nuclear activation (PNA) sample preparation .....	31
3.3.2 PNA instrumental setup and experimental conditions .....	32
3.3.3 PNA tracer concentration calculation .....	34
4 Errors and uncertainty .....	38
4.1 Tracers and samples .....	40
4.2 TIMS .....	41
4.3 PNA .....	42
5 Model development .....	44
5.1 Fractional absorption .....	44
5.1.1 Double tracer technique .....	45
5.1.2 Convolution integral technique .....	46
5.2 First-order kinetic compartment models .....	47
5.2.1 Theoretical a priori identifiability .....	48
5.2.2 Model development process .....	49
5.3 Dosimetry .....	53
6 Results and discussion .....	57
6.1 Investigations .....	57
6.2 Sample measurements and method comparison .....	58
6.2.1 TIMS and PNA detection limits .....	58
6.2.2 Combined uncertainty .....	61

6.2.3	Correlation of TIMS and PNA results.....	62
6.2.4	Measured data .....	65
6.3	Model development.....	69
6.3.1	Fractional absorption without compartment models.....	69
6.3.2	Tracer kinetics and compartment model structure .....	72
6.3.3	Proposed new model .....	81
6.4	Dosimetry.....	89
6.4.1	Reproducibility of ICRP ingestion dose coefficients.....	89
6.4.2	Influence of daughter radionuclide modelling on dose coefficients .....	90
6.4.3	Gender differences due to SEE values .....	91
6.4.4	Differences due to alimentary tract models.....	92
6.4.5	Dose coefficients of <sup>95</sup> Zr for the proposed new zirconium biokinetic model ..	93
6.4.6	Gender differences resulting from the use of the HAT model.....	93
6.4.7	Effect of fractional absorption on ingestion dose coefficients.....	95
6.4.8	Contribution of individual target tissues to effective dose.....	96
6.4.9	Summary of dosimetry .....	100
7	Conclusions.....	101
	Acknowledgements .....	103
	Bibliography.....	105
	Annex .....	I
A.	TIMS method development.....	I
B.	Algorithm for the calculation of absorption rates .....	VI

## Abstract

Internal radiation dosimetry relies on biokinetic models linking exposure and dose, since internal dose cannot be measured readily in exposed persons. The structure and parameters of these models are usually estimated from animal and, if available, human study data.

The purpose of the present work is to extend the limited knowledge about the element zirconium. Data on zirconium metabolism, especially fractional absorption, retention in the body and excretion, are obtained directly from humans by the use of enriched stable zirconium isotopes as tracers. Thermal ionisation mass spectrometry (TIMS) and proton nuclear activation (PNA) are optimised for the measurement of nanogram amounts of tracer zirconium in biological samples. Both methods are evaluated with respect to detection limit, uncertainty and practical applicability.

Blood plasma and urinary data from nine double tracer studies with up to 100 d duration serve as input for developing a new first order kinetic compartment model. The new model is based on the current zirconium model proposed by the International Commission on Radiological Protection (ICRP).

Ingestion dose coefficients for  $^{95}\text{Zr}$  are presented for the new model. Depending on gender and the chemical form of the ingested zirconium, the resulting dose coefficients differ from the current ICRP values by  $-87\%$  to  $+64\%$ , with a median deviation of  $-3.3\%$ . Effective doses vary between  $73\%$  and  $142\%$  from the ICRP value. The tissue-weighted contributions of individual dose coefficients to the effective dose are dominated by the colon ( $63 - 86\%$ ), followed by gonads ( $22\%$  in women,  $2 - 3\%$  in men), stomach, red bone marrow, urinary bladder wall, and bone surfaces (each  $> 1\%$ ).

## Zusammenfassung

Eine Probandenstudie über die Biokinetik des Elements Zirkonium im Menschen wurde durchgeführt, unter Anwendung der Doppelisotopentechnik mit angereicherten stabilen Isotopen als Tracer. Protonenaktivierungsanalyse und Thermionen-Massenspektrometrie wurden als Messmethoden zur Tracerkonzentrationsbestimmung in Blutplasma und Urin eingesetzt und optimiert. Die gewonnenen Daten stellen eine substantielle Erweiterung des bisherigen Wissensstandes dar und gaben Anlass zur Modifizierung des von der internationalen Strahlenschutzkommission veröffentlichten systemischen Modells für Zirkonium. Mit dem neuen Modell wurden für zwei verschiedenen chemische Formen von Zirkonium Ingestions-Dosiskoeffizienten zur Anwendung im Strahlenschutz berechnet.

## List of acronyms, symbols and abbreviations

This list comprises only expressions used commonly in different sections of the work. Expressions specific to single sections or equations are explained at their respective first occurrence.

<i>BDL</i>	Below detection limit
$D_T$	Absorbed dose to a target region $T$
<i>DL</i>	Detection limit
<i>E</i>	Effective dose
$f_I, f_A$	Fractional absorption (cf. section 1.4 for the difference of the two expressions)
GI tract	Gastrointestinal tract
GSF	National Research Center for Environment and Health in the Helmholtz Association, Neuherberg, Germany
GUM	ISO-Guide to the expression of uncertainties in measurement
HAT(M)	Human alimentary tract (model)
$H_T$	Equivalent dose to a target region $T$
i.v.	intravenous
ID(-MS)	Isotope dilution (mass spectrometry)
ICP-MS	Inductively-coupled plasma mass spectrometry
ICRP	International Commission on Radiological Protection
$\lambda_{i \rightarrow j}$	Transfer rate (of a substance) from a model compartment $i$ to compartment $j$
MLL	Maier-Leibnitz-Laboratory, Garching, Germany
NAA	Neutron activation analysis (INAA: instrumental NAA)
p.o.	peroral (used to denote tracer administration by ingestion)
PNA	Proton nuclear activation (analysis)
PSI	Paul Scherrer Institute, Villigen, Switzerland
$SEE(T \leftarrow S)$	Specific effective energy absorbed in a target region $T$ from a nuclear transformation in a source region $S$
TIMS	Thermal ionisation mass spectrometry
$t_i$	Irradiation time in PNA
$t_m$	Measurement or counting time in PNA
$t_w$	Waiting time in PNA between end of irradiation and start of measurement
$u(x)$	Standard uncertainty of a quantity $x$
$w_R$	Radiation weighting factor
$w_T$	Tissue weighting factor

# 1 Aim of the study

The aim of this study is to obtain and evaluate data on the human metabolism of zirconium in order to verify, improve or replace the current biokinetic model of this element as proposed by the International Commission on Radiological Protection (ICRP). Subsequently, ingestion dose coefficients will be recalculated to improve the internal radiation dosimetry estimates in cases of exposure to radionuclides of zirconium, in order to make them more realistic and reliable. The study is limited to intravenous and oral exposure in adults.

Internal radiation dose of exposed persons has to be modelled from available measurements outside the body, since it cannot be measured readily *in vivo*. To this purpose, the ICRP proposes biokinetic models for elements with dose-relevant common radionuclides, in order to calculate the number of radionuclide transformations in each organ of the body resulting from an intake of a radioactive substance.

For some elements, like strontium, uranium or plutonium, a substantial amount of data about their metabolic characteristics was accumulated in the last decades. Biokinetic models for such elements have evolved from basic, abstract models to complex multi-compartment models reflecting actual physiological processes (Leggett and Eckerman 1994).

Zirconium is used in various medical and technical applications, including nuclear energy technology, where radioisotopes of zirconium are produced by nuclear fission of uranium; examples are listed in sections 1.2 and 1.3 to illustrate the possibilities of human exposure to stable and radioactive zirconium. Although radioisotopes of zirconium were detected in nuclear fallout, e.g. after accidents or nuclear weapon tests, little information has been gathered on this element, and the structure of its biokinetic model is still very elementary. One reason may be that the element is insoluble in many of its compounds, and therefore poorly available for uptake into human metabolism. Furthermore, no model information is available in the field of stable zirconium toxicology, since no intensive research has been done on this element. Zirconium is not considered to be essential for the human metabolism; its compounds have low systemic toxicity, and are not considered genotoxic or carcinogenic (Merian 1984; U.S. National Library of Medicine 2005). As a consequence, the information included in the current ICRP model comprises only animal experiments, with one single exception (Mealey 1957).

The above-mentioned issues suggest that a systematic study with healthy humans can substantially improve the current knowledge of zirconium biokinetics and render a benefit to internal dosimetry.

## 1.1 *Natural occurrence of zirconium compounds*

Zirconium is a metal and a transition element of group 4 of the periodic table of elements, together with titanium and hafnium. In the earth's crust it is the 18<sup>th</sup> most common element with a mean concentration of 190 ppm (Emsley 2001). Its most common forms are the minerals zircon ( $ZrSiO_4$ ) or baddeleyite ( $ZrO_2$ ) with an oxidation state of +IV. In natural or commercially available form, zirconium contains hafnium with a varying fraction of up to a few percent. Zirconium is poorly water soluble, as can be seen in Tables 1.1 and 1.2 for various fluids in comparison to the occurrence in rocks or river sediments.

The estimations of dietary intake and abundance of zirconium in the human body vary by a large degree. Although the concentrations of zirconium in beverages are low, Minoia et al. (Minoia, Sabbioni et al. 1994) estimated that the intake from beverages contributes ~ 6.6 % to an overall weekly zirconium intake of 370  $\mu g$  for the Italian population. In contrast to this,

another source reported typical zirconium concentrations of 0.5 – 4.1  $\mu\text{g}\cdot\text{g}^{-1}$  in various foods and a daily intake of 3.5 mg (Ghosh, Sharma et al. 1992). Overall, recent measurements tend to find lower concentrations of zirconium in organic samples. An overview of zirconium concentrations in biological samples is given in Table 1.3.

**Table 1.1:** Zirconium concentration in rocks, sediments, fresh water and sea water. Original units were converted for comparability.

Sample	Concentration	Source
Various rocks	19 – 450 $\text{mg}\cdot\text{kg}^{-1}$	(Merian 1984)
River sediments, partially contaminated	101 – 1800 $\text{mg}\cdot\text{kg}^{-1}$	(Al-Jundi 2000)
River water	2 – 20 $\mu\text{g}\cdot\text{kg}^{-1}$	(Merian 1984)
	0.22 $\mu\text{g}\cdot\text{kg}^{-1}$	(Boswell and Elderfield 1988)
	20 – 500 $\text{ng}\cdot\text{kg}^{-1}$	(Merian 1984)
Sea water	7.3 – 18.2 $\text{ng}\cdot\text{kg}^{-1}$	(Boswell and Elderfield 1988)
	2.28 – 33.4 $\text{ng}\cdot\text{kg}^{-1}$	(McKelvey and Orians 1998)

**Table 1.2:** Zirconium concentrations in beverages, according to (Minoia, Sabbioni et al. 1994).

Beverage	Concentration
Table wine	$1.3 \pm 1.1 \mu\text{g}\cdot\text{l}^{-1}$
Mineral water	$4.3 \pm 9.5 \mu\text{g}\cdot\text{l}^{-1}$
Beer	$0.26 \pm 0.16 \mu\text{g}\cdot\text{l}^{-1}$
Tea infusion	$0.70 \mu\text{g}\cdot\text{l}^{-1}$
Instant coffee	$0.065 \pm 0.02 \mu\text{g}\cdot\text{l}^{-1}$

**Table 1.3:** Zirconium concentrations in biological samples. Original units were converted for comparability.

Sample	Concentration	Source
Guinea pig liver and bone	$<0.1 - 4 \mu\text{g}\cdot\text{g}^{-1}$ (dw)	(Osborn, Broering et al. 1981)
Plants	$0.3 - 2 \mu\text{g}\cdot\text{g}^{-1}$ (dw)	(Merian 1984)
Mammal muscle tissue	$0.08 \mu\text{g}\cdot\text{g}^{-1}$ (dw)	
Human lymph nodes (UK)	$0.3 \mu\text{g}\cdot\text{g}^{-1}$	(Hamilton, Sabbioni et al. 1994)
Human lymph nodes (Italy)	$0.7 \mu\text{g}\cdot\text{g}^{-1}$	
Pooled whole blood (UK)	$9.6 \pm 5.8 \mu\text{g}\cdot\text{l}^{-1}$	
Human serum	$0.9 - 7.4 \mu\text{g}\cdot\text{l}^{-1}$	(Morita, Kita et al. 1994)
Honey (USA)	$0.42 - 0.84 \mu\text{g}\cdot\text{g}^{-1}$	
Seal liver	$<1 - 362 \text{ng}\cdot\text{g}^{-1}$ (dw)	(Ikemoto, Kunito et al. 2004)
Seal kidney	$<1 - 157 \text{ng}\cdot\text{g}^{-1}$ (dw)	
Seal muscle	$<1 - 71 \text{ng}\cdot\text{g}^{-1}$ (dw)	
Seal hair	$13 - 4260 \text{ng}\cdot\text{g}^{-1}$ (dw)	
Animal tissues*	$0.3 - 4 \mu\text{g}\cdot\text{g}^{-1}$	(Engström, Stenberg et al. 2004)
Human serum	$90 - 160 \text{ng}\cdot\text{l}^{-1}$	(Rodushkin, Engström et al. 2004)
Human urine	$20 - 38 \text{ng}\cdot\text{l}^{-1}$	
Human blood	$<14 - 500 \text{ng}\cdot\text{l}^{-1}$	

(dw) Concentrations based on dry weight have to be divided by 3 – 5 depending on the tissue type to be comparable with wet weight measurements. (\*) The listed range is estimated from the means and standard deviations of the individual tissues, which were porcine muscle, fish muscle and liver, and rabbit liver, lung, kidney and brain.

Although no function of zirconium is known in the human metabolism, the element seems to be selectively transported, as indicated by different concentrations in various soft tissues. De Bartolo et al. found concentrations in blood plasma and total blood of Italian donors of  $1.4 \pm 0.3 \text{ ng}\cdot\text{ml}^{-1}$  and  $5.0 \pm 1.1 \text{ ng}\cdot\text{ml}^{-1}$ , respectively (de Bartolo, Cantone et al. 2000). An analogue enrichment of zirconium by a factor of  $\sim 10$  was found for renal cell carcinoma compared to healthy kidney cortex in a Polish study (Dobrowolski, Drewniak et al. 2002), in contrast to the behaviour of the chemically similar element titanium. Both findings suggest a specific transport process, in turn indicating an unknown metabolic function.

## **1.2 Applications of stable zirconium**

Yearly world production was reported in 2001 to be  $\sim 900,000$  tonnes zircon ore,  $\sim 7,000$  tonnes of zirconium metal, and  $\sim 25,000$  tonnes zirconium oxide (Emsley 2001).

In the middle of the 20th century, zirconium lactate was used in antiperspirants, and zirconium carbonate was used to treat poison ivy dermatitis in the USA (Baler 1966; Emsley 2001). The latter use was discontinued due to rare allergic reactions. Zirconium hydroxychloride has replaced the lactate in some antiperspirants.

Current technical applications of stable zirconium as metal, oxide, inorganic salt, or organic complex include but are not limited to chemical catalysts, solid oxide fuel cells, capacitors, dielectrics, paints and ceramic dyes, optical components, and surface coatings in paper production (Mel Chemicals 2007). By its use as catalyst, zirconium can be transferred into certain polymers, and was found in polyethylene (PE) and polypropylene (PP) in concentrations of  $0.5 - 100 \mu\text{g}\cdot\text{g}^{-1}$  (Diemer and Heumann 1999). Zirconium may be leached in small amounts from these polymers, which are used as laboratory equipment as well as in food packaging.

Ceramic zirconium, sintered from zirconium oxide and stabilized with yttrium oxide, is in commercial medical use in various implants, e.g. finger, toe and palm joints and dental implants (CeraRoot 2006; Moje 2007). Larger implants, e.g. femoral parts of knee joints, are also made from zirconium alloys (Katti 2004; Smith+Nephew 2007), in some applications with a thin covering ceramic layer of  $\text{ZrO}_2$  to combine metallic bulk properties with reduced wear at contact surfaces to polyethylene parts.

$\text{ZrO}_2$  is also used in polymethyl-metacrylate-based bone cement as a means to increase X-ray contrast. By fretting wear at the interface between bone cement and implant,  $\text{ZrO}_2$ -containing particles can be released, which was demonstrated in a wear chamber (Kunze, Wimmer et al. 1998).

From the latter medical applications, persons with certain implants may receive a small but continuous exposure to dissolved or particulate stable zirconium.

## **1.3 Applications of unstable isotopes of zirconium**

Neutron deficient zirconium isotopes, especially  $^{89}\text{Zr}$ , are produced as tracers for positron emission tomography with monoclonal antibodies (Zweit, Downey et al. 1991; Verel, Visser et al. 2003) by irradiation of yttrium targets with protons or deuterons. The produced activity reported in the work of Verel et al. was  $\sim 10^{10}$  Bq.

Radioactive zirconium isotopes with excess neutrons are produced in large quantities in nuclear fission reactors. The average mass of light fission fragments of  $^{235}\text{U}$  was calculated as 94.9 amu for incident thermal neutrons and 95.0 amu for incident non-moderated fission neutrons, i.e.  $^{95}\text{Zr}$  is one of the most common fragments in uranium fission (England and

Rider 1994). The relative yield of nuclei with masses 95 amu to 100 amu from  $^{235}\text{U}$  or  $^{238}\text{U}$  fission is  $\sim 5 - 6\%$  for each mass.

In addition,  $^{93}\text{Zr}$ ,  $^{95}\text{Zr}$  and  $^{97}\text{Zr}$  are generated by neutron capture reactions from stable zirconium isotopes in fuel rod claddings and other parts exposed in fission reactor cores. Zirconium is well-suited for such parts due to a combination of good corrosion resistance, a high melting point of 1852 °C, and a small cross section for thermal neutron capture, if the naturally present hafnium fraction of 1 – 3 % is removed. Thermal neutron capture cross sections of stable zirconium isotopes range from 0.011 barn ( $^{90}\text{Zr}$ ) to 1.17 barn ( $^{91}\text{Zr}$ ), with a mean cross section of 0.185 barn (Munter 1992). This is an order of magnitude less than the mean cross sections for many components of various steels (Cr, Mn, Mo, Fe, and V) or titanium, which lie in a range of 2.48 – 13.3 barn. Therefore, neutron-induced material transformation, which could eventually lead to material failure, is substantially reduced for zirconium in comparison to normal steel. Typically, zirconium is used in nuclear technology as ‘Zircaloy-2’, an alloy of zirconium with a total of  $\sim 2\%$  tin (Sn), iron (Fe), chromium (Cr) and nickel (Ni), or ‘Zircaloy-4’ without nickel (Tolksdorf 1974).

For the Chernobyl accident, the activity of  $^{95}\text{Zr}$  accumulated in the reactor was estimated as  $4.9 \cdot 10^{18}$  Bq, and the released activity as  $1.7 \cdot 10^{17}$  Bq (Pitkevich, Duba et al. 1996).

An overview of stable and medium to long-lived radioactive isotopes of zirconium, including natural abundances, half-lives and the most probable transformation processes and energies, is given in Table 1.4.

**Table 1.4:** Isotopes of zirconium with half-lives longer than 1 h.

The listed decay energies are the most abundant gamma energies and maximum beta energies. Values are cited from (Rosman and Taylor 1998; National Nuclear Data Center 2007) and rounded for visual clarity.

Isotope	Relative abundance (atom %)	Half-life	Decay mode	Decay Energies (keV)
$^{86}\text{Zr}$	-	16.5 h	EC, ( $\beta^+$ )	243 ( $\gamma$ )
$^{87}\text{Zr}$	-	1.68 h	$\beta^+$	511, (380) ( $\gamma$ ) 2266 ( $\beta$ )
$^{88}\text{Zr}$	-	83.4 d	EC	393 ( $\gamma$ )
$^{89}\text{Zr}$	-	78.4 h	EC, $\beta^+$	909, 511 ( $\gamma$ ) 902 ( $\beta$ )
$^{90}\text{Zr}$	$51.45 \pm 0.40$	stable		
$^{91}\text{Zr}$	$11.22 \pm 0.05$	stable		
$^{92}\text{Zr}$	$17.15 \pm 0.08$	stable		
$^{93}\text{Zr}$	-	$1.5 \cdot 10^6$ y	$\beta^-$	60.6 ( $\beta$ )
$^{94}\text{Zr}$	$17.38 \pm 0.28$	stable		
$^{95}\text{Zr}$	-	64.0 d	$\beta^-$	757, 724 ( $\gamma$ ) 368, 401 ( $\beta$ )
$^{96}\text{Zr}$	$2.80 \pm 0.09$	stable ( $> 3.9 \cdot 10^{20}$ y)	( $2\beta^-$ )	
$^{97}\text{Zr}$	-	16.7 h	$\beta^-$	743 ( $\gamma$ ) 1915 ( $\beta$ )

## 1.4 Current biokinetic model of the International Commission on Radiological Protection (ICRP)

The basic intention of radiological protection, represented by the ICRP, is to prevent or minimise damage by ionising radiation. The ICRP has published and updated recommendations to explain this intention, the last of which (ICRP 1991) was compiled in 1990 and is now under revision. A brief introduction into issues relevant to the current study is given in the following paragraphs.

Within the field of radiation protection, internal dosimetry is concerned with limiting the intake of radionuclides by workers or members of the public, in order to limit radiation damage by radionuclide transformations within the body. The resulting damage effects can be twofold; either deterministic radiation effects, whose severity depends on the amount of absorbed radiation above a certain threshold, or stochastic effects, e.g. the modification of DNA, leading to cancer or hereditary diseases. Exposure limits proposed by the ICRP are set to prevent deterministic effects and constrain the incidence of stochastic effects to a level “as low as reasonably achievable, economic and social factors being taken into account”.

The concept of ‘dose’ was introduced to quantify the effect of exposure to ionising radiation, in turn being able to give a quantitative estimate of the risk of stochastic effects, since their incidence is supposed to be related linearly to the dose.

The basic quantity is the ‘absorbed dose’  $D$ , defined as the energy of ionising radiation absorbed in a volume element, divided by the mass of this volume element. Its unit is  $\text{J}\cdot\text{kg}^{-1}$ , with the special name *gray* (Gy), defined as  $1 \text{ Gy} = 1 \text{ J}\cdot\text{kg}^{-1}$ . For practical purposes of dosimetry, the absorbed dose is usually averaged over a target region or tissue  $T$ .

Since radiation effects on tissues can be dependent on type and energy of radiation, it is useful for risk estimation to introduce radiation weighting factors  $w_R$  and calculate an ‘equivalent dose’  $H_T$  to a tissue  $T$  from the contributions of absorbed doses  $D_R$  from different radiation qualities  $R$ :

$$H_T = \sum_R w_R \cdot D_{T,R} . \quad (1.1)$$

Its unit is  $\text{J}\cdot\text{kg}^{-1}$ , with the special name *sievert* (Sv), defined as  $1 \text{ Sv} = 1 \text{ J}\cdot\text{kg}^{-1}$ . The value of  $w_R$  given in the current ICRP recommendations (ICRP 1991) is 1 for photons and electrons, 5 for protons, 20 for alpha particles, and 5 – 20 for neutrons, depending on their energy. It must be noted that the concept of tissue-averaged equivalent dose is usually not valid for localised effects, e.g. radiation damage from low-energy Auger electron emitters selectively attached to DNA.

Various tissues have differing sensitivities to radiation effects. This issue can be dealt with by tissue weighting factors  $w_T$ , which can be used to combine individual organ equivalent doses  $H_T$  to an ‘effective dose’  $E$ , estimating the risk of stochastic effects for the whole human organism. The effective dose is calculated by

$$E = \sum_T w_T H_T . \quad (1.2)$$

Its unit is also  $\text{J}\cdot\text{kg}^{-1}$ ; the special name *sievert* (Sv), defined as above.

In order to evaluate the ‘committed’ equivalent or effective doses ( $H_T(\tau)$  or  $E(\tau)$ ) from an intake of a given radionuclide, i.e. the dose received from transformations of this radionuclide occurring within a set time interval  $\tau$  after intake, the following steps are necessary:

- Estimation of the amount and time course of intake;

- identification of the organs and tissues to and from which the material is transferred and in which it is retained, and of the relevant excretion pathways;
- time course of retention and distribution in the body, and excretion from the body;
- calculation of the number of radionuclide transformations in relevant source regions  $S$ , i.e. organs or tissues containing the radionuclide, within the time interval  $\tau$ ;
- calculation of the fraction of radiation emitted from each source region  $S$  and absorbed in each target region  $T$ ;
- derivation of  $D_{T,R}$  and subsequent calculation of  $H_T(\tau)$  and  $E(\tau)$ .

Details on these steps are presented in section 5.3.

Exposure limits can be derived from the resulting relation between the incorporated amount of a radionuclide and the committed equivalent or effective doses. Estimated doses can also be used to judge the necessity of interventions in case of accidental incorporations, since many interventions, e.g. the administration of chelating agents to increase radionuclide excretion, can have adverse reactions.

Ingestion dose coefficients of  $^{95}\text{Zr}$ , i.e. the constant factors relating 1 Bq of ingested  $^{95}\text{Zr}$  to the respective equivalent and effective doses, were last published in ICRP publication 67 (ICRP 1993) and are listed in Table 6.8. Their calculation according to the steps above is discussed in section 5.3.

In 1979, in its Publication 30 (ICRP 1979), the ICRP issued a set of biokinetic models of the distribution of various radionuclides within the human body. These models serve to provide a means to calculate element uptake, distribution and retention in the human body, or allow for intake estimation from excretion measurements (bioassay measurements).

The general structure of most metabolic models in these publications consists of compartments, which contain the modelled substance, and substance transfers between the compartments. By design, the compartments represent functional units of the human metabolism rather than individual organs, although often some compartments can be identified with certain cell types, e.g. red bone marrow, or individual organs. The compartment structure of the ICRP zirconium model is illustrated in Figure 1.1.

The structure of many models, including that of zirconium, is unidirectional, i.e. there is no possibility of recycling once the substance has left a compartment. The transfers are described by first-order processes, i.e. that the change of substance concentration  $c_i$  within a compartment  $i$  is given by

$$\frac{dc_i(t)}{dt} = \sum_l \lambda_{l \rightarrow i} \cdot c_l(t) - \sum_j \lambda_{i \rightarrow j} \cdot c_i(t), \quad (1.3)$$

with  $\lambda$  being constant transfer rates. These transfer rates are related to the compartment emptying half-life by

$$T_{1/2,i} = \frac{\ln 2}{\sum_j \lambda_{i \rightarrow j}}. \quad (1.4)$$

In the current model depicted in Figure 1.1, ingested zirconium is introduced into the stomach and subsequently transported to the other compartments. In adults, zirconium absorbed from the gut is cleared from the transfer compartment with a half-life of 6 h, and distributed to mineral bone (50 %) and all other tissues (50 %), from where it is excreted with half-times of 10,000 d and 7 d, respectively (ICRP 1993). The urinary to faecal excretion ratio for both compartments is assumed to be 5:1.

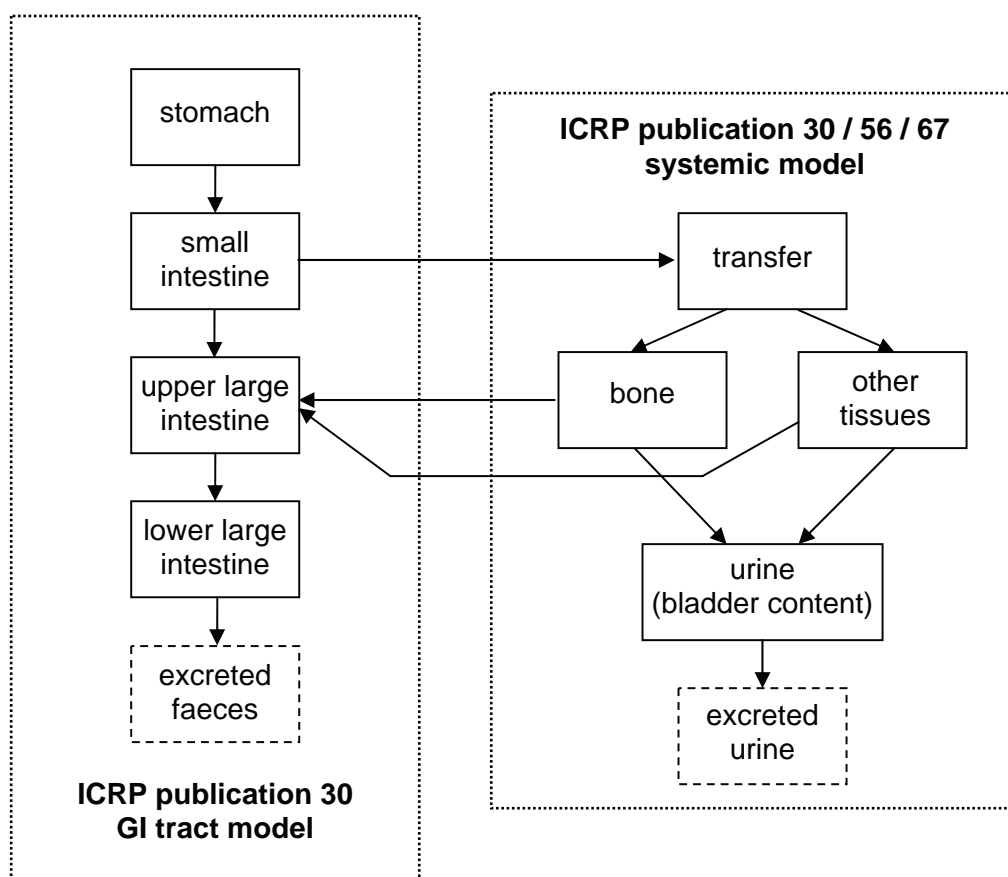


**Figure 1.1:** Current ICRP biokinetic model of zirconium. Radionuclide transformations in dashed compartments do not contribute to internal absorbed dose.

The initial models of ICRP publication 30 (ICRP 1979) have been repeatedly altered to include newer metabolic data and some evolved concepts in radiation protection, resulting in the following changes for zirconium:

- In publication 56, age-dependent biokinetic parameters, a larger fractional absorption from small intestine to transfer compartment, and dose calculations for members of the public were included (ICRP 1990).
- The concept of radiation quality factors based on linear energy transfer (LET) was changed to radiation weighting factors  $w_R$ , derived from relative biological effectiveness, in the new recommendations of the ICRP in publication 60 (ICRP 1991). This change was followed by a re-evaluation of the current ingestion dose coefficients in publication 67 (ICRP 1995) with some changes in tissue weighting factors and retention time in bone.
- A new respiratory tract model was published in publication 66 (ICRP 1994) and inhalation dose coefficients were presented in publication 71 (ICRP 1995) accordingly.
- A new model of the human alimentary tract (HAT) was introduced in publication 100 (ICRP 2006), allowing for absorption of substances from other organs than the small intestine. This model expands the gastrointestinal tract (GI) model used since publication 30 by the oral cavity and oesophagus, and features a different division of the colon into three compartments, namely right colon, left colon and rectosigmoid colon, instead of upper and lower large intestine. The model further optionally includes wall tissues within the alimentary tract, as well as teeth and oral mucosa. No dose coefficients of zirconium calculated with this model have been published yet.

A characteristic value of special importance for many radionuclides is the fractional absorption, i.e. the fraction of substance transferred from the alimentary tract into the systemic part of the model. It has two main consequences:

- If the amount of an element ingested shall be derived from urinary data by a bioassay measurement, the result is directly proportional to fractional absorption. Any associated dose estimate will be scaled by the fractional absorption value and also be subject to its uncertainty. This is relevant in occupational exposure monitoring, e.g. of thorium (Baglan, Cossonnet et al. 2001).
- For long-lived radionuclides with half-lives significantly longer than the transfer time of substances through the alimentary tract, e.g.  $^{137}\text{Cs}$  (30.2 y) or  $^{90}\text{Sr}$  (28.5 y), the internal absorbed dose is approximately directly proportional to the amount of substance transferred into the systemic circulation.

Since the transfer rates are constant over time, the fractional absorption from small intestine to transfer compartment can at any time be calculated by

$$f_1 = \frac{\lambda_{SI \rightarrow transfer}}{\lambda_{SI \rightarrow transfer} + \lambda_{SI \rightarrow colon}}. \quad (1.5)$$

In the new HAT model, the total fractional absorption  $f_A$  is identical to  $f_1$  as long as the uptake of an element only takes place from the small intestine. This is the standard assumption of the HAT model, unless information is available on specific uptake from other compartments of the alimentary tract; it also applies to zirconium. Therefore, in the current study,  $f_A$  and  $f_1$  are treated as synonyms, unless otherwise stated.

The value of  $f_A$  can be heavily dependant on the chemical form in which an element is ingested (Höllriegl, Röhmuß et al. 2004). For zirconium, the ICRP in its publication 67 adopted a value of 0.01 for adults and children in the general population, and 0.02 for infants of up to three months of age. Owing to its relevance for dose estimation, fractional absorption is one of the most interesting parameters investigated in the current work. Its evaluation is discussed in section 5, and results are presented in section 6.

## 2 Investigations with stable isotope tracers

Kinetic distribution of target substances in a steady state condition can be difficult to observe, especially if small changes, e.g. a slow flux between two large substance pools, shall be investigated. This is critical for biokinetic studies, since many substance concentrations in living beings are governed by dynamic equilibriums. Stable substance concentrations may easily be measured, but flux or reaction rates, which are attributed to metabolic activity, are more difficult to determine.

Tracer investigations attempt to bypass this problem by determining the kinetics of a tracer instead of the target substance, the tracee, with both substances being similar in respect to their metabolic characteristics. A meaningful tracer/tracee investigation should fulfil further requirements:

- (a) The tracer should not be present in the metabolism before the investigation.
- (b) The amount of applied tracer should be as small as possible in order to not disturb the normal tracee metabolism.
- (c) At least in studies with human test persons, a tracer substance must not be toxic, nor may its application cause harm to the persons under study.
- (d) The measurement process should not disturb the metabolism.

Depending on investigation design, stable tracers can be more complicated to measure and yield less information than radioactive tracers, which are detectable from outside the body. Although the latter are used e.g. in PET diagnosis, ethical concerns reflected in condition (c) prevent their application to healthy test persons, unless individually justified. In contrast, stable tracers can also be used for special test persons like pregnant women or children. Stable isotopes can be applied as tracers if more than one stable isotope of an element exists, and if the natural isotopic composition of an element is known and stable, at least within an investigation. These prerequisites are fulfilled for zirconium.

### 2.1 Double isotope technique and obtainable data

Except for sacrificial animal experiments, condition (d) limits the choice of sample types to blood, hair or various excreta, all of which can be obtained without anaesthesia. The information contained in such samples is limited to uptake into and clearance from these sample materials.

Especially for the determination of the fractional absorption of an ingested substance, the double tracer technique as introduced by De Grazia et al. (De Grazia, Ivanovich et al. 1965) is a potent method. The technique, which was originally performed with radioactive tracers and only one urine and two blood samples, was modified and applied to various elements over the last years (Cantone, De Bartolo et al. 1997; Giussani 1997; Veronese, Giussani et al. 2000; Höllriegl, Louvat et al. 2002).

Two tracers are applied simultaneously; one is administered orally (p.o.), the other injected intravenously (i.v.). It is assumed that, once in the systemic circulation, the two tracers are metabolised similarly. The concentration curves of the two tracers in blood plasma are compared, and the fractional absorption from the alimentary tract into the systemic circulation can be evaluated. The i.v. tracer serves as reference for the clearance processes from blood plasma, which would not be separable if using only a single ingested tracer.

Tracer excretion can be assessed by measurements of urine or faecal samples, yet urine samples have three advantages in the context of the intended tracer measurements:

- Urine sampling is easier and more acceptable than collection of faeces for many test persons.
- Urinary excretion from the body usually occurs more frequently, giving rise to a lesser uncertainty of the estimated excretion rate.
- Tracer excretion in faeces is a mixture of two components; tracer directly transferred through the alimentary tract, and tracer which has been transferred into the systemic circulation and excreted back to the alimentary tract, e.g. by biliary secretion. In contrast, tracer in urine must have entered the systemic circulation prior to excretion in the urinary pathway. Therefore, at least within the first few days after tracer administration, urine measurements are better suited to estimate excretion from the systemic circulation.

In summary, the double isotope technique with urine and plasma samples provides data on

- tracer absorption from the alimentary tract,
- tracer retention in plasma,
- and tracer elimination through the urinary pathway.

## **2.2 Preparation of tracer solutions**

Enriched stable zirconium isotopes were obtained as oxide powders from Campro Scientific GmbH, Germany and Chemotrade Chemiehandelsgesellschaft mbH, Leipzig, Germany, in 2000 and 2005. Table 2.1 lists the tracers and solutions used in the study.

Acidic stock solutions were prepared as follows:

- (a) 0.4 ml concentrated nitric acid ( $\text{HNO}_3$ ), 3.7 ml concentrated hydrofluoric acid (HF) and  $\text{ZrO}_2$  powder (20 – 100 mg, depending on the obtained amount) were placed in a sealable Teflon beaker.
- (b) The sealed beaker was kept at 140 °C for 3-5 h.
- (c) The solution was evaporated to dryness over 5 h.
- (d) The residue was redissolved either in 3.5 ml concentrated hydrochloric acid (HCl) and 1.5 ml concentrated  $\text{HNO}_3$ , or in 3 ml each of 6 M HCl and 8 M  $\text{HNO}_3$ , if necessary in an ultrasonic bath. In the latter approach, the solution was heated again to 140 °C for 4 h in the sealed vessel.
- (e) Milli-Q water was added, starting with 10 ml, until the desired concentration of 100 – 500  $\text{mg}\cdot\text{l}^{-1}$  was reached.

Injection ampoules were prepared from the stock solutions with the following further steps:

- (f) 10 ml Milli-Q water, 0.25 g potassium oxalate ( $\text{K}_2\text{C}_2\text{O}_4$ ), and 0.085 g oxalic acid ( $\text{H}_2\text{C}_2\text{O}_4$ ) were added to 10 ml or 40 ml of the  $^{90}\text{Zr}$  or  $^{96}\text{Zr}$  stock solution, respectively.
- (g) After dissolution was complete, 30 – 40 ml denatured ethanol and ~ 0.5 – 1 ml sodium hydroxide solution (NaOH, 50 %) were added, until at pH ~ 4 precipitation of zirconium oxalate crystals occurred.
- (h) The suspension was filtered and washed with denatured ethanol three times to maximise zirconium oxalate precipitation.
- (i) Crystals were washed with pure ethanol.
- (j) Cleaned crystals were dissolved in 25 ml Milli-Q water and 175 ml sterile 0.9 % NaCl solution.
- (k) 10 ml portions of this solution were filtered through a sterile filter into washed and autoclaved ampoules.

- (l) Ampoules were sealed by melting with a burner and again autoclaved.  
 (m) 10 % of the ampoules were selected randomly and subjected to microbiological analysis to check sterility.

From the stock solutions of  $^{90}\text{Zr}$ ,  $^{91}\text{Zr}$ , and  $^{96}\text{Zr}$ , two different oral tracer solutions were prepared. The standard drinking solution contained inorganic zirconium with sodium citrate ( $\text{Na}_3\text{C}_6\text{H}_5\text{O}_7$ ) added as buffer, and to keep zirconium in solution despite increasing pH to  $\sim 4$ . The alternative drinking solution contained zirconium in a soluble organic complex with oxalate anions.

Citrate solution was prepared by mixing 30 ml Milli-Q water and the desired volume of tracer stock solution, subsequently adding 120 mg sodium citrate per 7 mg zirconium, setting the pH to  $\sim 4$  by addition of NaOH (50 %), and adding Milli-Q water until the volume reached 100 ml.

Oxalate solution was either directly prepared from the desired amount of injection solution by dilution with Milli-Q water, or from dilution of a separately prepared zirconium oxalate solution. The latter was prepared as illustrated in steps f – j, but starting with the fourfold amount of ingredients and the following changes:

- Pure ethanol instead of denatured ethanol was used.
- The intermediate solution was cooled to 3 °C in a refrigerator following step g to promote crystal precipitation.
- Volumes of 100 ml Milli-Q water and 200 ml NaCl solution were added in step j instead of the previously given amounts.

Zirconium concentrations of all solutions were measured with inductively-coupled plasma optical emission spectrometry (ICP-OES) by the Central Inorganic Analysis Service of the GSF and are listed in Table 2.1.

**Table 2.1:** Data of isotopic tracers and tracer solutions.

Relative isotopic abundances are taken from suppliers' certificates. Concentration values refer to elemental content of zirconium.

Tracer	Relative isotopic abundance (atom %)					Solution type	Concentration (mg·l <sup>-1</sup> )	Chemical form
	$^{90}\text{Zr}$	$^{91}\text{Zr}$	$^{92}\text{Zr}$	$^{94}\text{Zr}$	$^{96}\text{Zr}$			
T-90	98.2	0.6	0.6	0.5	0.1	stock	553	acidic
						injection	30.7	oxalate
						Ox-1	72.3	oxalate
						Ox-2	102	oxalate
						Ox-3	133	oxalate
T-91	6.1	88.7	3.4	1.5	0.3	stock	351	acidic
T-94-S	3.8	1.5	2.5	91.2	1.0	stock	270	acidic
T-94-R						diluted	1.06	acidic
T-96-H	5.0	1.88	2.69	4.03	86.4	stock	94.2	acidic
						injection	11.6	oxalate
T-96-L	19.8	5.3	8.2	8.4	58.3	stock	100	acidic

## 2.3 Experimental scheme

The zirconium tracer study underlying the current work was approved by the Ethics Commission of the Medical Faculty of the Technische Universität München and supervised by Prof. Dr. M. Göttlicher (GSF). It was conducted in cooperation with Dr. N. Felgenhauer and Prof. Dr. T. Zilker of the Department of Toxicology in the II. Medical Clinic of the Technische Universität München, where the tracer administration took place. Tracer administration was limited based on body weight to  $0.01 \text{ mg}\cdot\text{kg}^{-1}$  of the i.v. tracer and  $0.1 \text{ mg}\cdot\text{kg}^{-1}$  of the p.o. tracer. Possible impairments to the test persons were covered by a special insurance.

Investigations were carried out according to the following pre-defined scheme:

- (a) Written informed consent was obtained from volunteers preceding investigations.
- (b) Test persons' health was checked by medical examination and a complete blood count. Further data retained from test persons are sex, age, weight, and body size.
- (c) Sampling vessels were labelled in advance.
- (d) One blank 24 h urine sample was collected one or a few days in advance.
- (e) Test persons had to be fasting overnight preceding the start of the investigation and further two hours thereafter.
- (f) Oral tracer solution was prepared fresh from stock solution in advance.
- (g) The test person was driven to the clinic where he or she would be kept under medical surveillance for the first 60 – 90 min of the investigation.
- (h) An indwelling catheter was intravenously inserted in one arm and fixed by the physician in charge.
- (i) 2-3 ml blood were drawn and discarded to avoid sample contamination by catheter material.
- (j) A blank blood sample of ~10 ml was drawn.
- (k) The investigation was started by an intravenous injection of one ampoule of i.v. tracer solution in the arm opposing the catheterized arm. The time of injection was noted in the investigation record form.
- (l) As soon and fast as possible, the test person drank the oral tracer solution. The actually administered amounts of both tracers were determined by weighing the beaker and syringe when empty, and when containing the tracers before and after application.
- (m) In pre-defined time intervals (confer below), blood samples of ~10 ml each were drawn. All urine was collected after the start of the investigation in collection intervals of 12 h or 24 h.
- (n) After 60-90 min the test person was driven back to the GSF, where consecutive blood samples were drawn by a physician or an assistant medical technician.
- (o) Two hours after tracer injection, the test person was offered breakfast, consisting of coffee, sugar, but no milk, and two bread rolls with butter and jam. Half an hour after breakfast, test persons were free to eat and drink at will.
- (p) The indwelling catheter was removed either if necessary, or 8 h after its insertion. After removal of the catheter, blood samples were drawn by butterfly needles.

Blood sampling times were scheduled for 5, 15, 30, 45, 60, 90 min, 2, 3, 4, 6, 8 h, as well as 30 d and 100 d after tracer injection. Urine should have been collected completely over the first 12 h, from 12 – 24 h, every 24 h until 7 d, and for 24 h each after 30 d and 100 d. All relevant sample data such as time after tracer injection, duration of drawing, time of centrifugation of blood samples, and urine sample weight were noted in a record form.

Blood samples were prepared for storage at the GSF as soon as possible by

- (q) centrifugation at 3,500 rpm for 10 min,
- (r) removing the plasma and freezing it,
- (s) removing and discarding the buffy coat, i.e. white blood cells and platelets,
- (t) cleaning the erythrocytes by rinsing with 5 ml of cold 0.9 % sodium chloride (NaCl) solution and centrifugation at 2,500 rpm for 2 min, with further two repetitions,
- (u) removal of two portions of 0.6 ml erythrocytes and addition of 0.6 ml Milli-Q deionised water (Millipore GmbH, Schwalbach, Germany) to each portion, then freezing.

Urine samples were weighed for later calculation of excreted tracer amounts. From each collected urine sample, two aliquots of 15 ml each and two of 100 ml each were mixed with 0.75 ml and 5 ml concentrated, sub-boiling distilled grade nitric acid (HNO<sub>3</sub>), respectively, and stored frozen until preparation for analysis.

## 3 Measurement methods

### 3.1 Requirements

Measurement methods for the tracer investigations described in the previous section must necessarily fulfil two requirements:

- They must be able to distinguish between different stable isotopes of the investigated element,
- and be sensitive enough to quantify or at least detect trace amounts of these isotopes in most samples.

The first necessary criterion suggests either mass spectrometric methods or activation analysis after induced nuclear reactions, making use of mass differences or internal nuclear structure as primary characteristics of stable isotopes of one element.

The necessary detection limit for zirconium isotopes can be obtained from a simple estimation. It is based on a reference person of 70 kg, with a blood plasma volume of  $\sim 3$  l, daily urine excretion of  $\sim 1$  l, and the administration of the maximum permitted amount of tracer, i.e. 700  $\mu\text{g}$  by injection or 7 mg by ingestion. The tracer is further assumed to be isotopically enriched to 100 %, and to distribute according to the current ICRP biokinetic model presented in section 1.4 with its standard parameters. Blood plasma and urine are considered as sample materials. In this case, the oral tracer would be the quantity constraining the necessary measurement detection limit, since the amount of tracer absorbed in plasma is  $7 \text{ mg} \cdot f_A$ , i.e. only 70  $\mu\text{g}$ , resulting in a maximum concentration in plasma of  $\sim 20 \text{ ng}\cdot\text{ml}^{-1}$ . The tracer is cleared from plasma with a half-life of 6 h, hence its estimated concentration will be  $1 \text{ ng}\cdot\text{ml}^{-1}$  after  $\sim 1$  d and  $0.1 \text{ ng}\cdot\text{ml}^{-1}$  after  $\sim 2$  d. Tracer concentrations in urine can be estimated from the literature data given in ICRP publication 56 (ICRP 1990) without using the model. Approximately 7 % of injected zirconium were reported to be excreted within one week after administration, i.e. the expected daily excretion is  $\sim 1$  %, resulting in an average urine concentration of  $0.7 \text{ ng}\cdot\text{ml}^{-1}$ .

Any measurement method applicable to the zirconium stable tracer investigations must therefore be able to detect  $\sim 1 \text{ ng}\cdot\text{ml}^{-1}$  or less of at least two zirconium isotopes in both blood plasma and urine.

Further practical requirements to suitable methods are:

- Interferences must be absent or at least correctable,
- methods should be available onsite or otherwise be readily accessible, so that various test measurements can be flexibly performed during method optimisation,
- and methods should be capable of providing an adequate sample throughput, since each investigation yields  $\sim 25$  samples.

### 3.2 Mass spectrometric methods

In order to find suitable examples for measurements of zirconium isotope ratios, from which a routine measurement method could be derived and optimised for biological samples, a literature search on the terms “zirconium” (in abstract, title or keywords) and “mass spectrometry” (in full text if possible) was conducted in June 2004. It revealed a total of 475 hits in three different search engines (www.sciencedirect.com, www.pubmed.com, and the GSF access to the ISI Web of Science). Many of these publications either dealt with

zirconium alloys or ceramics only as carrier or bulk material, or included zirconium products during sample preparation instead of measured samples, and hence were irrelevant for trace element analysis. The most common techniques concerned with measurements of zirconium were

- inductively coupled plasma mass spectrometry (ICP-MS), used for both multielemental trace element concentration measurements in various materials, including blood plasma or serum and urine, as well as for isotope ratio determinations;
- electrospray ionisation (ESI) or gas chromatography mass spectrometry (GC-MS), both concerned with organic molecules or (volatile) metal chelates (complexes);
- thermal ionisation mass spectrometry (TIMS), used for precise isotope ratio determinations in geological materials or concentration measurements with isotope dilution techniques.

The most relevant information for investigations with stable tracers is the precise determination of isotope ratios. TIMS is the accepted reference method for this purpose, with ICP-MS as a competing method. In contrast, ESI and GC-MS are predominantly used to determine organic chelates of zirconium or other trace elements (Crews, Ducros et al. 1994).

GC-MS instruments with electron impact ionisation are commonly available as relatively cheap benchtop systems with quadrupole mass analysers. By combining two different selection processes, i.e. a chromatography column and a mass filter, interferences in measurement are substantially reduced, and the method can be very sensitive. However, interferences can in turn be introduced by the use of the chelating agents. In addition, the chelating agents are composed at least of carbon, hydrogen and oxygen, and the measured isotope ratios have to be corrected for the isotope abundances of these elements, thus increasing the measurement uncertainty. It is therefore likely to be simpler and more accurate to directly measure inorganic elemental ions, instead of adding chelating agents to volatilize zirconium ions dissolved in plasma or urine in order to be able to determine the element with GC-MS.

The remaining two methods, ICP-MS and TIMS, in their application to samples containing trace amounts of zirconium, are briefly characterised for comparison in Table 3.1. Selected important characteristics are discussed thereafter. The information in this table and the following paragraphs is compiled from books and extensive reviews (Kienitz 1968; Adams, Gijbels et al. 1988; Crews, Ducros et al. 1994; Becker and Dietze 1998; Angerer and Schaller 1999) as well as from various shorter articles (Minster and Ricard 1981; Nomura, Kogure et al. 1983; Boswell and Elderfield 1988; Fassett and Paulsen 1989; Morita, Kita et al. 1994; Coedo, López et al. 1995; Xie and Kerrich 1995; Sahoo and Masuda 1997; Becker and Dietze 1998; Habfast 1998; Heumann, Gallus et al. 1998; McKelvey and Orians 1998; David, Birck et al. 1999; Diemer and Heumann 1999; Hirata and Yamaguchi 1999; Ramakumar and Fiedler 1999; Kunze, Koelling et al. 2000; Liang and Grégoire 2000; Yang and Pin 2000; Munker, Weyer et al. 2001; Wayne, Hang et al. 2001; Weyer, Munker et al. 2002; Yang and Pin 2002; Ide, Nakamura et al. 2003; Engström, Stenberg et al. 2004; Rodushkin, Engström et al. 2004; Schönbächler, Rehkämper et al. 2004; Walczyk 2004). Individual citations are given only if the discussed issue is treated specifically in the respective sources.

**Table 3.1:** Typical properties of inductively coupled plasma mass spectrometry (ICP-MS) and thermal ionisation mass spectrometry (TIMS). RSD = relative standard deviation

Method	ICP-MS	TIMS
sample pre-treatment	diluted with acids, or pure elemental solution after digestion and extraction from sample matrix	pure element after digestion and extraction from sample matrix
sample introduction	continuous flow of aerosol generated online from solution; diluted in argon; at atmospheric pressure	deposited (dried or electroplated) on metal filament (Re, Ta, W, Pt); thermally desorbed from filament in high vacuum
ionisation	plasma at 5,000 – 8,000 °C; ionisation yield 20 – 100 % for most elements; some multiply charged ions	hot metal surface at ~ 1,600 °C; ionisation yield ~ 0.1 – 10 %; singly charged ions predominant
ion selection	quadrupole double focussing sector fields	magnetic sector field
m/z resolution	300 – 12,000	~ 500
ion detection	single secondary electron multiplier single faraday cup multiple faraday cup (not for quadrupole ion selection)	single secondary electron multiplier single faraday cup multiple faraday cup (typical)
interferences	isobaric ions contribution from adjacent peaks doubly charged ions molecular / polyatomic ions: - argides (in particular $^{40}\text{ArX}^+$ ) - containing elements abundant in samples or acidic solvent, such as H, N, O, S, P, Cl	isobaric ions contribution from adjacent peaks doubly charged ions (rare) oxides (rare) cluster ions (rare)
quantification	standard samples, internal standards isotope dilution	isotope dilution
detection limit of zirconium	10 $\text{pg}\cdot\text{g}^{-1}$ – 10 $\text{ng}\cdot\text{g}^{-1}$ zirconium, depending on application; usually derived from $^{90}\text{Zr}$ and/or $^{91}\text{Zr}$	no value found, except for a minimum sample amount of ~ 17 ng (Boswell and Elderfield 1988)
achievable RSD of isotope ratios	30 ppm (91/90) to 120 ppm (96/90) in multicollector measurements (Schönbächler, Rehkämper et al. 2004)	20 – 70 ppm (Sahoo and Masuda 1997)

The most prominent difference between TIMS and ICP-MS is the mechanism of ion generation and the resulting ion yield.

In ICP-MS, a system of concentric tubes is used to generate a flow of sample aerosol into the centre of an argon plasma. The plasma is heated by an alternating magnetic field, generated by an alternating current in an induction coil surrounding the end of the tube system. The injected sample aerosol is successively dried, vaporised, and ionised in a local thermal equilibrium with the plasma.

The following paragraphs are based on a comprehensive article on ICP-MS, published in 1988 (Adams, Gijbels et al. 1988).

The degree of ionisation  $\alpha_p$  in a plasma is

$$\alpha_p = \frac{S}{n_e + S}, \quad (3.1)$$

with  $n_e$  the density of electrons.

S is the ionisation constant described by the Saha equation:

$$S = \frac{n_+ \cdot n_e}{n_0} = \left( \frac{2\pi \cdot m_e \cdot kT}{h^2} \right)^{3/2} \cdot \frac{2g_+}{g_0} \exp\left(-\frac{I}{kT}\right) \quad (3.2)$$

Here,  $n_+$  and  $n_0$  are the densities of singly charged positive ions and neutral atoms, respectively,  $g_+$  and  $g_0$  their respective statistical weights,  $m_e$  is the electron mass,  $h$  Planck's constant,  $k$  the Boltzmann constant, and  $T$  is the plasma (ionisation) temperature.  $I$  is the energy difference between the two considered states, i.e. in this case between atom and ion in their respective ground states.

Equation 3.2 is in principle valid only for a neutral, single element plasma at thermal equilibrium, i.e. with identical ion, electron, and neutral gas temperatures, defined by their respective kinetic energy distributions, and a commensurate excitation or ionisation temperature, defined by the occupation of excited electron states in the atoms or ions. As a further approximation in (Adams, Gijbels et al. 1988), the energy difference between the ground state and first excited state of gas atoms is identified with their ionisation energy  $I$ , relying on the fact that the differences of level energies of higher excitations are small.

Provided suitable experimental conditions, the atoms in the sample will approximate thermal equilibrium with the plasma atoms during their passage through the argon plasma, resulting in an analogue degree of ionisation. For a temperature of 8000 °C and an assumed electron density of  $3 \cdot 10^{21} \text{ m}^{-3}$ , the degree of ionisation  $\alpha_p$  will be  $> 90 \%$  for elements with an ionisation energy of up to 8 eV (including zirconium), and still  $> 10 \%$  for an ionisation energy of up to 11 eV.

Thermal ionisation in TIMS is realised by thermal desorption of ions from a heated metal surface, usually a narrow, flat filament. According to the temperature, valence electrons of atoms adsorbed to or near to the hot surface will occupy excited states or even be transferred into the conducting band of the bulk solid (Kienitz 1968) prior to desorption of the atom or ion. The ratio of ions and atoms desorbed from the surface is governed by the probability distribution of their electron states, described by the Saha-Langmuir equation:

$$\frac{N_+}{N_0} = \frac{g_+}{g_0} \exp\left(\frac{\Phi - I}{kT}\right) \quad (3.3)$$

$N_+$  and  $N_0$  are the numbers of positive ions and neutral atoms desorbed from the heated filament,  $g_+$  and  $g_0$  their respective statistical weights,  $\Phi$  the electron work function of the filament material,  $I$  the first ionisation energy of the adsorbed element,  $k$  the Boltzmann constant, and  $T$  the filament temperature in Kelvin.

Equation 3.3 is based on several assumptions or approximations, some of which are not strictly valid in certain circumstances:

- The ionisation energy  $I$  of an atom in close proximity to a conducting surface can be different from the ionisation energy  $I_0$  of a free atom.
- Equation 3.3 is valid only if the adsorbing atoms are in their ground state, i.e.  $I \sim I_0$ , and reach thermal equilibrium with the filament surface during their time near the surface.
- Especially in single filament sources, where desorption and ionisation take place on the same surface, this surface is often inhomogeneous. Due to sample or additive layers on the metal surface, the work function can be locally variable, resulting in surface areas with enhanced or inhibited ion desorption.

- In multiple filament sources, with one sample evaporation filament and one or more ionisation filaments without a sample layer, atoms can be lost by elastic scattering on the ionisation filament surfaces.

Depending on the filament material and temperature-constraining conditions, the ionisation yield, calculated as  $N_+/(N_0 + N_+)$ , can be below 1 %. This can be a severe drawback of the TIMS ion source, unless enough sample is available, or the low ion yield can be improved by applying additives to the filament surface(s), e.g. colloidal carbon, boron or rhenium suspensions, boric acid, or thin metal layers, in order to modify the work function  $\Phi$ .

Samples must be purified for TIMS to avoid a suppression of the ionisation of the target element. This purification is usually performed by chemical sample digestion with various acids and subsequent extraction of the relevant element, e.g. by column chromatography.

Although it is a time-consuming procedure and introduces the possibility of sample contamination, this purification is often also employed for ICP-MS to remove sources of spectral interference, i.e. polyatomic ions. These ions are produced from the abundant carrier gas of the ICP-MS ion source, argon, as well as from oxygen and halogens present in the sample, together with various trace elements from the sample. Possible argide interferences with zirconium include the elements Cr, Mn, Fe, Co, Ni, Ge, As, Se, and Br, some of which are present in human plasma and urine in concentrations exceeding those of zirconium. Therefore, for the analysis of trace amounts of zirconium, the necessary effort in sample preparation is similar for TIMS and ICP-MS.

Many of the polyatomic interferences can be removed from the relevant mass spectra peaks by using high-resolution sector-field ICP-MS instruments, e.g. the “Element” of the Central Inorganic Analysis Service of the GSF (Thermo Fisher Scientific (Bremen) GmbH, Germany). However, the transmission efficiency of this instrument is reduced by a factor of  $\sim 10$  if the mass resolution  $\Delta m/m$  is increased from 1:300 to 1:3000, or 1:3000 to 1:7500, thereby reducing the advantage of the increased ICP ionisation yield in comparison with TIMS. According to Prof. Schramel, the former head of the Central Inorganic Analysis Service, the high resolution mode is necessary to obtain reasonable concentrations of all stable zirconium isotopes, even from purified solutions (Schramel 2004).

A further advantage of ICP-MS is its high sample throughput. With an automated sampling system, up to a few hundred samples can be measured successively within one day. The measurement time of one sample, including a rinse cycle with diluted acid to avoid memory effects, is usually of the order of a few minutes. In contrast, only  $\sim 20$  samples can be placed on one TIMS sample carrier. The TIMS ion source with this sample carrier must be evacuated prior to measurement, implying a few hours of waiting time until a sufficiently low pressure is attained. Including the heating process, one sample measurement with TIMS can take from  $\sim 10$  min up to a few hours.

In summary, ICP-MS tends to be more sensitive than TIMS, while being hindered by more interfering species. For high sensitivity, both methods require purification of the relevant element(s) from organic samples. The sample throughput of ICP-MS is substantially higher, making it a preferable method for routine use.

At the GSF, both methods are available. As mentioned above, an ICP-MS instrument is run by the Central Inorganic Analysis Service, while two TIMS instruments (Finnigan MAT 262 and TRITON (Thermo Fisher Scientific (Bremen) GmbH, Germany)) are run by the working group Medical Physics in the Institute of Radiation Protection.

Both methods were tested by determining the isotope ratios of 20 zirconium standard solution samples (PLZR2-2Y; SPEX CertiPrep, Metuchen, NJ, USA), each containing ~ 2 ng of zirconium, with the ICP-MS Element and the TIMS TRITON.

The ICP-MS measurements did correctly reproduce the natural isotope ratio 91/90. However, even isobaric correction of molybdenum interference was not sufficient to correctly reproduce the natural isotope ratios 92/90 and 94/90, for which no other isobaric interference occurs. The mean ratio of 95/90 was 0.05. The presumed additional source of interference could not be separated by the mass spectrometer. Furthermore, preceding blank measurements yielded a count rate on mass 96 of the same order of magnitude as the count rate in the standard samples. Any possible correction, e.g. of molybdenum and ruthenium isobaric interference, would therefore have a large uncertainty. Since it was expected that experimental samples would have even stronger interferences due to incomplete separation of interfering elements from zirconium, ICP-MS was excluded as measurement method, due to the risk of measurement errors from interferences.

Zirconium in nanogram amounts, directly applied to rhenium filaments, could not be measured with TIMS on faraday detectors, since the ion signal was either too small or too unstable. However, the GSF TRITON features multiple channeltron detectors, whose ion counting capability was used for all zirconium measurements within the current study.

No reference method for zirconium measurements in low ng amounts was found in the literature. Therefore, a set of experiments was used to develop a measurement method, based especially on the work of Boswell and Elderfield (1988), whose lowest reported measured amount was 17 ng. A list of the extensive reference experiments in the current study is given in annex A, whereas only selected results are referred to in section 3.2.

In the current study, an optimal ionisation yield and good beam stability could be obtained by using a single rhenium filament, coated with a diluted graphite suspension. The longest measurement of a 1 ng sample of natural zirconium lasted ~ 3 h until total evaporation.

In the reference TIMS measurements performed in analogy to the ICP-MS test measurements, the isotope ratios had to be corrected for isobaric interference of molybdenum on masses 92, 94, and 96 from measurements on mass 95. The mean 95/90 count rate ratio was 0.017, i.e. about three times lower than in ICP-MS measurements. The count rates on the channeltron detectors were of the same order of magnitude than the count rates on the single secondary electron multiplier in the ICP-MS test measurements. The single standard deviations of the measured isotope ratios were typically in the range of 0.5 – 5 %; being highest for the ratio 96/90, which is both the most extreme ratio and most affected by the molybdenum isobaric correction.

All resulting zirconium isotope ratios were in consistence with the natural isotope ratios of zirconium (Rosman and Taylor 1998) within the published uncertainties and those resulting from the TIMS measurements. Therefore, TIMS was considered capable of measuring experimental samples of the intended tracer investigations with stable isotopes of zirconium.

### **3.2.1 Sample preparation for thermal ionisation mass spectrometry (TIMS)**

Blood plasma and urine samples were first subjected to microwave-assisted acidic pressure digestion. In a second step, zirconium was extracted by column chromatography to obtain pure zirconium salts, which can be optimally ionised in the TIMS ion source without interfering elements. The third step was the preparation and loading of TIMS sample carriers. The digestion and extraction procedure was derived from previous experiences with biological samples in the working group Medical Physics. It was optimised for zirconium

based on literature examples of zirconium extraction from various materials (Boswell and Elderfield 1988; David, Birck et al. 1999; Münker, Weyer et al. 2001; Weyer, Münker et al. 2002; Schönbacher, Rehkämper et al. 2004) and supplier's recommendations on the treatment of chromatography resin. Special credit goes to Vera Höllriegl and Pascale Louvat for separation method development, and to Vera Höllriegl and Beate Saath for sample preparation and all further chemistry-related operations.

The sample carrier loading procedure was inspired by previous TIMS measurements of zirconium (Minster and Ricard 1981; Nomura, Kogure et al. 1983; Boswell and Elderfield 1988; Sahoo and Masuda 1997; Rasmussen 2004), and was optimised for small amounts of zirconium.

Chromatography columns were prepared as follows:

Ln Resin material, with a particle size of 100-150  $\mu\text{m}$ , and column assembly parts were purchased from Eichrom Environment, SAS, Bruz, France. The resin consisted of polymer beads covered with HDEHP (di(2-ethylhexyl) orthophosphoric acid) as extractant. Prior to the first use, the loose resin was repeatedly elutriated in 0.1 M  $\text{HNO}_3$ ; floating particles were removed. Aliquots of the resin slurry were filled into polypropylene columns of 8 mm inner diameter. During filling, air bubbles were removed by stirring the resin with a glass rod in order to prevent the columns from becoming impermeable for solutions. The resin was firmly fixed in place by porous polypropylene frits to prevent loss of resin and disturbances when adding sample solutions or acids during chromatography. The typical height of the resin beds was 20 mm, resulting in a resin volume of  $\sim 1$  ml. Assembled columns were successively rinsed with 5 ml 6M HCl, 5 ml 2 M hydrofluoric acid (HF), and 15 ml 0.1 M  $\text{HNO}_3$  prior to their first use. They were stored in 0.1 M  $\text{HNO}_3$  at 3°C.

Sample preparation was done for several samples in parallel and included the following steps:

- (a) Spiking of 1 ml urine or 500  $\mu\text{l}$  plasma with 5  $\mu\text{l}$  of reference tracer solution T-94-R, commensurate to a tracer mass of 5.3 ng
- (b) incubation at 37 °C in a heating cabinet over 8 h
- (c) addition of 1 ml concentrated  $\text{HNO}_3$  (sub-boiling distilled grade)
- (d) microwave digestion in quartz vessels over 10 min at 600 W output power, 2 samples at a time (limited by the design of the microwave oven from Hans Kürner Analysentechnik, Rosenheim, Germany)
- (e) transfer of the samples from quartz vessels to Teflon beakers ( $\sim 10$  ml volume)
- (f) evaporation to dryness at 120 °C over 4 h on a hot plate with extraction of the acid vapour to avoid cross-contamination of samples
- (g) redissolution of the residue in 1 ml of a mixture of 0.5 M  $\text{HNO}_3$  and 0.01 M hydrofluoric acid (HF) by using an ultrasonic bath over 15 min
- (h) preconditioning of the Ln resin columns with 5 ml of the latter acid mixture, followed by loading of the sample solution directly on the top frit, i.e. when the sinking fluid level coincides with the upper fringe of the resin
- (i) rinsing the emptied Teflon beakers with 1 ml of the latter acid mixture and loading this solution on the respective columns

In every following chromatography step, the solutions were not applied until the fluid level on the columns reached the upper fringe of the resin, in order to prevent mixing of the different solutions. Extraction chromatography was continued by:

- (j) applying 5 ml of 4 M HCl
- (k) applying 20 ml of 6 M HCl

- (l) elution of zirconium with 12 ml of a mixture of 3 M HCl and 0.1 M HF; the first 4 ml were discarded, the following 6 ml collected in a Teflon beaker, the following 2 ml again discarded.

The resulting zirconium solution was evaporated to dryness under the same conditions as in step (f) above. Chromatography columns were regenerated for repeated use by consecutive rinsing with 5 ml 6 M HCl, 5 ml 2 M HF, again 6 M HCl, 5 ml 2 M HF, and 15 ml 0.1 M HNO<sub>3</sub>.

TIMS sample carriers, i.e. single rhenium filament assemblies, were prepared onsite from filament holders (Thermo Fisher Scientific (Bremen) GmbH, Germany) and a zone-refined rhenium ribbon (Rhenium Alloys Inc., Elyria, OH, USA) of 99.995 % purity, 0.7 mm width and 38 µm thickness. Rhenium filaments were cut to appropriate length and electrowelded to filament holders. The assembled sample carriers were washed in 99.9 % denatured ethanol in an ultrasonic bath and successively baked out in high vacuum over 30 min at 4.5 A, corresponding to a temperature of ~ 1,600 °C. Baking was used both for cleaning the filaments after handling, as well as to reduce the isobaric signals of trace impurities of molybdenum from the filament. Reference experiments with blank sample carriers during method development showed that the main fraction of molybdenum resulted from filaments rather than from samples.

For application to TIMS, samples were re-dissolved each in a droplet ~ 3 µl of concentrated HNO<sub>3</sub> of sub-boiling distilled grade, by placing the Teflon beakers in an ultrasonic bath over 15 min. As a means to enhance ionisation yield and beam stability when using rhenium single filaments, the filaments were coated with a diluted graphite suspension (1 part 'Aquadag' from Acheson Colloids Company, Port Huron, MI, USA; diluted with 15 parts Milli-Q water). A droplet of 1 µl of graphite suspension was deposited on the rhenium filament surface and dried at 1.2 A. The redissolved sample was consecutively transferred from its Teflon beaker to the filament and dried at 1.2 A, followed by 1 µl of diluted graphite suspension to form a covering layer. After drying, the heating current was increased to 1.5 A for ~ 10 s.

Before reuse, the Teflon beakers were cleaned by

- rinsing with tap water, cleaning with a soft brush, and allowing to dry,
- dissolving large remnants of samples in 1 ml HNO<sub>3</sub> conc. (analytical grade) using an ultrasonic bath over 15 min,
- rinsing with distilled water and allowing to dry,
- filling with 10 ml HNO<sub>3</sub> conc. (analytical grade), letting trace impurities dissolve over more than 48 h,
- again rinsing with distilled water and allowing to dry,
- subjecting the beakers to a flow of hot HNO<sub>3</sub> vapour over 5 h,
- and finally rinsing them with Milli-Q water and allowing to dry.

This laborious method proved to be necessary after contamination from concentrated tracer stock solutions, which were prepared in specific Teflon beakers, was found in some samples. Neither the ultrasonic bath nor the acid vapour cleaning alone were sufficient to prevent memory effects. It was furthermore necessary to individually clean each beaker to avoid cross-contamination.

Up to 21 samples at a time, including at least one standard sample of 2 ng natural zirconium, were assembled on a sample carrier wheel and introduced into the TRITON ion source chamber. Prior to measurement, the source chamber was pumped out, aiming at a pressure of ~ 10<sup>-7</sup> hPa.

### 3.2.2 Description of the TIMS instrument and measurement

The TRITON thermal ionisation mass spectrometer is shown in Figure 3.1.

The ion source chamber (to the left in Figure 3.1) features the sample carrier wheel, a heating current system with glide contacts, and the ion optics. The filament temperature can be monitored by a pyrometer.

A 90° magnet is used to deflect the ions according to their mass-to-charge ratio, optionally supported by two quadrupoles. These quadrupoles serve to deform the beam in measurements which use two or more magnet settings and static multicollectors. The detector distance between neighbouring isotopic ion beams is dependent on the central ion mass selected by the magnet. Since the detectors are not moved when the magnet current is changed, the ion beam can not be centred on all detectors with all magnet settings. By using the quadrupoles it is possible to deform the beam slightly and correct such small deviations.

The ion detection system of the TRITON consists of three subsystems:

- A set of nine carbon faraday cups, movable individually either direct or indirect by 4 motors, and used for high-precision isotope ratio measurements with strong ion beams;
- a single secondary electron multiplier for low signals or large isotope ratios; in the latter case, the more abundant isotope is measured with a faraday cup and the less abundant isotope with the SEM;
- a set of up to 8 channeltron detectors, mounted onto selected faraday cups. This arrangement is specific to one or a few elements, since the relative distances of the detectors can not easily be altered.

The instrument is operated exclusively by a software suite provided by the manufacturer. This software provides access to all necessary operational tests and measurements, as well as to diagnostic information.

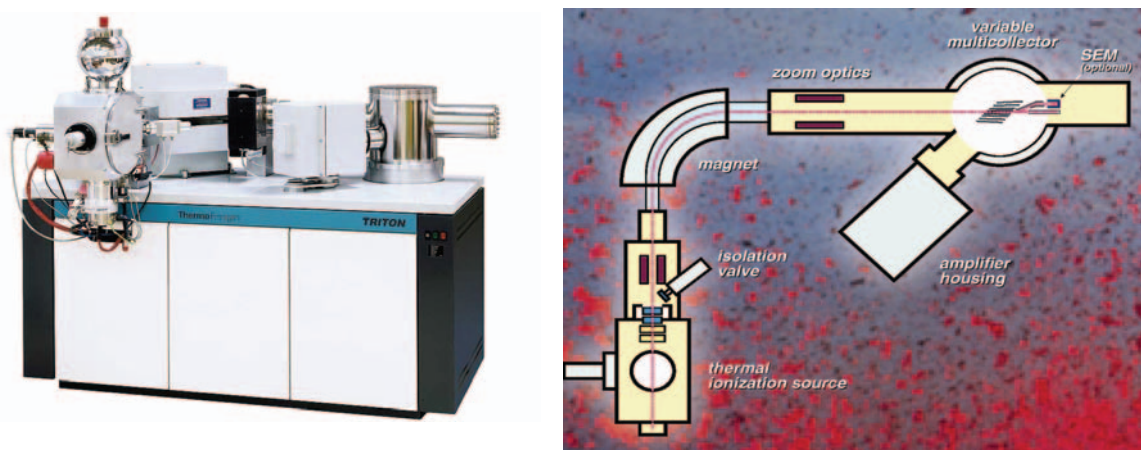


**Figure 3.1:** Photograph and scheme of the TRITON instrument (courtesy of Thermo Fisher Scientific (Bremen) GmbH, Germany)

A typical sample measurement of zirconium samples in the current study proceeds according to the following scheme:

- The sample is heated slowly to a temperature where ion beam formation can be expected, trying to avoid sample loss due to local stress deformations from an inhomogeneous temperature distribution, or complete untimely evaporation. The heating scheme is  $500 \text{ mA} \cdot \text{min}^{-1}$  up to 2500 mA, then  $350 \text{ mA} \cdot \text{min}^{-1}$  up to 3500 mA,

followed by  $200 \text{ mA}\cdot\text{min}^{-1}$  up to  $4500 \text{ mA}$ , and finally  $100 \text{ mA}\cdot\text{min}^{-1}$ , until a signal of  $^{90}\text{Zr}$  can be observed which is sufficient to focus the ion beam.

- The ion beam is focused to obtain optimal transmission through the instrument. To this purpose, an automated optimisation routine included in the software was alternated with fine tuning of the filament position. The combination of both focusing operations can improve the ion count rate by several orders of magnitude. This is a critical step, especially for small samples, since excessive heating instead of good focussing can easily consume the sample within a few minutes.
- When the ion beam is focused and sufficiently stable, the measurement routine is started. In an initial reference measurement, the magnet current setting is calibrated to centre the beam on the detectors; this measurement takes  $\sim 5 - 10 \text{ min}$ . The standard measurement then consists of 50 measurement cycles, grouped in 5 blocks of 10 cycles. In each cycle, the count rates of the masses 90, 91, 92, 94, 95, and 96 amu are recorded for 16.7 s simultaneously by the channeltron detectors, followed by a measurement of the  $^{90}\text{Zr}$  count rate on all detectors for 2 s each, in order to correct yield deviations. The measurement routine calculates all count rate ratios relative to  $^{90}\text{Zr}$ , taking into account the relative detector yields, the molybdenum isobaric correction, the detector dead time and dark noise, as well as the temporal change of the count rates. The isotope ratio measurement takes  $\sim 25 \text{ min}$ .

The measured data can be viewed during and after measurement with the instrumental software. The calculation of isotope ratios is interactive in that only the count rates of each cycle are stored as numbers; all derived quantities can be recalculated or modified in case an error is found. The results can be exported as ASCII files. They were further evaluated with Microsoft Excel.

Two specific issues related to the channeltron detectors and the TIMS ion source are worth noting in the context of ion count rate ratios:

The measured ratios of zirconium isotopes in investigation samples varied from 0.004 to 1. Setting at  $1000 \text{ s}^{-1}$  the minimum count rate level for the most abundant isotope, the minimal count rate of the least abundant isotope is  $4 \text{ s}^{-1}$ . The maximum channeltron dark noise of  $0.1 \text{ s}^{-1}$  then would account for 2.5 % of the signal in the worst case. However, the actual effect of detector dark noise would still be lower due to the dark noise correction. In standard measurements, typical count rates  $> 10^4 \text{ s}^{-1}$  were attained for the most abundant isotopes.

Detector dead time effects and fast changes in detector yield can be avoided by limiting the heating current in a way that the most abundant isotope yields a count rate below  $10^5 \text{ s}^{-1}$ . The change in detector yield over time was observed during the peak centring phase of the measurements. All channeltron amplifying voltages were changed several times during the study to correct adopt to ageing effects. This was especially necessary for the channeltrons on masses 90 amu and 94 amu, since  $^{90}\text{Zr}$  and  $^{94}\text{Zr}$  were the most abundant isotopes in most samples, resulting in consistently high count rates.

In a thermal ion source, the probability of atom or ion emission from the surface is dependent on the mass of the particle. Lighter ions of an element are preferably emitted, leading to a depletion in light ions over time and a change in measured isotope ratios, an effect termed ‘mass fractionation’. In high-precision isotope ratio measurements, this effect is usually corrected by using a known isotope ratio of the investigated element as reference (Habfast 1998). However, in the current study, each zirconium type (i.e. the different tracers and natural zirconium) contains all of the naturally-occurring isotopes in non-negligible amounts. This makes internal mass fractionation correction impossible, because none of the zirconium isotope ratios are known in mixed samples.

Two total evaporation experiments during method development showed that the change in zirconium isotope ratios was negligible for the ratio 91/90 until ~ 70 % of a sample was evaporated, while during a routine measurement, typically only 10 – 50 % of a sample were consumed. The change in isotope ratios 92/90, 94/90, and 96/90 was greater, but still below 1 % during a typical measurement duration.

Care must be taken, however, if a sample is nearly depleted during measurement, indicated by a declining signal despite a continuous increase of the heating current. In such an extreme case, the relative change in the isotope ratio 96/90 can exceed 10 %. Since no reliable correction mechanism is available, such sample measurements should be rejected and repeated.

Repeated measurements of laboratory standards, with 2 ng natural zirconium per sample, have shown that the change of isotope ratios due to mass fractionation is usually negligible compared to the random fluctuations of the isotope ratio in the course of a typical measurement procedure. No significant systematic deviations of any measured isotope ratio were found in comparison to the IUPAC recommended ratios for natural zirconium (Rosman and Taylor 1998), or in comparison to the certified ratios for the isotopically enriched tracers.

A further source of mass-dependent bias is ‘mass discrimination’ introduced by the ion detector. Secondary electron multipliers (SEM) have different electron emission efficiencies for ions with differing velocities (Adams, Gijbels et al. 1988). This bias can be assessed in the same way as thermal ionisation mass fragmentation, i.e. by comparison of the measured count rates with reference isotope ratios or abundances. However, the effect is negligible if the detector is operated in ion counting mode, and if the ions of all isotopes generate enough secondary electrons to exceed the SEM’s pulse-generating threshold value. Therefore, the channeltron measurements in the current study should not be subject to mass discrimination effects.

### 3.2.3 Tracer concentration calculation with the isotope dilution technique

Thermal ionisation mass spectrometry does not allow for absolute calibration, because the ion yield of the thermal ion source can vary by orders of magnitude between different samples with identical filament heating current and focussing voltages of the ion optics system. A similar variation can occur for individual samples depending on the focussing voltages. Thus, the direct measurement of zirconium mass or concentration in a sample is not possible.

In order to enable concentration measurements by TIMS, isotope dilution (ID) can be implemented. The basic concept of this technique is the mixture of an elemental sample ( $E$ ) with a ‘spike’ ( $S$ ), i.e. a known amount of the same element with artificially altered isotope ratios (Fassett and Paulsen 1989). The mass  $m_E$  of the natural element in the sample can then easily be derived from the measured isotope ratios  $R_M = Y_M/X_M$  and the relative isotopic abundances  $h_x$  and  $h_y$  in spike  $S$  and natural element  $E$  (the two types present in the measured sample  $M$ ;  $aw$  denotes atomic weight):

$$m_E = \frac{m_s \cdot aw_E}{aw_S} \cdot \frac{h_{y,S} - h_{x,S}R_M}{h_{x,E}R_M - h_{y,E}} \quad (3.4)$$

This method is very accurate, since few processes cause significant alterations in the isotope ratio of a sample, and natural isotope ratios of most elements are well-defined world-wide. After spike and sample have been thoroughly mixed to ensure a homogenous distribution of

all isotopes, a sample loss during chemical processing has no influence on the isotope ratios, and thus the derived element concentration.

This concept is used for the tracer concentration measurements by ID-TIMS in the current study, however adapted to four different ‘types’ of zirconium in each sample. In the following, the term ‘type’ denotes zirconium with a specific isotopic composition, in the sense that each tracer (T-90, T-91, etc.), as well as natural zirconium, is a different type of zirconium. The term ‘species’ has been used for this purpose in the literature, but ‘species’ also denotes characteristic chemical forms of an element, and thus can be misunderstood.

It is further important to distinguish between *type concentration*, i.e. the mass of zirconium of a certain type per mass of sample, and *isotope concentration*, i.e. the mass of a certain isotope of zirconium per mass of sample, since each type contains all isotopes in non-negligible abundances.

In the application to the current double tracer study, four types must be considered in each sample:

- orally administered tracer (either T-90, T-91, T-96-L, or T-96-H)
- intravenously injected tracer (either T-90 or T-96-H)
- natural zirconium, present in the sample or introduced as contamination
- reference tracer or ‘spike’ (T-94-R)

The concentration of each type can straightforwardly be calculated, similar to Equation 3.4, if the number of stable isotopes is equal to or greater than the number of types in the sample, including the reference tracer. The calculation for four types is principally simple, yet demands a high effort due to many mixed products of isotope abundances or ratios. Therefore, the calculation was done with the symbolic programming language Mathematica 5 (Wolfram Research Inc., Champaign, IL, USA). The major steps are described in the following paragraphs, expressed generally to be transferable to various isotopic mixtures or elements.

Consider a measured sample  $M$ , consisting of  $N_M$  atoms, composed of five different (stable) isotopes  $i$  ( $i = v, w, x, y, z$ ) according to the relative abundances  $h_{M,i}$ :

$$N_M = N_M \cdot (h_{M,v} + h_{M,w} + h_{M,x} + h_{M,y} + h_{M,z}) = N_{M,v} + N_{M,w} + N_{M,x} + N_{M,y} + N_{M,z} \quad (3.5)$$

The number of atoms  $N_{M,i}$  of each isotope in  $M$  is in turn composed of contributions from all types  $T$  ( $T = A, B, C, D, M$ ):

$$N_{M,i} = N_M \cdot h_{M,i} = N_A \cdot h_{A,i} + N_B \cdot h_{B,i} + N_C \cdot h_{C,i} + N_D \cdot h_{D,i} \quad (3.6)$$

If the resulting system of equations is solved under the assumption that the number of atoms of one type is known, e.g.  $N_D$ , the number of atoms of all other types is obtained in analogy to Equation 3.4.

The numbers of atoms can be converted to masses by scaling with the atomic weights of the respective isotopic mixtures:

$$m_T = N_T \cdot aw_T = N_T \cdot \sum_{i=v}^z h_{T,i} \cdot im_i \quad (3.7)$$

Here,  $im_i$  denotes the respective isotope masses.

In order to obtain a direct link between the masses  $m_T$  and measured values, i.e. isotope ratios, the relative abundances  $h_{T,i}$  can be described by the isotope ratios  $R_{T,ij}$ . This conversion has no effect on the mass values, but is relevant for the calculations of their uncertainties (cf. section 4). In some samples, the measured isotope ratios are strongly correlated, and their correlation

coefficients can be easily included in the uncertainty calculation, according to Equation 4.2, if the masses are related to isotope ratios.

$$R_{T,ij} = \frac{N_{T,i}}{N_{T,j}} = \frac{h_{T,i}}{h_{T,j}} \quad (3.8)$$

$$h_{T,i} = \frac{R_{T,ij}}{R_{T,yj} + R_{T,wj} + R_{T,xj} + R_{T,yj} + R_{T,zj}} \quad (3.9)$$

The isotope  $j$  has a special role in Equation 3.9 as a reference isotope. In the current study,  $^{90}\text{Zr}$  was chosen for this purpose, since it was the most or second most abundant isotope in all relevant types. As a consequence, its measured count rate was relatively high in all samples, limiting the uncertainty of isotope ratios. In addition, no isobaric interferences exist for  $^{90}\text{Zr}$ . The complete expressions for the masses  $m_T$ , in analogy to Equation 3.4, include the mass of the reference type  $m_D$ , the ratio of atomic weights  $aw_T/aw_D$ , and 24 mixed products of 4 isotope ratios each in numerator and denominator, which is the reason why they are not shown here. It was considered to simplify the solutions by neglecting small terms; however, most isotope ratios varied significantly between samples due to the use of various tracers, and no generally small terms were identified.

In order to reproduce the results from the IDMS evaluation, it is necessary to note that the choice of isotopes in the calculation is basically arbitrary, if more isotopes are available than types are present in the sample. It is reasonable to choose isotopes which are most abundant in one type in order to optimise the uncertainty (Yu, Fassett et al. 2002). However, this criterion is not sufficient in the case of T-90, since  $^{90}\text{Zr}$  is the most abundant isotope both in T-90 and in natural zirconium. Therefore either  $^{91}\text{Zr}$  or  $^{92}\text{Zr}$  has to be chosen as fourth isotope in investigations with T-90, in addition to  $^{94}\text{Zr}$  (T-94-R) and  $^{96}\text{Zr}$  (T-96-H or T-96-L). In practice, the respective samples were evaluated with both isotope combinations, yielding two results of one measurement. As a general rule, if no specific errors could be found, the weighted mean of both results was used as effective value. The uncertainty of these effective values was taken to be the arithmetic mean of the individual uncertainties, since the calculation of the weighted uncertainty would imply that the two results are independent measurements, artificially lowering the uncertainty value.

For practical purposes, MS Excel worksheets were developed specifically for each tracer combination in order to calculate all tracer concentrations, as well as the respective absolute and relative uncertainties, directly from the measured data. Uncertainties were calculated as described in section 4, in particular by Equation 4.2.

With the help of these files, routine data evaluation could be performed without manual transcription, except for sample name and measurement data, thus constraining a typical source of errors.

### 3.3 Activation analysis

Nuclear activation analysis is based on excitation or transformation reactions of nuclei, induced by sample bombardment by a particle beam. In general, radioactive reaction products are detected and quantified by gamma spectrometry, either during the irradiation (prompt gamma activation analysis), or after a suitable waiting time (delayed gamma activation analysis). Depending on the reaction product nuclei, other radiation types may be measured

(e.g.  $\beta^+$  or  $\beta^-$ ), however, gamma radiation is most frequently used due to its penetrating ability, thus limiting errors due to sample size and facilitating sample handling.

Irradiated samples can either be measured directly, or the radionuclide of interest can be separated chemically from the sample to reduce spectral interferences and background generated by activated matrix elements. The first approach is termed instrumental activation analysis, the second radiochemical activation analysis.

The concentration of (trace) elements in a sample is calculated from the measured counts in the respective peaks of the gamma energy spectrum, taking into account the time of irradiation and measurement, waiting time, the respective reaction cross sections, beam particle flux, geometry of irradiation and measurement, as well as any further necessary corrections. To facilitate this calculation, often known amounts of internal and external standards are irradiated under the same conditions as the samples; by comparison of sample and standard measurements, some of the above-mentioned corrections can be cancelled out, possibly reducing the uncertainty of the concentration calculation.

Photons, protons, neutrons, deuterons, as well as alpha particles can be used as beam particles. The type of beam particle and the intended type of reaction determine the energy needed for the beam particles. Charged particles must exceed energies of a few MeV to penetrate the coulomb barrier of the target nuclei, while neutrons may have any energy, depending on the favoured reaction. For large sample sizes, the loss of energy and intensity of the particle beam has to be taken into account in the concentration calculation of trace elements.

For the measurement of trace amounts of zirconium, two techniques were initially considered for the current study (the cited publications are also the source for the following paragraphs, unless otherwise stated):

- Instrumental neutron activation analysis (INAA) with thermal neutrons, which is a very common technique suitable for many elements (Erdtmann 1992; de Goeij 2000; Glascock 2003); several high-flux sources of thermal neutrons are available at the research reactor FRM II in Garching, Germany.
- Proton nuclear activation analysis (PNA) (Cantone, Molho et al. 1982), which was already demonstrated to be applicable for zirconium in biological samples (Cantone, de Bartolo et al. 1997; de Bartolo, Cantone et al. 2000; Veronese, Giussani et al. 2003).

Both techniques rely on delayed gamma spectrometric measurements of radioactive product nuclei. Prompt gamma activation analysis would mean that only one sample could be measured at a time with a given instrumental setup, which would have been impractical considering the available resources during the study. In addition, single sample measurements would have constrained the number of samples, since it was expected that each sample would need several hours measurement time due to low tracer concentrations.

The following advantages are typical for nuclear activation analysis:

- Depending on the beam particle type and energy, many elements can be activated in the same irradiation, making activation analysis capable of multielement analysis.
- For many nuclei, characteristic values like radionuclide half-life, decay energy and reaction cross sections are well-known, allowing for a reasonable estimate of measurement uncertainty. For this reason, activation analysis has often been used as a reference technique for validation of other measurement methods.
- Many applications require only basic sample processing prior to irradiation, reducing the risk of contaminations. Encapsulation, e.g. in polyethylene, quartz vials, or aluminium foil, can be sufficient for solid samples. Liquid samples can be dried and

pressed to prevent aerosol generation and sample loss by evaporation of water due to energy absorbed from beam particles.

- The energy range of nuclear reactions is well above that of chemical bonds, hence the influence of the sample matrix on the reaction yield is often negligible.
- Radioactive activation products cannot be confounded with stable isotopes of the same element in gamma spectrometric measurements. As a consequence, any necessary chemical processing after irradiation (e.g. to remove interfering elements) is practically immune to contamination with the naturally occurring element.

Typical drawbacks of activation analysis are:

- Activation of natural samples often yields a mixture of radionuclides with interfering emission lines in the gamma energy spectrum. A suitable choice of the lines used for element quantification can avoid this effect. However, a substantial background can be produced by Compton scattering of gamma photons with sufficiently higher energy than the observed line, thus obscuring the observed peak and reducing the detection limit.
- Spectral interferences can be reduced by chemical separation of the element of interest from the sample. An internal standard is necessary in this case to correct for losses during separation.
- In certain samples, matrix elements present in large concentrations can quench the beam particles. As an example, activation analysis of trace elements in a cadmium-containing alloy by thermal neutrons is difficult, since cadmium has a large mean absorption cross section of  $2520 \pm 50$  barn for thermal neutrons. The same is true for the presence of boron with an absorption cross section of  $767 \pm 8$  barn (Munter 1992).
- The access to suitable irradiation facilities sets constraints to the sample throughput of activation analysis. A typical irradiation time of elements with small reaction cross sections is of the order of hours to days. If only few samples can be measured at a time, e.g. due to a short activation product half-life, the total number of samples is limited.
- Depending on the type of reaction, only selected isotopes of one element can be activated and measured in one irradiation. Limiting factors can be energy dependence and magnitude of cross sections, product nuclide half-lives and specific activities, as well as stable product nuclides.

Thermal neutrons, with an energy of up to 0.55 eV, are most frequently used for neutron activation analysis due to the large thermal neutron fluxes in research reactors. At the FRM II, fluxes of up to  $4 \cdot 10^{14} \text{ cm}^{-2} \text{ s}^{-1}$  were expected at various irradiation positions in 2003 (Link, Pulz et al. 2003).

Typically, thermal neutrons are absorbed by irradiated nuclei of mass X, leading to the emission of a gamma photon and a product nucleus of mass X+1. In the case of zirconium, three radionuclides can be generated from this type of reaction, namely  $^{92}\text{Zr} (n,\gamma) ^{93}\text{Zr}$ ,  $^{94}\text{Zr} (n,\gamma) ^{95}\text{Zr}$ , and  $^{96}\text{Zr} (n,\gamma) ^{97}\text{Zr}$ . The characteristic data of these reactions is presented in Table 3.2.

The product radioisotope  $^{93}\text{Zr}$  is a pure beta emitter with a very long half-life and a low absorption cross section for thermal neutrons. Due to these characteristics, it is not suitable for neutron activation analysis in trace amounts. The cross sections of the other two reactions are even lower, however both product nuclei,  $^{95}\text{Zr}$  and  $^{97}\text{Zr}$ , emit gamma radiation of an energy readily measurable by gamma spectrometry. The half-lives permit sample transport and processing, thus both nuclides are in principle measurable by NAA.

The lowest detection limit of zirconium found in the literature in 2003 was 10 ng zirconium in animal tissues; reported in (Osborn, Broering et al. 1981) and being based on the reaction

$^{94}\text{Zr}$  ( $n,\gamma$ )  $^{95}\text{Zr}$  after a 100 h irradiation with a flux of  $1\cdot 10^{14}$   $\text{cm}^{-2}\text{s}^{-1}$  and radiochemical separation to remove interferences. This detection limit might be improved slightly, e.g. by using high purity germanium crystals with a better energy resolution instead of Ge(Li) detectors for gamma spectrometry, or a modified separation technique. However, it was not expected at the beginning of the current study that  $^{96}\text{Zr}$  would also be measurable, since its absorption cross section is smaller than that of  $^{94}\text{Zr}$ , and its half-life shorter, resulting in less time available for sample transport and processing.

Since no expertise on NAA was available at the time within the working group Medical Physics at the GSF, contact was sought with the Institute of Radiochemistry at the Technische Universität München (TUM). The successive discussion and personal communication (Lierse v.G. and Lin 2004) made clear that a simultaneous measurement of  $^{94}\text{Zr}$  and  $^{96}\text{Zr}$  in low ng amounts in biological samples would practically be impossible with the available resources.

In contrast, PNA has been shown to have detection limits of 1 ng  $^{90}\text{Zr}$  and 2 ng  $^{96}\text{Zr}$  per g of human blood plasma (Veronese, Giussani et al. 2003) without chemical separation of zirconium from plasma samples. Therefore, the method was adopted for the current study.

**Table 3.2:** Data on ( $n,\gamma$ ) reactions of zirconium isotopes in NAA.

Cross sections are taken from (Munter 1992), half-lives and energies from the NuDat 2 database (National Nuclear Data Center 2007).

Reaction	Absorption cross section (mb)	Product half-life	Product decay energies (keV)
$^{92}\text{Zr}$ ( $n,\gamma$ ) $^{93}\text{Zr}$	220	$1.5\cdot 10^6$ y	60.6 ( $\beta$ )
$^{94}\text{Zr}$ ( $n,\gamma$ ) $^{95}\text{Zr}$	49.9	64.0 d	757, 724 ( $\gamma$ ) 368, 401 ( $\beta$ )
$^{96}\text{Zr}$ ( $n,\gamma$ ) $^{97}\text{Zr}$	22.9	16.7 h	743 ( $\gamma$ ), 1915 ( $\beta$ )

### 3.3.1 Proton nuclear activation (PNA) sample preparation

The sample preparation for PNA was usually done for all samples of one irradiation at once, since the risk of cross-contamination was low due to the small volatility of dissolved zirconium. It consisted of the following steps:

- Mixing of  $\sim 0.8$  g blood plasma or 18 ml urine with a 100  $\mu\text{l}$  of  $^{51}\text{V}$  standard solution, followed by incubation overnight,
- partial pressure digestion of urine samples with a mixture of 7.2 ml  $\text{HNO}_3$  and 1.2 ml of  $\text{H}_2\text{O}_2$  (this step was necessary because untreated urine samples are hygroscopic and viscous, and thus were not feasible for tablet pressing),
- drying in a fume hood overnight (plasma samples) or evaporation to dryness on a hot plate (urine samples,  $\sim 30$  h at  $120$   $^\circ\text{C}$ ),
- grinding to a fine powder in an agate mortar and pressing into tablets of  $\sim 9$  mm diameter and 1 – 2 mm thickness.

The resulting tablets were encased in aluminium sample holders consisting of a base plate, a thin sheet of aluminised Mylar foil, an intermediate plate with a hole of 10 mm, in which the tablet was placed (shown in Figure 3.2), another sheet of Mylar foil, and aluminium shielding plates of 0.20 – 0.92 mm thickness. The shielding thickness must be constant within each distinct irradiation to ensure sample comparability, but can be varied between irradiations according to the tracers used. For simultaneous activation analysis of both  $^{90}\text{Zr}$  and  $^{96}\text{Zr}$  at the 20 MeV proton beam at the MLL, 0.7 mm were found to be optimal owing to a slight

background suppression relative to 0.2 mm and 0.5 mm. Depending on the shielding thickness, the mean incident proton energy on the sample surface varies in the range of 12.8 – 17.6 MeV, as modelled with the SRIM2003 software (Ziegler, Biersack et al. 2003). For each irradiation and sample type, i.e. plasma and urine, up to three standard samples were prepared following the above approach, with the addition of a known amount of tracer solution in step (a).

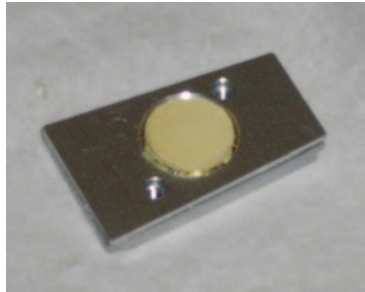


**Figure 3.2:** PNA plasma sample tablet on a partially assembled aluminium casing.

### 3.3.2 PNA instrumental setup and experimental conditions

In 2004, Augusto Giussani proposed to transfer the instrumental setup used in (Veronese, Giussani et al. 2003) from its former location at the Paul Scherrer Institute (PSI) in Villigen, Switzerland to a proton beam source in Garching, Germany. Proton irradiations could not be continued at the PSI, since the facility's cyclotron was modified for other purposes. Prof. Dr. R. Krücken (TUM) and the staff of the Maier-Leibnitz-Laboratory (MLL) in Garching, Germany, made it possible to establish the instrumental setup at the tandem accelerator of the laboratory as a proton beam source.

A photograph of the instrumental setup is shown in Figure 3.3. The end of the evacuated beam line is visible at the right margin; the setup is connected to it by a rotary flange. From right to left, in beam direction, the setup consists of the following structures:

- A cubic chamber with slit apertures built of iron plates for beam control (close-up view in Figure 3.4); these plates serve as a control of beam width and position since the absorbed beam protons give rise to a current which can be measured in the control room.
- A 25  $\mu\text{m}$  titanium foil, sealing the beam line; the foil is cooled by pressurised air, whose flow is controlled by the valve visible in Figures 3.3 (top) and 3.5 (upper left).
- The casing of the rotary disc holding the samples; in the frontal view of the open casing in Figure 3.5, the small blue spot on the right side of the disc marks the irradiated area. For control of the beam current, a faraday cup can be moved in and out of the beam by a pneumatic cylinder (Figure 3.5 on the right). The front plate of the disc casing also features a system for automated sample removal. Figure 3.6 shows two mounted samples, fixed by clips which can be pushed down by the removal system, releasing the sample.
- The connection of the external cooling system for the rotary disc; the coolant is transferred along the axis to channels inside the disc.
- A transmission gear and a step motor for rotating the disc during irradiation.

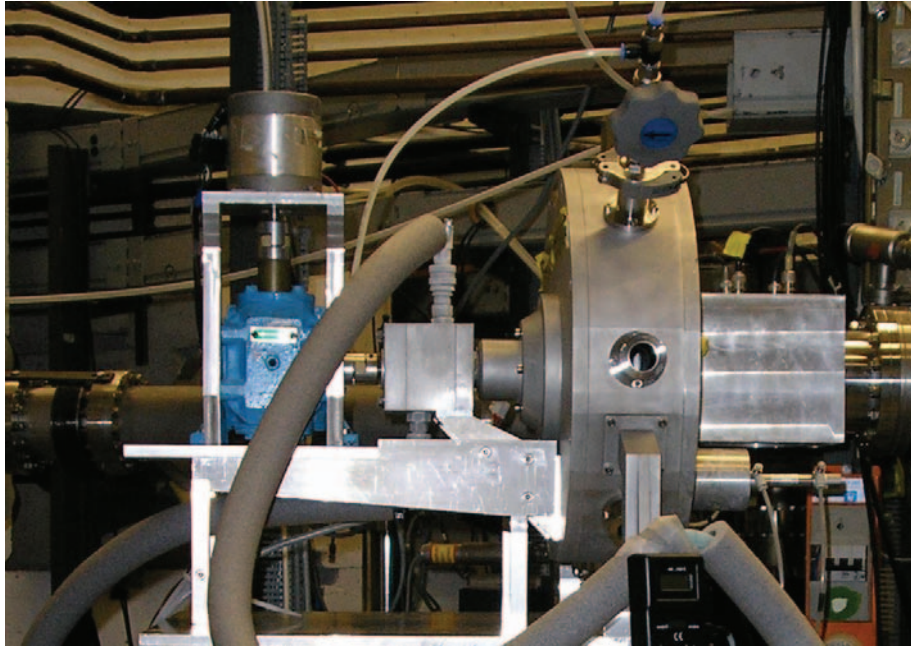


**Figure 3.3 (left):**  
Main parts of the  
PNA instrumental  
setup.

**Figure 3.4 (right):**  
Beam shape control  
Each of the four iron aperture plates  
is connected to a galvanometer in the  
control room by a coaxial cable.

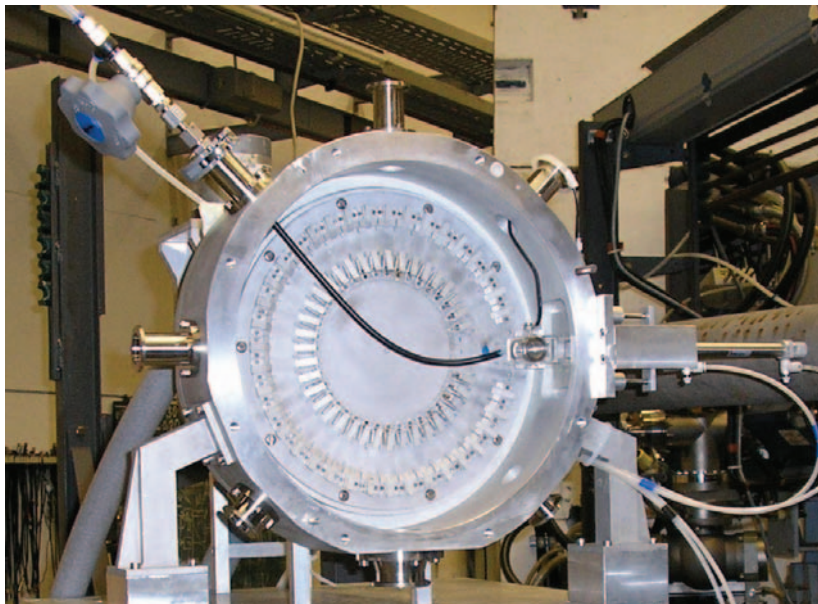


**Figure 3.5(left):**  
Front view of the rotary disc  
in the opened PNA setup.  
The valve in the upper left  
corner controls the inlet of  
pressurised air through the  
black tube, in order to cool  
the titanium foil sealing the  
beam line during irradiation.



**Figure 3.6 (right):** Two encapsulated samples,  
mounted onto the rotary disc of the PNA setup.

The base plate of the setup is supported by vertically adjustable trestles, which are placed on a trolley together with the cooling system. Potentially activated cooling fluid leaking from the system, or water condensed on the cold setup, are retained on the trough-shaped upper plane of the trolley. The complete system is mobile and can be easily removed from the beam line between irradiations.

By cable connections to the accelerator control room, the step motor, disc position, pneumatic cylinders, aperture plate and faraday currents, as well as a CCD camera signal can be controlled or monitored remotely.

A typical irradiation is carried out according to the following schedule:

- (a) The setup is connected to the beam line and the end of the beam line is pumped out, aiming at a pressure below  $10^{-5}$  hPa.
- (b) The samples are mounted on the rotary disc.
- (c) The cooling system is started a few hours prior to the start of the irradiation.
- (d) The MLL operators configure the ion source and set the beam shape, which is eventually controlled by a quartz crystal at the location of the samples.
- (e) When the correct shape is obtained, the crystal is removed and the disc casing is closed. Subsequently, the disc rotation is started and the irradiation is begun.
- (f) During irradiation, the beam shape and position can be controlled by the currents from the aperture plates. The rotation of the disc axis and the coolant temperature at the outlet of the setup are monitored from the control room via a CCD camera. In regular intervals, the beam current prior to the setup and the coolant temperature are recorded.
- (g) Irradiation is discontinued overnight, since no operator is present between 12:00 a.m. and 8:00 a.m.
- (h) 8 h after end of the irradiation, the setup is opened, all samples are removed and placed in a transport box, and the setup is disconnected from the beam line and moved to a storage area to avoid frequent public passage of the activated setup.
- (i) The samples are transported to the GSF by the GSF technical security.
- (j) The sample casings are removed in a fume hood; samples are placed in flat and fluid-tight sample carriers for gamma spectrometry.
- (k) The samples are consecutively measured by gamma spectrometry.

The gamma spectrometric measurements of all samples were performed by A. Geisler, U. Gerstmann, and O. Meisenberg on cylindrical HPGe detectors at the radioanalytical laboratory (RADLAB) of the GSF.

Typical experimental conditions for irradiations at the MLL are summarised in Table 3.3.

### 3.3.3 PNA tracer concentration calculation

Incident protons of energies of  $\sim 10 - 30$  MeV induce primarily (p,xn) reactions in the target. The type of reaction can be selected by a suitable selection of the mean proton energy because the reaction cross sections  $\sigma(E)$  peak at different energies, i.e. the product yield is energy dependent. An overview of possible reactions of zirconium isotopes is given in Table 3.4. The table is sorted by the peak energy of the reaction cross sections.

**Table 3.3:** Characteristic data of proton irradiations at the MLL.

Experimental condition	Typical value (range)
Irradiation time	36 – 48 h within 3 d
Proton energy (MeV)	20
Beam current ( $\mu\text{A}$ )	1.7 (0.8 – 3.2)
Incident proton energy on sample surface* (MeV)	14.5 (12.8 – 15.8)
Mean proton energy loss in 1 mm dry plasma* (MeV)	$\sim 3$
Coolant reservoir temperature	- 15 °C
Disc temperature during irradiation	- 4 °C to + 10 °C
Gamma dose rate at the setup after irradiation <sup>†</sup> ...	
... at the rear side of the disc casing <sup>†</sup>	$\sim 1 \text{ mSv}\cdot\text{h}^{-1}$ , directly at the surface
... in front of the disc (open casing) <sup>†</sup>	$1 \text{ mSv}\cdot\text{h}^{-1}$ , 10 – 15 cm above the disc surface
Delay between end of irradiation and gamma spectrometric measurement (waiting time $t_w$ ):	
$^{90}\text{Zr}(\text{p,n})^{90}\text{Nb}$ ( $T_{1/2} = 14.6 \text{ h}$ )	41 h (10.6 h – 18 d)
$^{96}\text{Zr}(\text{p,2n})^{95}\text{Nb-g}$ ( $T_{1/2} = 35 \text{ d}$ )	47 d (32 d – 77 d)
Measurement time $t_m$	
$^{90}\text{Zr}(\text{p,n})^{90}\text{Nb}$ ( $T_{1/2} = 14.6 \text{ h}$ )	15 h (1.4 h – 3 d)
$^{96}\text{Zr}(\text{p,2n})^{95}\text{Nb-g}$ ( $T_{1/2} = 35 \text{ d}$ )	3 d (4.6 h – 7 d)

(\*) Proton energy losses in and outside of samples were modelled using the SRIM software (Ziegler, Biersack et al. 2003), based on 25  $\mu\text{m}$  titanium foil, 35 mm air, 700  $\mu\text{m}$  aluminium shielding, and 1 mm dry plasma. (†) These dose rates were measured at the time of sample removal, i.e. 8 h after end of irradiation.

**Table 3.4:** Reaction cross sections of zirconium isotopes irradiated with protons in the energy range 5 – 30 MeV, taken from the EXFOR database (NNDC 2004). Half-lives and gamma energies were obtained from the NuDat 2 database (National Nuclear Data Center 2007).

Reaction	Optimal energy (MeV)	Maximum of reaction cross section (barn)	Product half-life	Product $\gamma$ energies (keV)
$^{96}\text{Zr}(\text{p,n})^{96}\text{Nb}$	8	0.6	23.4 h	778, 569, 1091
$^{92}\text{Zr}(\text{p,n})^{92}\text{Nb-m}$	9	0.7	10.15 d	934
$^{90}\text{Zr}(\text{p,n})^{90}\text{Nb}$	10-15	0.9	14.6 h	1129, 2319, 141
$^{96}\text{Zr}(\text{p,2n})^{95}\text{Nb-g}$	13-17	0.8	35 d	766
$^{96}\text{Zr}(\text{p,2n})^{95}\text{Nb-m}$	13-17	0.3	87 h	236 ( $\rightarrow\text{g}$ ); 204
$^{91}\text{Zr}(\text{p,2n})^{90}\text{Nb}$	19-24	0.9	14.6 h	1129, 2319, 141
$^{90}\text{Zr}(\text{p,x})^{89}\text{Zr}$	20-30	1.2	78.4 h	1713
$^{90}\text{Zr}(\text{p,2n})^{89}\text{Nb-m}$	22-25	0.2	66 m	588, 507
$^{96}\text{Zr}(\text{p,n+p})^{95}\text{Zr}$	24-30	0.2	64.0 d	757, 724
$^{91}\text{Zr}(\text{p,x})^{89}\text{Zr}$	$\leq 30$	$\leq 0.6$	78.4 h	1713
$^{92}\text{Zr}(\text{p,3n})^{90}\text{Nb}$	$\leq 30$	$\leq 0.6$	14.6 h	1129, 2319, 141

Generally, the proton energy is not varied during an irradiation, thus the selection of proton energy determines the isotopes which can be detected in the sample, taking into account the mean energy loss of beam particles in solid samples. As can be seen from Table 3.4, only 2 – 3 isotopes can effectively be determined by PNA at a fixed energy. The optimal combination concerning detection limits after simultaneous activation was attributed to the reactions  $^{90}\text{Zr} (p,n) ^{90}\text{Nb}$  and  $^{96}\text{Zr} (p,2n) ^{95}\text{Nb}$ -g in (Veronese, Giussani et al. 2003).

The product nuclide activity  $A_{x,k',0}$  generated from the irradiation of isotope  $k$  of an element  $x$  can be described by Equation 3.10 (Erdtmann 1992)

$$A_{x,k',0} = \frac{m_x a_{x,k} N_A}{M_x} (1 - e^{-\lambda_{k'} t_i}) \int_{E=0}^{\infty} \sigma_{k,k'}(E) \phi(E) dE \quad (3.10)$$

with the following terms:

- $m_x$  mass of element  $x$  in the irradiated sample
- $a_{x,k}$  abundance of isotope  $k$  in element  $x$
- $N_A$  Avogadro's number ( $6.022 \cdot 10^{23} \text{ mol}^{-1}$ )
- $M_x$  atomic weight of element  $x$
- $\lambda_{k'}$  decay constant of the radionuclide  $k'$  produced from the target nuclide  $k$
- $t_i$  irradiation time
- $\sigma(E)$  reaction cross section for the production of  $k'$  from  $k$
- $\phi(E)$  proton flux

The fraction term on the right side of Equation 3.10 describes the number of target isotopes  $k$  in the sample. The production probability of nuclide  $k'$  per atom of  $k$  is given by the integral term. Finally, the term in brackets describes the dynamic equilibrium of production and loss by transformation of the radionuclide  $k'$ . This term is important to optimise the irradiation time; an increase in irradiation time far beyond the mean lifetime  $\lambda^{-1}$  of the radionuclide of interest  $k'$  causes a relative increase of the background from long-lived radionuclides in comparison to the signal of  $k'$ .

The count number  $N_{k'}$  measured by gamma spectrometry is the produced activity  $A$  of the radionuclide  $k'$ , corrected by the waiting time between irradiation and measurement  $t_w$ , the measurement time  $t_m$ , the detector efficiency  $\eta$ , and the yield  $Y(E_\gamma)$  of the measured gamma energy  $E_\gamma$  per transformation (Erdtmann 1992):

$$N_{k'} = A_{x,k',0} \cdot \frac{1 - e^{-\lambda_{k'} t_m}}{\lambda_{k'}} \cdot e^{-\lambda_{k'} t_w} \cdot \eta \cdot Y(E_\gamma) \quad (3.11)$$

If all parameters of Equations 3.10 and 3.11 are known, the mass of an element,  $m_x$ , or the isotope mass  $m_x \cdot a_{x,k}$  can be directly calculated. The detector efficiency  $\eta$  includes the energy-dependent probability of detection per volume of detector material and the solid angle covered by the detector.

The direct calculation of elemental or isotopic masses can often be complicated, e.g. by unknown values or large uncertainties of  $\eta$ ,  $\sigma(E)$  or  $\phi(E)$ , or by interruptions of the irradiation which would have to be corrected for. The use of a known amount of internal standard in all samples, as well as an (external) standard sample with a known amount of the isotopes of interest, can overcome these problems.

If all samples, including the standard sample, are irradiated under the same conditions and measured on the same detector, the values of  $t_i$ ,  $\sigma(E)$ ,  $\phi(E)$ , and  $\eta$  are identical for all samples. In this case, the isotope mass  $m_{k,s} = m_{x,s} \cdot a_{x,k}$  in a sample can be derived from the isotope mass

$m_{k,0}$  in the standard sample, the respective peak areas in the gamma spectra, and the respective waiting and measurement times:

$$m_{k,s} = m_{k,0} \cdot \frac{N_{k',s}}{N_{k',0}} \cdot \frac{e^{-\lambda_k \cdot t_{w,0}} (1 - e^{-\lambda_k \cdot t_{m,0}})}{e^{-\lambda_k \cdot t_{w,s}} (1 - e^{-\lambda_k \cdot t_{m,s}})} \quad (3.12)$$

If several gamma spectrometers must be used due to a large number of samples, their relative efficiency can either be calibrated by the measurement of the standard sample on each detector and by relating their efficiencies  $\eta$  in analogy to Equation 3.12, or by using Equation 3.12 for the measurements of each detector separately.

An internal standard, added in identical amounts to all samples, can be used to scale the peak areas  $N_{k',s}$  and  $N_{k',0}$  to correct for possible deviations between samples, e.g. partial sample irradiation, or variations in sample placement on the detectors (given a similar detector efficiency for the gamma energies emitted by  $k'$  and the activation product of the internal standard). Partial sample irradiation can occur if the beam is smaller than the samples, and the samples have different areas facing the beam.

During the study,  $^{51}\text{V}$  was used as internal standard, resulting in the activation reaction  $^{51}\text{V}(\text{p},\text{n})^{51}\text{Cr}$ . The gamma emission at 320 keV was used to quantify  $^{51}\text{Cr}$  in the samples.  $^{51}\text{Cr}$  has a radioactive half-life of 27.7 d (National Nuclear Data Center 2007).

The concentration calculations of the measured samples and consequentially the raw data of the PNA results in section 6.2, although discussed, repeated and sometimes corrected by the author, have been performed originally by Dr. Augusto Giussani, who shall hereby be given the full credit for the fundamental evaluation of PNA measurement data. He also evaluated the peak areas in the gamma spectra with the software ALPI (Bianco 1989).

The further analysis of PNA method characteristics (e.g. detection limit and correlation with TIMS data) was done by the author.

## 4 Errors and uncertainty

To give a quantitative, reproducible indication of the quality for the measurement results included in this work, measurement uncertainties were calculated based on the recommendations in the “Guide to the expression of uncertainties in measurement” (GUM) (ISO, BIPM et al. 1995).

According to the concept of this guide, the uncertainty of a measurement result is attributed to random variations, due to a lack of knowledge of the measurand value and a lack of exact definition of influencing quantities during measurement. Measurement errors and known systematic deviations of a measurand from its true value are not included and should be corrected.

A stated uncertainty is given as a range in which measurement results are found with a fixed level of confidence around the estimated value of the measurand. With this condition, various probability distributions are allowed for quantities, although a normal distribution is usually assumed. In the current study, the level of confidence is 68 %, corresponding to a coverage factor of 1, unless otherwise stated.

If uncertainties are evaluated by statistical means from repeated observations of single quantities, they are termed “type A standard uncertainties”. Uncertainties  $u(y)$  of a quantity  $y$  can be expressed as standard deviations of the mean  $s_M(y)$  of repeated observations  $q_k$ , if the results are symmetrically distributed:

$$u(y) = s_M(q) = \sqrt{\frac{\sum_{k=1}^n (q_k - q_M)^2}{n(n-1)}} \quad (4.1)$$

Here,  $q_M$  represents the mean of a number  $n$  of observations.

If uncertainties cannot be evaluated from repeated observations by statistical means, they have to be estimated from other sources of information, e.g. known upper and lower bounds, previous measurements, or data given in specifications or certificates. Such uncertainties are termed “type B standard uncertainties” and are treated in the same way as type A standard uncertainties.

For measurement results obtained from a functional relation  $f$  of different influencing quantities  $x_i$ , “combined standard uncertainties”  $u_c(y)$  are stated. They are calculated from the individual quantities’ standard uncertainties based on a first-order Taylor series approximation:

$$u_c(y) = \sqrt{\sum_{i=1}^N \left( \frac{\partial f}{\partial x_i} \right)^2 u^2(x_i) + 2 \sum_{i=1}^{N-1} \sum_{j=i+1}^N \frac{\partial f}{\partial x_i} \frac{\partial f}{\partial x_j} u(x_i) u(x_j) r(x_i, x_j)} \quad (4.2)$$

The second term with the correlation coefficients  $r(x_i, x_j)$  can be neglected if is comparatively small, i.e. if all influencing quantities are uncorrelated, or if the combined uncertainty is dominated by large, uncorrelated components. It can, however, be important for simultaneous measurements of multiple quantities with the same instrument, e.g. different isotope ratios of

one TIMS sample. Another relevant case is a repeated procedure with the same instrument, as is e.g. volume determination by a repeated pipetting process with a fixed volume.

Depending on the probability distribution of a measurand, different estimates of its expected value can be given in a type A evaluation. Commonly, a normal or at least symmetrical distribution is assumed for a measurand, and the estimate of the expectation value is stated as the arithmetic mean  $\mu_a$  of the measurement results. In case only a small number of observations is available, the weighted arithmetic mean  $\mu_w$  is calculated in the current study, in order to avoid a biased value of  $\mu_a$  due to single uncertain observations. The weighted arithmetic mean is calculated as

$$\mu_w = \frac{\sum_{k=1}^n x_k w_k}{\sum_{k=1}^n w_k} \quad (4.3)$$

with the weight  $w_k$  being the inverse square of the uncertainty attributed to the value  $x_k$ , i.e. its inverse variance. The uncertainty of  $\mu_k$  was calculated in one of three ways, with the first option as the standard evaluation method for this type of uncertainty in the current study:

- If a small number of independent values were available as input to  $\mu_w$ , the variance  $v_w$  of  $\mu_w$  was calculated by weighting the variances of the contributing values, under the assumption that all contributing values were elements of the same population:

$$v_w = \sigma_w^2 = \frac{\sum_{k=1}^n \sigma_k^2 w_k^2}{\left(\sum_{k=1}^n w_k\right)^2} = \left(\sum_{k=1}^n \frac{1}{\sigma_k^2}\right)^{-2} \quad (4.4)$$

This uncertainty calculation was e.g. used for the determination of the uncertainties of average concentrations from measurements of activated PNA samples as related to different standard samples, or determined by different peaks in the  $\gamma$  energy spectra. In these cases,  $n$  was typically 2.

- The uncertainties for the model parameters in Table 6.6 were in contrast based on the standard deviation of the mean, according to Equation 4.1. The uncertainties of the 6 parameters common to all investigations ( $n = 9$ ) were as low as 1.1 – 6.4 % of the parameter value range if calculated according to Equation 4.4, but 10 – 13 % if calculated according to Equation 4.1. The respective expected values of the standard deviation of the mean of 9 samples would be  $\sim 10$  % of the range for a rectangular distribution, and  $\sim 6.4$  % for a normal distribution cut off at 99 % coverage, according to the GUM. Thus, in order to avoid an underestimation of uncertainty, the standard deviation of the mean was used as parameter uncertainty.
- If two values of  $x_k$  were the result of *two different evaluations of the same measurement*, the uncertainty was calculated as the arithmetic mean of the uncertainties  $u_k$ , as an estimate of the uncertainty of a *single measurement*. This option was used solely for the calculation of tracer concentrations from IDMS measurements, as indicated in section 3.2.3, to avoid artificially lowering the uncertainty.

For lognormally distributed results, the geometric mean  $\mu_g$  is a more meaningful estimate of the expected value. If, finally, none of the above-mentioned distributions is appropriate for a measured data set, the median  $\mu_m$  is given, since it is less susceptible to bias caused by outliers.

The following subsections comprise a list of the standard uncertainties of various quantities contributing to tracer measurements. Combined uncertainty values of tracer measurements in samples are discussed in the results section.

With one exception, only ‘measurement’ uncertainties are covered in the following three subsections, and are subsequently used as input for the modelling procedure. The term ‘measurement’ in this context relates to quantities that are relevant for the assessment of measurement method performance. Additional uncertainties are quite probably introduced into the study mainly by actions of test persons, e.g. drinking speed and nutritional preferences. Another source of uncertainty may be biological variability, which can result in substantial deviations of a smooth trend in tracer concentration over time (Lindsey, Jones et al. 2001). The combined uncertainty from the latter sources and the former ‘measurement’ uncertainty is termed ‘experimental’ uncertainty within this work.

The distinction between ‘measurement’ and ‘experimental’ uncertainty is intentional, since the capabilities of the TIMS and PNA methods for tracer measurements shall be compared without masking them by large common uncertainty components. For sample analysis and modelling, the modelling software SAAM II provides a way to judge the actual combined experimental uncertainty by weighting the goodness of fit of the different sample and tracer types. The uncertainty of the fit parameters given by SAAM II then reflects the combined ‘experimental’ uncertainty.

#### **4.1 Tracers and samples**

Uncertain quantities related to the orally and intravenously administered tracers included isotope ratios, tracer concentrations and the amounts of tracer solution applied during the investigations.

The isotope ratios of all tracers were measured repeatedly by TIMS and compared to the corresponding manufacturers’ certificates, showing only small differences. TIMS measured ratios were used for the TIMS evaluation, since a possible small systematic bias introduced by the instrument would then be present both in normal samples and tracer reference measurements, thus minimizing its effect. Type A relative standard uncertainties on tracer isotope ratios of  $9 \cdot 10^{-4} - 1$  were calculated as 0.07 – 2.6 %. These relative standard uncertainties were approximately lognormally distributed with a geometric mean of 0.39 %. The certified isotope ratio values were used for the PNA evaluation with an estimated relative uncertainty of 1 %.

Tracer concentration in stock solutions was measured by the GSF Central Inorganic Analysis Service with inductively coupled plasma optical emission spectrometry (ICP-OES). Type B relative standard uncertainties from one to three measurements per tracer solution were estimated to be ~ 1.5 %.

The amount of tracer solution applied to test persons is dependent on the type of tracer application and the applied volume. Ampoules and drinking cups were weighed to measure the amount of solution injected or ingested. For intravenous injection, the measurement standard uncertainty of the tracer solution amount applied was determined by the weighing process and estimated to be ~ 0.1 % (relative uncertainty), and larger than 5 mg (absolute uncertainty). The relative measurement standard uncertainty for oral application was larger, since multiple pipetting processes with up to three pipettes were involved. Its estimates range

from 0.45 % to 0.65 %, with a minimal absolute uncertainty of 0.08 ml. Both standard uncertainties are qualified as type B, since they are based on manufacturers' data.

Input quantities relevant to sample drawing and preparation were blood plasma and urine density, collected urine volume or mass, and the amounts of plasma or urine used for measurement.

For healthy persons, plasma density was estimated as  $1.027 \pm 0.006 \text{ g}\cdot\text{ml}^{-1}$ , urine density as  $1.020 \pm 0.015 \text{ g}\cdot\text{ml}^{-1}$  (1994; ICRP 2002).

The collected amount of urine was measured initially with a standard uncertainty of 25 ml. In later studies, it was weighed, with a smaller standard uncertainty of 0.25 g. This corresponds to relative standard uncertainties in the range of 0.01 % to 8 %.

An additional uncertain component concerning urine collection is associated with non-uniform urine production and the limited number of voids per day or sampling interval. In the current study, each tracer concentration measurement in urine is attributed to a sampling period of fixed duration, usually 12 h or 24 h. Usually, the start and end of each sampling period do not coincide with a urinary void; in contrast, a test person may delay a void over the end of a sampling period and thus shift a part of the produced urine amount from one sampling period to the next. A relative standard uncertainty of 17 % for this effect is adopted from the ICRP estimate of the number of voids per day of 6 (ICRP 1995). This uncertainty component is an exception to the 'measurement' uncertainty concept. It is necessary to avoid bias between plasma and urinary data during the fitting process in modelling in some cases where only few urinary data are available in a study, but is not used in the method uncertainty comparison in order not to mask the smaller uncertainty components for the different methods.

During sample preparation, volumes of 1 – 18 ml urine and 0.5 – 0.8 ml plasma were determined by pipetting from the collected samples. The attributed relative standard uncertainties were 0.6 % and 1.0 % for urine and plasma volume, respectively, as long as completely fluid samples were processed. The minimal absolute uncertainty was 5  $\mu\text{l}$ .

## **4.2 TIMS**

As described in section 3.2.3, tracer concentrations from TIMS/IDMS measurements were calculated from the reference tracer concentration, the isotope ratios of all zirconium types in the specific sample, the measured isotope ratios, and the relative atomic masses of the isotopes. The combined standard uncertainty was calculated using Equation 4.2. The correlation term was important in this case, since correlation coefficients near unity were observed for several samples and isotope ratios. The calculations were done using the Mathematica 5 program (Wolfram Research Inc., Champaign, IL, USA).

The combined uncertainty of the reference tracer concentration was assessed with a series of 15 isotope dilution TIMS measurements. No difference was observed between two sets of mixing volumes (2  $\mu\text{l}$  and 500  $\mu\text{l}$ ) and mixture equilibration times ( $\sim 1 \text{ min}$  and  $> 1 \text{ h}$ ). Further preliminary tests with plasma and urine samples showed that the mixing process was equally robust for reference tracer added to biological samples. The type A relative standard uncertainty of reference tracer concentration, including the mixture process, was 3.9 %. The large uncertainty of the reference tracer concentration was likely a consequence of the processed small volumes of diluted reference tracer solution (T-94-R; 1  $\mu\text{l}$  minimum), which are prone to large losses during pipetting. For most samples, this uncertainty was the dominant component of the combined measurement uncertainty of TIMS tracer concentration measurements, as can be seen in Table 4.1.

Similar to the isotope ratios of tracers stated above, zirconium isotope ratios in investigation samples have type A relative standard uncertainties in the range of 0.03 % to 4.2 %, with a median value of 0.11 %. The minimal absolute standard uncertainty was  $1.3 \cdot 10^{-5}$ .

Relative atomic masses were taken from a database provided by NIST (Coursey, Schwab et al. 2005). The relative uncertainties given by this source were smaller than  $10^{-5}$  %, and thus were neglected during the combined uncertainty calculation.

**Table 4.1:** Overview on relative standard uncertainties of quantities relevant for TIMS/IDMS measurement.

Source	Estimated or expected value (%)	Range (%)
Tracer isotope ratios	0.39 (median)	0.07 – 2.6
Tracer concentration	1.5	
Tracer solution volume i.v.	0.1	
Tracer solution volume p.o.	0.64 (median)	0.45 – 0.65
Plasma density	0.6	
Urine density	1.5	
Collected urine amount	-	0.01 – 8
Urine voids per day*	17	
Plasma sample volume	1.0	
Urine sample volume	0.6	
Reference tracer concentration	3.9	
Sample isotope ratios	0.11 (median)	0.03 – 4.2
Relative atomic masses	$< 10^{-5}$	

(\*) Not included in the TIMS measurement uncertainty, but a component of the experimental uncertainty.

### 4.3 PNA

The most critical procedure during PNA measurement was the evaluation of gamma spectra. In many samples, the relevant peaks were small, interfered with other peaks, and were obscured by high background count rates. Therefore the uncertainty of peak statistics and peak definition was the dominant part of the combined uncertainty of tracer concentrations in PNA. For this reason, some comparably smaller relative uncertainties could be neglected in the evaluation of the combined standard uncertainty.

The standard counting uncertainties of the relevant peaks were determined by the peak evaluation software and varied in a wide range. For a fixed proton energy spectrum, the most important quantities influencing these counting uncertainties are irradiation time and current, waiting time after irradiation, and thus evolution of the signal-to-background ratio, counting time, and relative detector efficiency. The ranges of relative standard uncertainties for the different peaks are shown in Table 4.2, separated into external standard samples and experimental samples.

For plasma samples, with their sometimes inevitable gel-like consistency, the relative pipetting uncertainty was estimated as 5 %.

**Table 4.2:** Overview on relative standard uncertainties of quantities relevant for PNA measurement.

Source	Estimated or expected value (%)	Range (%)
Tracer isotope ratios <sup>†</sup>	1	
Tracer concentration <sup>†</sup>	1.5	
Tracer solution volume i.v. <sup>†</sup>	0.1	
Tracer solution volume p.o. <sup>†</sup>	0.64 (median)	0.45 – 0.65
Plasma density <sup>†</sup>	0.6	
Urine density <sup>†</sup>	1.5	
Collected urine amount <sup>†</sup>	-	0.01 – 8
Urine voids per day*	17	
Urine sample volume <sup>†</sup>	0.6	
Plasma sample volume	5	
320 keV from <sup>51</sup> Cr (standard)	0.9 (median)	0.17 – 15
t <sub>w</sub> ~ 2 d		
320 keV from <sup>51</sup> Cr (standard)	0.7 (median)	0.16 – 3.6
t <sub>w</sub> ~ 1.5 mo		
141 keV from <sup>90</sup> Nb (standard)	4.5 (median)	0.26 – 27
141 keV from <sup>90</sup> Nb (sample)	10 (median)	3.0 – 52
1129 keV from <sup>90</sup> Nb (standard)	8.3 (median)	1.5 – 27
1129 keV from <sup>90</sup> Nb (sample)	30 (median)	14 – 92
766 keV from <sup>95</sup> Nb (standard)	3.3 (median)	2.6 – 12
766 keV from <sup>95</sup> Nb (sample)	15 (median)	4.9 – 39

(\*)Not included in the PNA measurement uncertainty, but a component of the experimental uncertainty. (†) Neglected in the PNA uncertainty evaluation.

## 5 Model development

A set of experimental data, although possibly comprehensive, generally consists of discrete measured values. A suitable model can allow for interpolation and extrapolation in a multi-dimensional parameter space, offering further insights or enabling predictions beyond the set of previously collected data.

The methods, tools, and assumptions which were used to evaluate measured data in this study are discussed in this section. Three major topics are addressed:

(a) Fractional absorption

As introduced in section 1.4, the fractional absorption  $f_A$ , i.e. the fraction of substance transferred from the alimentary tract into the systemic circulation, is an important parameter for internal dose estimates. Various techniques are available for the determination of this parameter (Roth and Werner 1985), two of which are dealt with in section 5.1.

(b) First-order kinetic compartment models

The ICRP uses this class of models to estimate the distribution and retention of most radionuclides in the human metabolism, as well as to calculate the number of radionuclide transformations giving rise to internal absorbed doses. Since the aim of this work is to support, improve or replace the current biokinetic model of zirconium (cf. section 1.4), this type of model was exclusively used in this study. A software method for simple numeric solution of this class of models is introduced in section 5.2. The treatment of measured values below method detection limit in modelling, and the concept of and tools to assess theoretical a priori identifiability of models is also presented.

(c) Calculation of ingestion dose coefficients

The ICRP provides a framework for calculating dose coefficients, which is adopted in this study, and briefly introduced in section 5.3. Care has been taken to calculate the dose coefficients in this study in accordance to ICRP standards in order to attain comparability of new, calculated dose coefficients with the current, published ICRP values (ICRP 1993).

### 5.1 Fractional absorption

Fractional absorption  $f_A$  can be derived from the transfer rates of a first-order kinetic compartment model (Equation 1.5), if a model is available. The quality of this approach relies both on the appropriateness of the model, as well as on the uncertainty of the relevant parameter values. A large amount of data may be needed for a well-defined and appropriate model.

However, information about fractional absorption can also be obtained from comparatively simple investigations with fewer assumptions concerning the metabolism under study (Werner, Roth et al. 2002).

One very basic technique is the measurement of the fraction of an orally (p.o.) administered substance which is directly excreted in faeces, i.e. passed through the alimentary tract without being absorbed. This method requires the complete collection of faeces within a few days after administration, with only one substance concentration measurement of the collected sample. It is however limited in its informative value due to endogenous excretion of the substance, which can yield a biased result, i.e. an artificially low fractional absorption value. In addition, this method is not suitable if  $f_A$  is of the order of the relative measurement

uncertainty (e.g. 1 %), since the measured excreted amount of substance will not be significantly different from the ingested amount in this case, hence the measured value of  $f_A$  is zero. Hence, this method is presumably not applicable for zirconium.

For elements with low fractional absorption values it is preferable to measure the amount of absorbed substance rather than the remaining excreted amount. Various techniques have been reviewed concerning their effectiveness for radioisotopes of calcium (Roth and Werner 1985), but not all of them are applicable for stable zirconium tracers:

- Absorbed radioactive isotopes may be quantified by whole-body counting, but the exposure to radioactive substances without special necessity is generally not accepted. In addition, inhomogeneous tracer distribution in the body, excretion processes prior to measurement (i.e. loss of tracer), and retention of non-absorbed tracer in the alimentary tract may be sources of errors.
- The tracer concentration in plasma, which can easily be obtained from a single plasma sample, can allow for the quantification of  $f_A$ . This technique requires a scaling factor which relates the plasma concentration at the time of measurement to the whole-body concentration after completed absorption. It is therefore only applicable if further information on the metabolism of the element is available, e.g. plasma content of the body, and clearance rate of the tracer from plasma.
- The double tracer technique circumvents the latter problem by using a second, intravenously (i.v.) administered tracer. This tracer can serve as a reference for clearance processes from the plasma and thus provide the scaling factor relating oral tracer concentration in plasma with whole-body absorbed amount. The central assumption of this technique is that both tracers are metabolised identically after simultaneous administration. This assumption can be wrong if one (or both) of the tracers are strongly bound to (different) chelating agents or molecules, and the tracer distribution depends more on the binding agent than on the element itself. In principle, the double tracer technique requires only one plasma or urine sample, probed after the absorption process from the alimentary tract is completed. This method is discussed below in section 5.1.1.
- The convolution integral technique is a modified extension of the double tracer technique, and discussed in section 5.1.2. In brief, it uses the time course of the concentrations of one orally and one intravenously administered tracer to derive the time-dependent absorption rate. The fractional absorption is then calculated from the time integral of the absorption rate. This technique relies on the same basic assumption as the double tracer technique. It requires several plasma samples, but also yields additional kinetic information.

### 5.1.1 Double tracer technique

The double tracer technique was introduced by de Grazia et al. (1965) for the determination of the intestinal absorption of calcium. De Grazia et al. originally used radioisotopes of calcium as tracers, but the method is applicable to stable tracers, too, if three or more stable isotopes are available for an element. In special cases, even two stable isotopes may be sufficient, if the isotope ratio is suitable for the preparation of isotopically-enriched tracers, and if the natural element content in plasma or urine can be corrected for.

The generalised experimental procedure of the double tracer method consists of:

- Simultaneous administration of both tracers, one ingested orally and one injected intravenously, usually after overnight fasting to establish a metabolic reference condition;

- a waiting period which is sufficient to complete the absorption process (e.g. 6 – 24 h, depending on the form in which the oral tracer was administered, either as solution or with a meal);
- probing of one urine or plasma sample and measurement of the tracer concentrations.

The fractional absorption  $f_A$  can then be calculated from the tracer concentrations  $c_i$  and the administered masses of tracer  $m_i$ :

$$f_A = \frac{c_{po} \cdot m_{iv}}{c_{iv} \cdot m_{po}} \quad (5.1)$$

With the experimental scheme of double tracer investigations as presented in section 2.3, a multiple determination of the  $f_A$  value is possible. It should yield similar results if the assumption of identical behaviour of both tracers is valid.

In the current study, only plasma samples within  $\sim 7 - 48$  h after tracer administration were evaluated due to constraints imposed by the measurement detection limits. The results are presented in Table 6.5 in section 6.3.1.

### 5.1.2 Convolution integral technique

While the double tracer technique evaluates concentration data in plasma or urine after completed absorption, the convolution integral technique focuses on the kinetics of the absorption process in plasma.

For this purpose, the tracer concentrations in plasma are described by time-dependent concentration functions  $c_{po}(t)$  and  $c_{iv}(t)$ , which are normalised on the respective administered amount of tracer. Since no specific model is presumed, these functions can simply be derived from the measured concentrations, e.g. by stepwise linear interpolation, or by fitting a suitable curve to the data. The latter approach was used in this work and is further explained in section 6.3.1.

In general,  $c_{iv}(t)$  is observed to decline continuously after its bolus injection into the circulation. In contrast,  $c_{po}(t)$  rises from an initial zero value to a peak value and declines afterwards.  $c_{po}(t)$  can be interpreted as a linear superposition of infinitesimal short bolus entries  $a(\tau)d\tau$  of oral tracer from the gut into the blood plasma, which are afterwards cleared from the plasma in the same way as the intravenous tracer. This relation can be formulated as convolution integral

$$c_{po}(t) = \int_0^t a(\tau) c_{iv}(t - \tau) d\tau, \quad (5.2)$$

which is a special case of a Volterra integral equation. It may be solved by Laplace transformation, yielding a simple equation for the transformed functions:

$$A(s) = \frac{C_{po}(s)}{C_{iv}(s)} \quad (5.3)$$

The reverse transformation leads to a function  $a(t)$  which describes the absorption rate; its time integral is the (total) fractional absorption  $f_A$ .

The reverse transformation can however be complicated. Instead of an analytical solution, it is also possible to apply a numerical approach to the reverse Laplace transformation. In the current work, a short Fortran program (volterra.f, cf. annex B) written by Paul Roth, GSF, was used for the calculation of absorption rates and fractional absorption values for the investigations with stable isotopic tracers of zirconium. Previously, the same program had

been applied to evaluate absorption rates in studies with calcium, iron and molybdenum (Roth, Giussani et al. 1998), as well as in studies with strontium (Li, Höllriegl et al. 2006).

## 5.2 First-order kinetic compartment models

First-order kinetic compartment models are a rather simplistic approach to describe the distribution of substances in metabolism, since common processes like diffusion or enzyme-catalysed biochemical reactions may not be modelled in this way. Nevertheless, this class of models is often successfully used to describe metabolic and endocrine systems, including the distribution of many trace elements. In the following, some important concepts of this approach are presented, based on a book by E. Carson, C. Cobelli, and L. Finkelstein (1983).

Each compartment can be interpreted as a store of the modelled substance, e.g. in a common chemical form, in a certain location within the body, or both. Its functional relation with other compartments can be described by a balance equation of mass, concentration, or amount of substance:

$$\frac{dc_i(t)}{dt} = \sum_l R_{l \rightarrow i} - \sum_j R_{i \rightarrow j} \quad (5.4)$$

$R_{l \rightarrow i}$  are general transfer rates of substance from compartment  $l$  to compartment  $i$  and can be associated with physical substance transfers or chemical reactions. The transfer rates are often dependent on the mean concentration in the respective source compartment. If this dependence can be formulated as  $R_{l \rightarrow i} = \lambda_{l \rightarrow i} \cdot c_l(t)$ , with positive, constant coefficients  $\lambda$ , the model is a linear, first-order kinetic compartment model, and Equation 5.4 can be written in the form of Equation 1.4:

$$\frac{dc_i(t)}{dt} = \sum_l \lambda_{l \rightarrow i} \cdot c_l(t) - \sum_j \lambda_{i \rightarrow j} \cdot c_i(t). \quad (5.5)$$

With a set of initial values or boundary conditions for  $c_i(t)$ , the resulting system of coupled differential equations may be solved analytically (Sanchez and Lopez-Fidalgo 2003), but is usually solved numerically (Birchall and James 1987). The solutions of  $c_i(t)$  are sums of exponential functions with constant coefficients.

One application of the ICRP biokinetic models is the estimation of internal dose after accidental intakes of radionuclides. In this case, the initial intake of a substance is usually modelled as a bolus at  $t = 0$ , i.e. the concentration in the intake compartment(s) is set to a positive initial value, while all other concentrations  $c_i(0)$  are set to zero.

A general modelling approach can be split up into the following basic steps:

- Compartmentalisation of the metabolic system, including transfer processes
- Description of this system by appropriate differential equations
- parameter estimation from experimental data

If the model structure is fixed and parameter values are available, the concentrations or amounts of substance in each compartment can be evaluated. If the model is physiologically valid, it may be used to extrapolate these quantities for time periods beyond the experimentally obtained data. This is the aim of biokinetic modelling in the ICRP framework, as the internal dose from the transformations of radionuclides should be estimated for exposed persons, from the time of exposure, up to an age of 70 y.

## 5.2.1 Theoretical a priori identifiability

A given set of experimental data may be described by various models, depending on the variance of the data. The comparative distinction between models is a matter of practical identifiability, i.e. the available data and its uncertainty allow the modeller to decide whether a model is in accordance with the data or not.

However, before starting the modelling process, it must be tested whether the experimental design is sufficient to theoretically make unique estimates of all parameters of the proposed model (Carson, Cobelli et al. 1983). For this test, the data obtainable from the experiment is assumed to be ideal, i.e. without errors and of negligible uncertainty. Three possible outcomes can be distinguished:

- At least one parameter has an infinite number of solutions. In this case, the model is not identifiable and must be modified to obtain deterministic results for all parameters. A simple example for a model which is not identifiable with a given experiment is presented in Figure 5.1.
- All parameters have a finite number of solutions, at least one of them more than one. The model is then locally theoretically a priori identifiable, but additional information is necessary to distinguish between multiple solutions. An example relevant to the zirconium biokinetic model is given in Figure 5.2.
- All parameters have only one solution. Such models are globally theoretically identifiable from the experimental design, and parameter estimation is possible without further constraints.

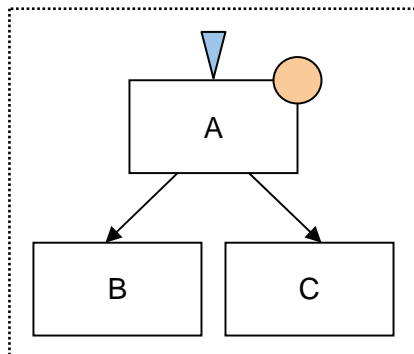


**Figure 5.1:** Example for non-identifiability of a first-order kinetic compartment model.

The triangle indicates tracer injection into compartment A, the circle indicates tracer concentration measurement. The (ideal) measurement in A yields the sum of  $\lambda_{A \rightarrow B}$  and  $\lambda_{A \rightarrow C}$ , but the ratio of these parameters is not defined by the measurement, thus infinite solutions for both parameters exist and the model is not identifiable.

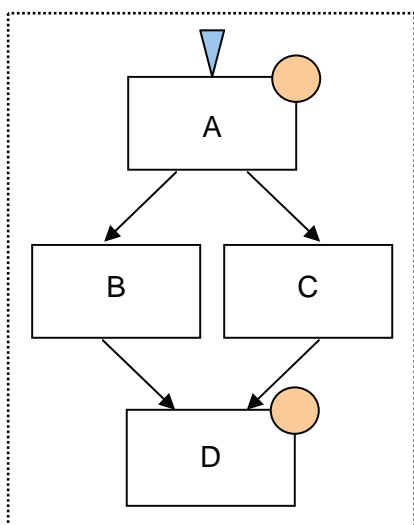


**Figure 5.2:** Example for a locally identifiable model.

The triangle indicates tracer injection into compartment A, the circles indicate tracer concentration measurements. The time course of tracer influx into compartment D allows for two unique solutions of the transfers from A; however due to the symmetry of B and C, two solutions are possible for each transfer parameter. This structure is similar to the current systemic model of zirconium, A being the transfer compartment, B and C mineral bone and ‘other tissues’, and D urinary bladder contents. In the ICRP model, unique identification is possible, since it is known that the turnover rate of bone is lower than that of ‘other tissues’, hence the B and C can be distinguished.

The analysis of theoretical a priori model identifiability can be very complex, depending on the model. For this reason, a specialised software, GLOBI2 (Audoly, D'Angio et al. 1997), was used to check theoretical identifiability of all model candidates. The underlying experimental scheme for the tests was always set according to the procedure described in section 2, i.e. tracer administration to the alimentary tract and transfer compartment, and tracer measurements in the transfer compartment and urine. The volume of the transfer compartment was assumed as unknown.

The results of the a priori identifiability tests are stated in the figure captions of the respective model graphs in section 6.3.2.

## 5.2.2 Model development process

Various compartmental model candidates were evaluated in the current study, inspired by certain observations of measured data, the current ICRP biokinetic model, and experiences during the modelling process itself. Therefore, detailed information on the development of models is given together with these observations in section 6.3.2, while the tools and concepts used for model evaluation are discussed in the current section.

The general approach to each modelling cycle contained the following steps:

- A new model structure was designed, or a previously evaluated model was altered, according to observations made from the measured data.
- The new structure was tested for theoretical identifiability. If necessary, the model structure was again altered in order to be identifiable with the fixed experimental scheme presented in section 2.
- If at least locally a priori identifiable, the model was built, solved and fitted to investigation data sets with the modelling software SAAM II described below.
- Parameter values were adopted from ICRP publications 67 and 100 (ICRP 1993; ICRP 2006) if applicable, or estimated from these default values to obtain similar time courses of tracer concentrations. Parameter limits were set to 0 (lower limit) or 10 times the starting values (upper limits). If a parameter reached its upper limit during fitting, the respective upper limit was increased one-time by a factor of 10.
- The subjective accordance between fitted model and data was examined in order to decide whether the issues leading to the model design were resolved. If the model led to an improvement, certain statistical parameters calculated by SAAM II were evaluated to quantitatively compare the goodness of fit.

The modelling software SAAM II (Saam Institute 1992-2002; Barrett, Bell et al. 1998) was used to describe and solve all compartmental models in the current work, as well as to fit models to data and thus evaluate the respective parameters.

This software allows constructing compartmental models by drawing the compartments and transfers; the associated differential equations are generated by the software, according to the model structure. For a given experimental setup (duration, tracer administration etc.), the model is then solved numerically.

Experimental data, including uncertainties, can be provided to SAAM II by pre-formatted text files. Multiple data sets, i.e. measured data of different tracers in different compartments, can be handled at once during a fit of the model.

The following description of SAAM II's features is taken from its tutorial and documentation. It shall illustrate the possibilities of the program, its mode of operation, and the options

selected for compartment modelling in this work, in order to enable a reproduction of the results presented in sections 6.3.2, 6.3.3, and 6.4.

Several options are available for fitting in SAAM II; however, the objective function  $R$ , which is minimised during a fit process, is always calculated as given in Equation 5.6. In this objective function, the squared deviation of each data point to its respective model estimate is weighted by its variance. By variation of the parameters, the fit process continues until convergence, i.e. until the relative change in the objective function falls below a previously specified value per iteration. As a default in the current work, this threshold value  $\delta$  was set to  $10^{-4}$ . An alternative criterion for convergence is if the change in each parameter  $p_k$  falls below a threshold value dependent on  $\delta$  and the permitted range of parameter values. As a default, this convergence criterion was set to  $p_k \cdot 10^{-3}$ .

$$R(\mathbf{p}) = \frac{1}{M} \left( \sum_{j=1}^J \sum_{i=1}^{N_j} \left( \log(V_{i,j}) + \frac{\left( y_{i,j} - s(\hat{\mathbf{p}}, t_{i,j}) \right)^2}{V_{i,j}} \right) + X \right) \quad (5.6)$$

The terms in this and the following equations are:

- $\mathbf{p}$  (estimate of the) vector of adjustable parameters
- $M$  total number of data points;  $M = N_1 + \dots + N_J + N_b$
- $N_j$  number of data points in data set  $j$
- $N_b$  number of Bayesian parameters
- $J$  number of data sets
- $y_{i,j}$  the  $i$ -th datum in the  $j$ -th data set
- $s(\mathbf{p}, t_{i,j})$  the model prediction corresponding to  $y_{i,j}$
- $V_{i,j}$  the variance of  $y_{i,j}$ , according to the specified variance model (cf. below)
- $v_j$  (estimated) variance parameter in the  $j$ -th data set
- $X$  abbreviation for further terms of the objective function related to Bayesian estimation

Bayesian estimation, i.e. the implementation of information concerning parameter values in a studied group similar to the subject(s), can be optionally used for parameter estimation. If it is used for one or more parameters of the model ( $N_b > 0$ ), the term  $X$  is introduced in the objective function. It accounts for the deviation of the respective parameters from their population estimates (mean values  $m_{p,k}$ ), weighted by the respective population standard deviations  $\sigma_{p,k}$ :

$$X = \sum_{k=1}^{N_b} \frac{(p_k - m_{p,k})^2}{\sigma_{p,k}^2} + \log(\sigma_{p,k}) \quad (5.7)$$

In the current work, Bayesian estimation was only used in the final step of parameter estimation of the model proposed in section 6.3.3.

SAAM II implements a generalised variance model for all data points without individual uncertainty values. The variance model is based either on compartment model estimates or data values.

Even if the input data file for SAAM II contains explicit uncertainties for each data point, the type of variance model must be specified. The data based option, described in Equation 5.8, was exclusively used in the current work:

$$V_{i,j}\left(y_{i,j}, \hat{v}_j\right) = \hat{v}_j \cdot (A + B \cdot y_{i,j}^C) \quad (5.8)$$

For a weighting factor  $v_j = 1$ , a combination of the weighting parameters  $(A, B, C) = (0, B, 2)$  is equal to a constant relative standard deviation of  $\sqrt{B}$ , whereas  $(A, B, C) = (A, 0, 0)$  defines a constant absolute standard deviation  $\sqrt{A}$  for all data points with unspecified variance. The latter option was used as a default, according to the uncertainties given as absolute uncertainties; however explicit individual uncertainty values do override the value of  $\sqrt{A}$ , making the value of  $A$  arbitrary.

The variance model also allows using the specified uncertainties without further weighting, i.e.  $v_j = 1$  ('absolute' variance model), or the estimating the weighting factor from model and data according to Equation 5.9 for each data set  $j$  ('relative' variance model):

$$\hat{v}_j = \frac{1}{N_j} \sum_{i=1}^{N_j} \frac{\left(y_{i,j} - s\left(\hat{\mathbf{p}}, t_{i,j}\right)\right)^2}{V_{i,j}(y_{i,j}, 1)} \quad (5.9)$$

Both options were used during the evaluation of various models (cf. section 6.3.2) in order to judge the effect of uncertainty estimates on fit results. The weighting factor  $v_j$  can be different for the four data sets, thus emphasising the influence of one or more sets over the others. Care must be taken in the interpretation of the resulting factors, since a data set with very few data points may yield a 'perfect' fit due to overfitting.

If the model structure is physiologically reasonable and simple enough to avoid overfitting, the value of  $v_j$  can be used to review the uncertainties. Values of  $v_j$  substantially different from 1 indicate that some sources of uncertainty beyond the previously quantified components from section 4 are influential.

## Treatment of data below detection limit

In the different data sets obtained from tracer measurements, a varying portion of values lies below detection limit (BDL). BDL values should not be included in modelling without critical consideration, since they cannot be clearly attributed to the existence of a tracer in an analysed sample. Various strategies have been proposed to deal with values below quantification limit (BQL) (Beal 2001), which is a similar problem as BDL values, in that its topic is unreliable, small-value data.

With the SAAM II software only simple solutions are possible, i.e. BDL or BQL data can be discarded or substituted by a specified value, which may not be an optimal solution (Lindsey, Jones et al. 2001).

Substitution by zero or complete omission can both introduce bias into parameter estimations for clearance kinetics. Actual concentrations in a first-order kinetic model are always greater than zero after tracer application, thus if BQL or BDL values are set to zero, clearance is overestimated by artificially forcing the fitted concentration curve towards zero. In contrast, if BQL or BDL values are completely omitted, the lowest concentrations available for fitting are above BQL or BDL respectively, which can also result in a false estimation of clearance. For a population kinetic analysis of a single-compartment model, replacing BQL values by values between zero and QL was shown to allow acceptable parameter estimation regardless of the different uncertainty options associated to these values (Hing, Woolfrey et al. 2001). Especially for absorption processes and declining quantities, a mixed treatment has been

proposed, in which BQL data are discarded except for the first BQL value after the peak of the absorbed substance concentration (Duval and Karlsson 2002; Beal 2005).

Based on this background, a substitution method is adapted for the zirconium data used for compartment modelling in the current study:

- If replaced, BDL values are set to DL/2 with associated uncertainties of DL/4, similar to a common treatment of BQL values in the aforementioned literature.
- BDL values of tracer concentrations in plasma directly following the last above-DL measurement were replaced and included in the analysis. All other plasma BDL data were discarded. The aim of this solution is to use the limited BDL information to draw fits towards the range between zero and DL, even if values are not detectable during the later phase of a study.
- BDL values in urine are only replaced if they are between two above-DL values, or if they directly succeed the last above-DL value in an investigation.

This conservative substitution approach should avoid a large bias on model parameters while still placing little weight on BDL observations.

## Model comparison

Apart from the subjective assessment of fit quality by visually comparing data and model graphs, three quantities generated by SAAM II were used to judge the relative fit quality of different model candidates.

The first of these quantities is the minimised value of the objective function  $R(\mathbf{p})$  as defined in Equation 5.6. For any unique data set with accordingly unique unweighted variances, a lower value means that the residuals, i.e. the differences between each data point and its respective model estimate, are smaller on average, thus the modelled curve is closer to the data. However, this value can be misleading; a large number of parameters may lead to a ‘perfect’ fit of a completely unsuitable model. As an extreme example, consider a data set consisting of  $n$  data points  $y_i(x_i) = 0$ . These data may either be described by a model function  $y(x) = 0$ , or by a polynomial of an order greater than or equal to  $n$ , if its roots coincide with the  $x_i$ .

Two other quantities were used to compare models; these were the Akaike information criterion (*AIC*) and the Bayesian information criterion (*BIC*). They are calculated by SAAM II as follows:

$$AIC = \frac{1}{2} (R(\mathbf{p}) + \log(2\pi)) + \frac{N_p}{M} \quad (5.10)$$

$$BIC = R(\mathbf{p}) + \log(2\pi) + \frac{N_p \log(M)}{2M} \quad (5.11)$$

In these expressions,  $M$  is the total number of data points as defined above, and  $N_p$  is the number of adjustable parameters  $p$ , including the number of variance parameters  $v_j$  if relative weighting is used. Both expressions are based on the (minimised) value of the objective function, but penalise the number of adjustable parameters. The addition of one parameter to a model may thus lead to a worse AIC or BIC score despite of a lower minimised value of  $R(\mathbf{p})$ . In such a case, this additional parameter is likely not necessary.

## Parameter uncertainty

After a successful fit, SAAM II reports the optimised parameter values  $\hat{p}_k$  together with an estimated standard deviation  $\sigma_k$ . This standard deviation is derived from the diagonal elements of the covariance matrix of parameters, which is calculated by SAAM II during the fitting process:

$$\sigma_k = \sqrt{E\left[\left(p_k - \hat{p}_k\right)^2\right]} \quad (5.12)$$

Unfortunately, it was not found out in this study what distribution is used by SAAM II to generate the ‘random’ values of  $p_k$  during the calculation of the covariance matrix. The estimates of SAAM II were found to differ significantly from those of another modelling software, NONLIN (Heatherington, Vicini et al. 1998). However, with the data from the current study, the uncertainty values were reproducible under identical conditions, and similar under similar conditions (e.g. with slight variations in the data), thus the parameter uncertainties may still serve as a means to judge improvement by a change in model structure.

The uncertainties of the final parameter estimates of the proposed new biokinetic model in section 6.3.3 were not based on SAAM II estimates, but evaluated from the parameter values as standard deviations of the mean, according to section 4.

## 5.3 Dosimetry

In accordance to the concept of radiation protection and dose, presented in section 1.4, the ICRP provides dose coefficients linking an intake of activity with the equivalent doses  $H_T$  received from this activity. These coefficients allow for a quick, tentative dose assessment in the case of a known intake, without the need for laborious calculations. In the same way, an estimate of the whole-body effective dose coefficient can be made. The unit of dose coefficients is  $\text{Sv}\cdot\text{Bq}^{-1}$ .

The descriptions and expressions in this section are based on ICRP publications 30 (ICRP 1979), 38 (ICRP 1983), 56 (ICRP 1990), 60 (ICRP 1991), 66 (ICRP 1994), 67 (ICRP 1993), and 100 (ICRP 2006).

Dose coefficients are calculated from the number of transformations  $U_{S,i}(\tau)$  of a radionuclide  $i$  in the time period  $\tau$  as predicted from the respective element’s biokinetic model for each source region  $S$ . A further set of coefficients, the specific effective energies (SEE), is then used to characterise the equivalent dose received by a target region  $T$  per transformation in  $S$ :

$$H_T(50) = \sum_S \sum_i U_{S,i}(50) \cdot SEE_i(T \leftarrow S) \quad (5.13)$$

Equation 5.13 presents the simplified expression for the committed equivalent dose in adults, which is also exclusively used in the current study, since only investigations with adult test persons were performed. However, the ICRP has also given recommendations concerning dose calculations for infants and children. In the case of intake at an early age, biokinetic model parameters and SEE values have to be interpolated between age groups, and the right side of Equation 5.13 must be evaluated by integration over time. The characteristic time period  $\tau$  is 50 y as a default for intake in adults, and the time from intake up to an age of 70 y for intake at a younger age.

The number of transformations  $U_S(50)$  was calculated with the SAAM II software. For this purpose, each compartment  $C_S$  of the respective biokinetic model was linked to a closed compartment  $C_{S,0}$  receiving the transformed radionuclides. The respective transfer rates  $\lambda$  were set according to the radionuclide half-lives in analogy to Equation 1.4. With an experiment duration of 50 y and a unit intake of activity, the contents in the closed compartments  $C_{S,0}$  are equal to  $U_S(50)$ .

In ICRP publication 67, only ingestion dose coefficients for  $^{95}\text{Zr}$  were published, presumably because this isotope of zirconium is most commonly produced in nuclear technology, and has a half-life of 64 d which makes it relevant for internal dose calculations after accidental release into the environment.  $^{95}\text{Zr}$  has a radioactive daughter nuclide,  $^{95}\text{Nb}$ , which occurs in both its metastable (m) as well in its ground state (g) in the decay chain of  $^{95}\text{Zr}$  (Figure 5.3). The transformations of  $^{95}\text{Nb}$  must also be taken into account in the dose coefficient calculation of  $^{95}\text{Zr}$  (Eckerman; ICRP 1983).

In order to model these daughter nuclides, two biokinetic models of niobium were linked with the zirconium biokinetic model (one each for  $^{95}\text{Nb-m}$  and  $^{95}\text{Nb-g}$ ). The radionuclide transformations of these daughter nuclides were assessed in the same way as illustrated above. However, only one nuclide at a time can be evaluated in this way without a loss of activity to the closed compartments; thus, the procedure had to be done for each nuclide separately.

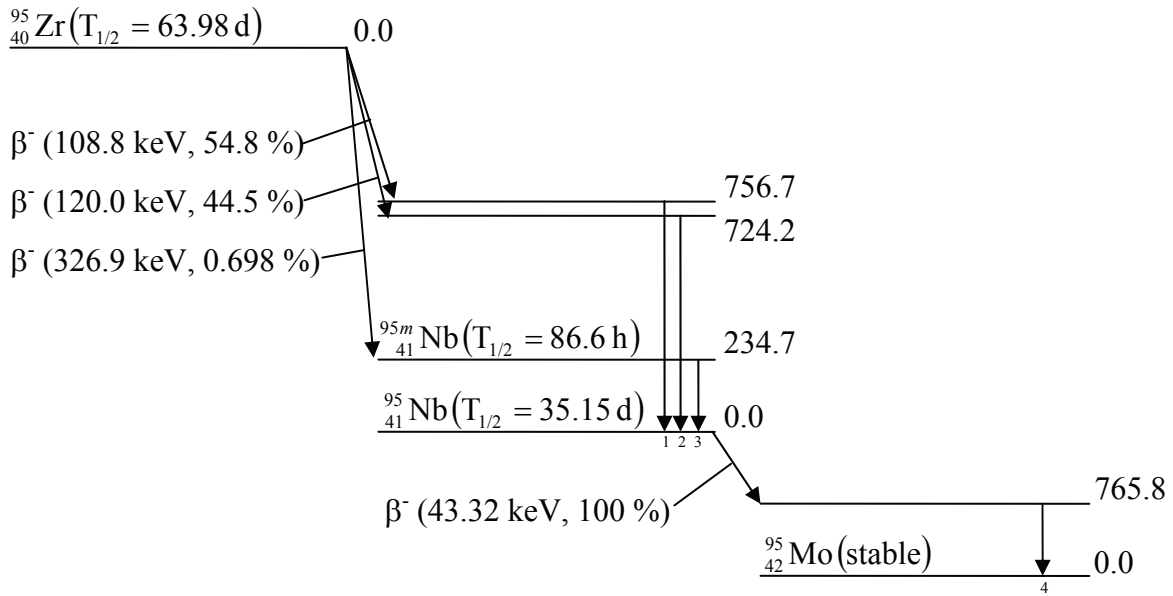


**Figure 5.3:** Simplified decay scheme of  $^{95}\text{Zr}$  and its daughter products according to ICRP publication 38 (ICRP 1983). Excitation energies of the nuclides are stated in keV, as are the mean  $\beta^-$  energies; the levels are not drawn to scale. The  $\gamma$  emission yields  $Y$  are (1) 55.0 %, (2) 44.5 %, (3) 25.9 %, and (4) 100 %. X-rays, Auger electrons and internal conversion electrons are not shown, although they contribute to the released energy, especially for the transformation of  $^{95}\text{Nb-m}$  to  $^{95}\text{Nb-g}$ .

The specific effective energy  $SEE_i(T \leftarrow S)$  is defined as

$$SEE_i(T \leftarrow S) = \sum_k \frac{w_{R,k} Y_k E_k A F_k(T \leftarrow S)}{m_T}, \quad (5.14)$$

with  $w_{R,k}$  being the radiation weighting factor of radiation  $k$ ,  $Y$  the yield of radiation  $k$  per transformation,  $E_k$  the energy of radiation in J,  $m_T$  the mass of target region  $T$ , and  $A F_k(T \leftarrow S)$  the absorbed fraction of radiation  $k$  in  $T$  per transformation in  $S$ . Apart from geometrical

relations of source and target regions, the  $AF$  values are dependent on type and energy of nuclear transformations, according to the penetration depth of each radiation caused by a transformation. Usually, non-penetrating radiations like alpha and beta particles, recoil atoms, and fission fragments, are assumed to be absorbed within the source region. Exceptions to this general assumption are source regions distributed over the whole body ('whole body' and 'other tissues'), the radiosensitive target regions in bone (red bone marrow and endosteal tissue), as well as walled compartments (e.g. stomach, intestine, colon and urinary bladder, where the wall is the target region and the contents are the source).

Tabulated  $SEE$  values were taken from the SEECAL software package (Eckerman 1993), which was also used to calculate the ingestion dose coefficients in ICRP publication 56 (ICRP 1990). These coefficients were derived from mathematically defined phantoms of the human body, termed MIRD phantoms. This type of phantom will shortly be replaced by voxel phantoms based on CT data; yet no reference  $SEE$  values for the new phantoms were available at the time of the study.

The committed effective dose over 50 y is calculated from the individual dose coefficients in analogy to Equation 1.2. The tissue weighting factors  $w_T$  used in the current study are presented in Table 5.1, taken from ICRP publication 67 (ICRP 1993).

**Table 5.1:** Tissue weighting factors  $w_T$

Tissue or organ	Tissue weighting factor $w_T$
Gonads	0.20
Red bone marrow	0.12
Colon	0.12
Lung	0.12
Stomach	0.12
Bladder	0.05
Breast	0.05
Liver	0.05
Oesophagus	0.05
Thyroid	0.05
Skin	0.01
Bone surface	0.01
Remainder	0.05

Several of the tissue doses or dose coefficients covered by the tissue weighting factors are subject to a special treatment:

- The gonad dose included in the effective dose coefficients given by the ICRP is the higher value of both ovaries and testes dose coefficients, weighted by the gonads weighting factor. Since the dose coefficient calculations in the current study are gender-specific, this approach was not adopted. The calculated effective dose coefficients in section 6.4 always contain the gender-appropriate dose coefficient, weighted by the gonads weighting factor. The gender-specific calculation leads to significant differences in the contribution of the gonad dose to the effective dose, as conceivable in Figures 6.22 – 6.26.
- As recommended in ICRP publication 67, the colon dose coefficient is composed of the dose coefficients of its sections by  $H_{colon} = 0.57 \cdot H_{ULI} + 0.43 \cdot H_{LLI}$ .
- The lung dose coefficient is composed of the dose coefficients to the thoracic tissues, i.e.  $H_{lung} = 0.333 \cdot H_{bronchial} + 0.333 \cdot H_{bronchiolar} + 0.333 \cdot H_{alveolar-interstitial} + 0.001 \cdot H_{lymphatics}$ . The dose coefficients of extrathoracic tissues (ET) of the respiratory tract are included

in the remainder region, combined as  $H_{ET} = 0.001 \cdot H_{\text{anterior nose}} + 1 \cdot H_{ET2} + 0.001 \cdot H_{\text{lymphatics}}$ . The regions in ET2 are posterior nasal passages, larynx, pharynx, and mouth.

- The remainder dose coefficient is composed of the dose coefficients of all further target regions, weighted by their relative mass contribution. The respective target regions and their masses are given in Table 5.2. The uterus is taken to contribute only to female effective dose coefficients in the current study.

Some compartments of the HAT model are not included in the SEECAL *SEE* values, nor is the oesophagus included as a target region in the SEECAL software. Therefore, the following adaptations were made:

- Oral cavity and oesophagus were introduced as additional source regions *S*. For the purpose of dose calculation, the oral cavity was identified with the brain, and the oesophagus with the thymus, since the members of both organ pairs are in close proximity to each other and have similar sizes, resulting in a small error if the same *SEE* values are used within each region pair. Furthermore, the masses of these tissues are small, and the error introduced by removing them from the ‘other tissues’ source region is also small.

In brief, the following equations were used for the relevant values of  $SEE(T \leftarrow S)$ , with existing SEECAL values marked by \*:

$$SEE(T \leftarrow \text{oral cavity}) = SEE^*(T \leftarrow \text{brain})$$

$$SEE(T \leftarrow \text{oesophagus}) = SEE^*(T \leftarrow \text{thymus})$$

$$SEE(\text{brain} \leftarrow \text{oral cavity}) = 0$$

$$SEE(\text{oesophagus} \leftarrow \text{oesophagus}) = SEE^*(\text{thymus} \leftarrow \text{thymus})$$

$$SEE(\text{thymus} \leftarrow \text{oesophagus}) = 0$$

The calculation of the thymus and oesophagus dose coefficients is therefore not identical, in that the latter includes the self-absorbed dose component  $U_{\text{oesophagus}}(50) \cdot SEE(\text{oesophagus} \leftarrow \text{oesophagus})$ , whereas this contribution is neglected for the thymus dose. The effect of this difference can be seen in Table 6.10. The brain dose coefficient is also calculated without self absorption, i.e. the brain, as a surrogate for the oral cavity, is used as source region for all target regions except for itself.

- The upper large intestine is identified with the right colon, i.e.  $U_{ULI}(50) = U_{RC}(50)$ .
- The lower large intestine is taken to be composed of the left and rectosigmoid colon;  $U_{LLI}(50) = U_{LC}(50) + U_{RS}(50)$ .

**Table 5.2:** Masses of tissues contributing to the remainder dose coefficient, as used by the SEECAL software.

Target region	Mass (male, g)	Mass (female, g)
Adrenals	14	14
Brain	1400	1200
Small intestine wall	640	600
Kidneys	310	275
Extrathoracic tissues	15.47	12.71
Muscle	28000	17000
Pancreas	100	85
Spleen	180	150
Thymus	20	20
Uterus	80*	80

(\*) The uterus dose coefficient is included in ICRP dose coefficients, but not in the male dose coefficients calculated in the current study.

## 6 Results and discussion

### 6.1 Investigations

Until July 2007, 22 investigations with stable isotopic tracers of zirconium were performed at the GSF, 9 of which as preliminary investigations from 1998 to 2003, preceding the current work. Within this study, 13 further investigations were performed since 2005.

Investigations were prioritised for measurement based on the following criteria:

- chronologic progression, i.e. it was intended to keep the storage time of samples as short as possible and measure the earliest investigations first;
- inclusion of both sexes, to evaluate potential metabolic gender differences;
- and inclusion of two different chemical forms of oral tracer solution, to estimate the effect of chemical form on fractional absorption.

Table 6.1 gives an overview of the investigations for which measurements were performed during this study. The first two-digit number in the investigation code identifies test persons, the last two digits denote the investigation.

Due to the considerable expenditure of time for measurements, and the deadline set for this work, only measured TIMS data from 9 investigations and PNA data from 2 investigations are included in the current evaluation. One further investigation (Zr.20.08) was subjected to measurement, but given the small amount of tracer administered, all TIMS and most PNA measurement results were below the respective method detection limits.

**Table 6.1:** Overview of investigations subjected to measurement within this study.

If no additional solution code is given for p.o. tracers, the tracer was administered with sodium citrate.

Investigation (code)	Sex	Age (y)	i.v. tracer		p.o. tracer		Collected samples	
			Type	( $\mu\text{g}$ )	Type	(mg)	Plasma	Urine
Zr.01.03	m	60	T-90	280	T-96-H	6.46	17	3
Zr.20.08	f	31	-	-	T-90	1.79	16	11
Zr.21.09	f	26	T-90	287	T-96-L	5.93	11	11
Zr.22.10	m	39	T-90	277	T-96-L	6.93	14	11
Zr.24.11	f	48	T-90	218	T-96-L	6.84	15	11
Zr.11.12	f	55	T-90	274.5	T-91	6.27	15	11
Zr.20.14	f	31	T-96-H	109	T-91	6.95	15	11
Zr.26.15	m	28	T-96-H	110	T-90 / Ox-2	7.04	14	10
Zr.25.16	m	29	T-96-H	104	T-90 / Ox-1	6.79	15	11
Zr.20.19	f	32	T-96-H	113	T-90 / Ox-3	6.91	13	9

According to the standard investigation protocol described in section 2.3, 16 plasma and 11 urine samples should be collected for each investigation. However, there are deviations from this standard:

- Usually, one blood sample was skipped while returning from hospital to workplace.
- The last samples (30 d and/or 100 d) were not available at the time of measurement for Zr.26.15 and Zr.20.19.
- In Zr.21.09 no sufficient blood volume could be obtained for some sampling times.
- Zr.01.03, one of the preliminary investigations, was limited to 33 h duration with a unique sampling scheme.

Within the evaluated investigations, Zr.01.03 is a special case beyond its different sampling scheme. It is one of the preliminary experiments whose plasma samples were already measured with PNA, the results being published in 2002 and 2003 (Veronese, Cantone et al. 2002; Veronese, Cantone et al. 2003; Veronese, Giussani et al. 2003). The reasons for its inclusion in the current study are the following:

- the scarcity of new PNA data due to the small sample throughput of the method, combined with the intent of PNA and TIMS method comparison;
- the possibility to compare the PNA measurements of Zr.01.03 at the Paul Scherrer Institute in Villigen, Switzerland with new measurements (Zr.20.14 and Zr.25.16) at the Maier-Leibnitz-Laboratory in Garching, Germany, and the GSF;
- and the first-time inclusion of urine data.

Further preliminary investigations have not been included, since they were either limited to only one tracer (i.v. or p.o.), or the oral tracer was administered in combination with a meal, or samples could not be measured before the deadline.

## **6.2 Sample measurements and method comparison**

TIMS measurements for this study encompass ~700 samples, from which 256 belong to the above-mentioned investigations, including some repeated measurements. The remaining measurements were performed for various preliminary experiments in method development, or were reference measurements of various tracer solutions or quality assurance measurements. Annex A gives a list and short descriptions of these further experiments.

In four irradiation periods in 2006, 24 reference samples, 67 samples from 3 investigations (Zr.20.08, Zr.20.14, Zr.25.16), and 12 standard samples were analysed by activation. The reference samples were used to assess the method detection limit and to optimise irradiation and measurement conditions. 61 of the investigation samples were measured with gamma spectrometry to obtain  $^{90}\text{Zr}$  concentrations, resulting in 31 detectable concentration values. 38 concentration values of  $^{96}\text{Zr}$  were detected in further 40 gamma spectrometric measurements. The main reason for the small yield of  $^{90}\text{Zr}$  results was the fast decay of its activation product  $^{90}\text{Nb}$  in comparison to the allocated time for measurement, combined with high background signals which brought about a high limit of detection. Thus only few samples with high amounts of  $^{90}\text{Nb}$  could be reasonably well measured in a time frame of ~7 d. Generally, counting time was limited due to (a) only 2 – 3 HPGe crystals being used for each sample type and irradiation to limit the influence of detector variability, and (b) reaction product decay and corresponding loss of signal intensity.

### **6.2.1 TIMS and PNA detection limits**

Yu et al. (2002) presented a detection limit calculation for isotope dilution mass spectrometry (IDMS), based on the standard uncertainty of IDMS concentration measurements, and derived according to ISO recommendations in the GUM (ISO, BIPM et al. 1995). This detection limit formulation comprises individual detection limits of the isotopes involved, isotope abundances of the unspiked sample, and the corresponding isotope ratio in the spike. Its most prominent feature is that its value depends on the difference of isotope ratios in spike and unspiked sample.

Since the uncertainties of zirconium IDMS measurements are also calculated according to GUM, a detection limit for the tracers could be deduced in an analogue way. However, there are some limitations to an analytical solution:

- Isotope ratios or abundances in spike, tracers and sample have uncertainties of up to a few percent, i.e. although precisely calculated, the detection limit can only be reasonably specified with a similar uncertainty.
- The detection limits of the individual isotopes are dominated by background count rates from zirconium and interfering molybdenum from the rhenium filaments. Molybdenum count rates vary in a wide range of about  $2 \text{ s}^{-1}$  to  $2 \cdot 10^4 \text{ s}^{-1}$ .

Considering the effort needed to deduct individual detection limits for all tracers in contrast to the uncertainty of the resulting limits, an empirical approach is preferred, which is based on the definition of detection limit DL by Currie (Currie 1968):

$$DL = 4.65 \cdot \sigma_B \quad (6.1)$$

$\sigma_B$  is the standard deviation of the background and is estimated by the standard deviation of the mean of repeated blank observations.

Using the latter approach, tracer concentrations in ng per sample are evaluated from 28 blank samples, i.e. plasma and urine samples before tracer application, plasma samples with only one tracer, and oral tracer concentrations in plasma samples collected within five minutes after tracer ingestion. The latter values may be considered as blank values since the amount of oral tracer in plasma is negligible during the first few minutes after ingestion. No significant differences have been observed between p.o. tracer concentrations before and up to 5 min after tracer ingestion, as well as between plasma and urine samples measured by TIMS. Three values were excluded from the evaluation, since they were considered erroneous after comparison with the distribution of all other results. The excluded results were 2.07 ng of T-91, as outlier to 15 other values in the range of -0.34 ng to +0.24 ng, and 5.3 ng and 45.6 ng of T-90, as outliers to 24 other values ranging from -0.83 ng to +0.77 ng.

For each tracer, the mean and median concentrations in blank samples as well as the standard error and detection limit of the tracers are presented in Table 6.2. It can be seen that one principle of the approach of Yu et al. (2002) still applies for the empirical detection limits; tracers whose isotope abundances differ by a larger amount from those of the reference tracer (or other species in the mixed sample) can be detected in smaller quantities. Thus T-96-H has a lower detection limit than T-96-L, and T-90 has a high detection limit since  $^{90}\text{Zr}$  is the second most abundant isotope in all tracers and the most abundant isotope in natural zirconium.

**Table 6.2:** Blank measurements of stable tracers with ID-TIMS

<b>Tracer (enrichment)</b>	<b>T-90 (98.2 %)</b>	<b>T-91 (88.7 %)</b>	<b>T-96-L (58.3 %)</b>	<b>T-96-H (86.4 %)</b>
Number of blank measurements	24	15	18	17
Mean (ng)	0.097	0.024	0.024	0.059
Median (ng)	0.049	0.050	0.038	0.030
$\sigma_B$ , standard deviation of the mean (ng)	0.081	0.037	0.033	0.019
Detection limit (ng)	0.376	0.171	0.155	0.090

Especially for T-90, the detection limit in samples containing a low amount of zirconium can be lower, since in this case the difference between unspiked and spiked sample is more prominent.

The values above have been evaluated from measurements with both high and low background of natural zirconium, since both types of measurements are occurring in the

study. One main contribution to natural zirconium in measured samples is attributable to the purity of hydrochloric acid used during sample preparation. As long as high-purity ‘suprapure’-grade hydrochloric acid (Merck KGaA, Darmstadt, Germany) was used for extraction chromatography, approximately 0.1  $\mu\text{g}$  of natural zirconium background was present in each sample. If, before use, hydrochloric acid of the same grade was purified by distillation at temperatures below its boiling point (‘distillacid BSB-939-IR’, Berghof Products + Instruments GmbH, Eningen, Germany), the amount of natural zirconium per sample was reduced to approximately 4 ng per sample. This change in natural zirconium background affects the detection limit by a factor of  $\sim 10$ .

Detection limits of PNA are based on a set of 24 reference plasma samples which were activated and analysed to optimise the procedure at the MLL. They are calculated according to Equation 6.1, with  $\sigma_B$  being the gamma spectrometric background uncertainty at the respective energy as determined by the evaluation software. The isotope detection limits of both  $^{90}\text{Zr}$  and  $^{96}\text{Zr}$  are greatly influenced by waiting time after end of irradiation, and either measuring time, or ratio of waiting time over measuring time. Aluminium shielding thickness has little effect on detection limit when varied from 0.2 – 0.7 mm. Detection limits and optimal conditions are summarised in Table 6.3.

**Table 6.3:** Detection limits and optimal conditions for PNA measurement of zirconium isotopes. Plasma sample volumes used for measurement were  $\sim 0.8$  ml.

Activation reaction	$^{90}\text{Zr}(\text{p},\text{n})^{90}\text{Nb}$	$^{96}\text{Zr}(\text{p},2\text{n})^{95}\text{Nb}$
Gamma energy (keV)	141	766
Isotope detection limit (ng)	1.8	1.6
Waiting time (d)	< 4 d	30 – 50 d
Further optimal condition	$t_w/t_m < 3$	$t_m \sim 5 - 7$ d

In summary, both measurement methods are capable of zirconium tracer measurement in the concentration range needed for biokinetic investigations. TIMS generally can detect smaller amounts of any zirconium tracer type. PNA is able to quantify pure natural zirconium content in blank samples by measurement of  $^{90}\text{Zr}$ , if the concentration is sufficiently high. In the current state, TIMS is not capable of background quantification, due to contamination with natural zirconium introduced during sample digestion and extraction chromatography.

Detection limits have only been calculated for tracers or tracer isotopes, but not for natural zirconium. The reason was that concentration measurements of natural zirconium were subject to bias in TIMS, and usually impossible in PNA because T-90 was present as tracer in most investigated samples. However, it is possible to define an upper limit for the concentration of natural zirconium in samples by determining its minimal concentration in all TIMS samples and in PNA blank samples.

Referring to Table 6.2 and considering natural zirconium similar to a tracer, a TIMS detection limit of  $\sim 0.1 - 0.4$  ng per sample can be estimated for natural zirconium, depending on the tracers present in the sample. This range is commensurate with  $0.2 - 0.8$   $\text{ng}\cdot\text{ml}^{-1}$  in plasma and  $0.1 - 0.4$   $\text{ng}\cdot\text{ml}^{-1}$  in urine due to a simple scaling with the processed sample volume. The PNA detection limit of 1.8 ng  $^{90}\text{Zr}$  per sample corresponds accordingly to a detection limit of 4  $\text{ng}\cdot\text{ml}^{-1}$  in plasma and 0.2  $\text{ng}\cdot\text{ml}^{-1}$  in urine.

In the single urine blank sample measured by PNA, no zirconium was detected. TIMS measurements of urine samples, using sub-boiled HCl during sample preparation, show concentrations of natural zirconium in the range of  $1.2 - 8$   $\text{ng}\cdot\text{ml}^{-1}$ .

From the two plasma blank samples measured by PNA, concentrations of  $7.3 \text{ ng}\cdot\text{ml}^{-1}$  and presumably erroneous  $360 \text{ ng}\cdot\text{ml}^{-1}$  were evaluated. TIMS measurements of natural zirconium in plasma have shown a range of  $1.5 - 9 \text{ ng}\cdot\text{ml}^{-1}$ . The total number of TIMS plasma samples with low background, i.e. with sub-boiled HCl used during sample preparation, was  $\sim 80$ . The concentration ranges in urine and plasma evaluated from TIMS measurements are remarkably similar and may be the result of the common remaining contamination with natural zirconium from purified acids used during sample preparation. Thus it is likely that the concentrations of natural zirconium in urine and plasma are in the range of or even lower than  $\sim 1.5 \text{ ng}\cdot\text{ml}^{-1}$ . This is consistent with the lowest concentrations in published data presented in the introduction in section 1.2 (de Bartolo, Cantone et al. 2000; Heitland and Köster 2006).

## 6.2.2 Combined uncertainty

Combined uncertainties are calculated as described in section 4 for all measurements. Relative uncertainties are preferred for comparison, since absolute uncertainties are dependent on tracer concentration or count rates and vary by a large amount.

An overview on relative combined uncertainties of tracer concentrations is given in Table 6.4. Blank samples are not included in the data given in this table, since relative uncertainties approach infinity for concentrations approaching zero with small but finite absolute uncertainties. This problem is specific to TIMS in this case, since isotope dilution calculations can yield zero or negative type concentrations if a sample contains more than two types. In gamma spectrometric measurements in PNA, small signals are usually not resolvable as peak in the gamma spectrum and therefore no result at all is obtained.

**Table 6.4:** Overview on relative combined uncertainties in sample measurements by TIMS and PNA.

<b>TIMS</b>			
Tracer	Sample type	Median (%)	Range (%)
T-90	Plasma	4.37	4.33 – 15.0
T-91	Plasma	4.75	4.46 – 25.0
T-96-L	Plasma	4.57	4.39 – 19.6
T-96-H	Plasma	4.35	4.33 – 20.7
T-90	Urine	4.76	4.48 – 28.5
T-91	Urine	4.74	4.52 – 64.0
T-96-L	Urine	4.91	4.53 – 7.9
T-96-H	Urine	4.49	4.47 – 18.1
<b>PNA</b>			
Tracer	Sample type	Median (%)	Range (%)
T-90	Plasma	32.7	7.4 – 90
T-96-H	Plasma	16.3	6.1 – 39
T-90	Urine	30.0	13.8 – 71
T-96-H	Urine	12.3*	6.5 – 56*

(\*) Only 3 measurements.

TIMS relative combined uncertainties usually are in the range of 4.3 – 5 %. The combined uncertainty in these samples is dominated by the standard uncertainty of the reference tracer (spike) concentration of 3.9 %. Larger relative uncertainties are either related to samples with small tracer concentrations, or to samples with a low ion yield during measurement, resulting in large uncertainties of the measured isotope ratios. The difference between the tracer types is small.

PNA uncertainties show a substantially higher variability. The minimal and maximal relative combined uncertainties are increased by a factor of ~1.5 over the respective TIMS values, while the median uncertainty is strongly dependant on the tracer. The latter is increased by a factor of ~3.5 for T-96-H and ~7 for T-90 in comparison to TIMS.

One reason for these discrepancies may be that TIMS measurements can be standardized, e.g. by setting operational ranges for ion optics focus voltages, heating current and temperature of the sample carrier, as well as desirable count rates. In contrast, PNA measurement results strongly depend on irradiation conditions, as well as waiting time and counting time, which are variable by design since samples are measured consecutively.

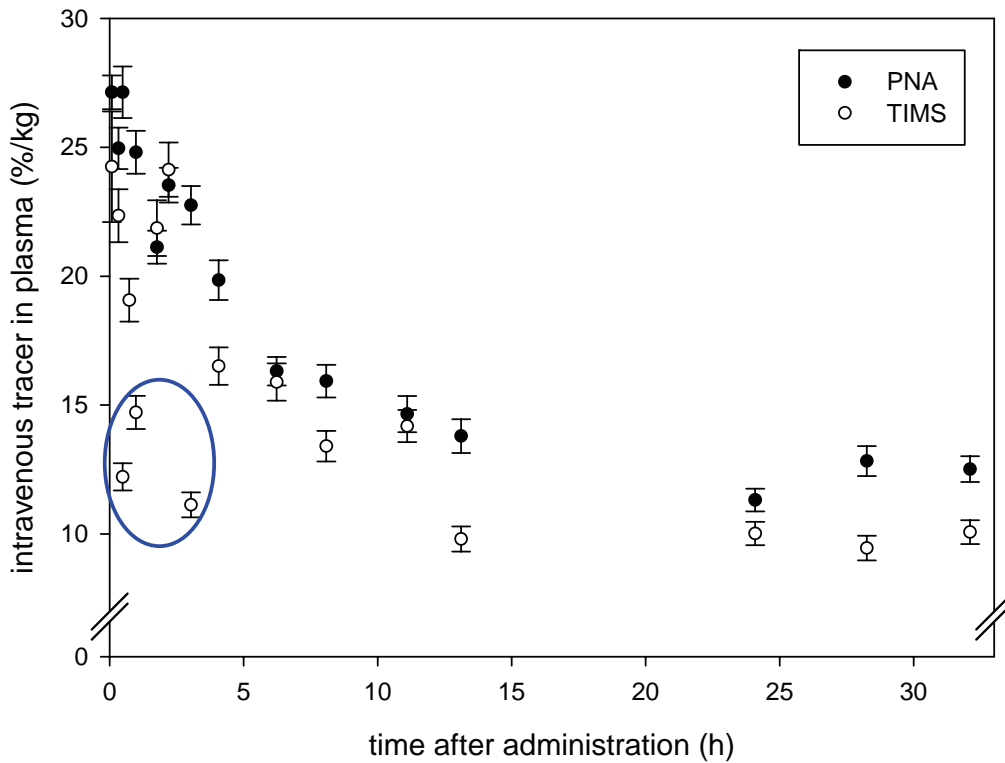
### 6.2.3 Correlation of TIMS and PNA results

Since both methods are capable of and available for measuring tracer concentrations in investigation samples, a decision must be taken as to which samples should be subjected to which method. Rather than using two methods in parallel to improve sample throughput, it was decided to profit from the two techniques by validating the results of one by the other. This is especially expedient because the PNA and TIMS measurement processes rely on different physical mechanisms and do not share a common sample preparation. If an error or systematic deviation is inherent in one method, it should be discoverable by comparison.

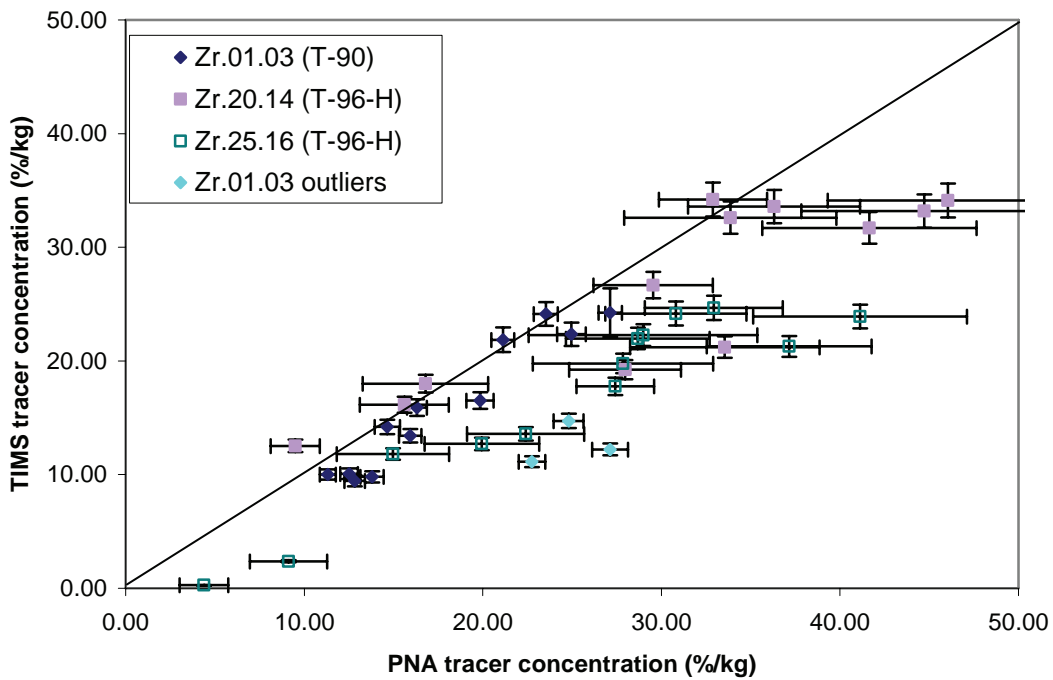
As an example, Figure 6.1 shows the values of i.v. tracer in plasma in investigation Zr.01.03, measured by PNA (black circles) and TIMS (white circles). The results are largely similar, with a tendency of larger concentration values from PNA measurements. The three data points marked as outliers are likely biased by a TIMS measurement error, since their values compare well within the rest of the PNA measurements for this investigation, but lie ~ 25 – 50 % below the preceding and succeeding TIMS values. This shows the potency of method comparison, since if only results of one method were available, it would not be clear if results are biased due to measurement errors or deviations inherent in the original samples. However, due to the good correlation with PNA data for the remaining 12 samples, an error in the TIMS measurement of the 3 ‘outlier’ samples seems more plausible.

Figure 6.2 shows a direct comparison of i.v. tracer concentration measurements in plasma samples independent of time after administration. It can be seen that PNA results tend to be higher than TIMS results, but that both methods’ results show a substantial correlation despite the large uncertainties. Due to the generally large variation and uncertainty in Zr.20.14 and Zr.25.16, it is not reliable to exclude individual samples as outliers from further evaluation, in contrast to Zr.01.03.

Data of Zr.20.14 and Zr.25.16 show a larger deviation between TIMS and PNA, the PNA measurement uncertainties being also larger. This might be attributable to a change in activation and measurement procedures, since the PNA values of Zr.01.03 are adopted from an irradiation made at the Paul-Scherrer-Institute (PSI) in Villigen, Switzerland (Veronese, Cantone et al. 2003; Veronese, Giussani et al. 2003), while the other samples were irradiated at the MLL and measured at the GSF in 2006.



**Figure 6.1:** Concentration data of i.v. tracer in plasma from investigation Zr.01.03. The ellipse marks three TIMS measurements considered as erroneous outliers. Tracer concentrations are given as % of the administered tracer amount per kg of plasma.



**Figure 6.2:** Comparison of PNA and TIMS measurement of i.v. tracer concentration in plasma samples. The diagonal line indicates identical values for both methods. Tracer concentrations are given as % of the administered tracer amount per kg of plasma. The three outlying values of Zr.01.03 are identical with those marked in Figure 6.1.

Another possible and more likely explanation for bias introduced in PNA measurement is a contribution of other activation product transformations to the peak which is used for  $^{96}\text{Zr}$  quantification. If this contribution is small and cannot be resolved due to limited resolution of the gamma spectrometers, the signal attributed to  $^{95}\text{Nb}$  and thus  $^{96}\text{Zr}$  is positively biased in all measurements. However, for the external standard this effect is small, thus the sample concentrations calculated in relation to this standard will be too high. The contribution of this effect to  $^{96}\text{Zr}$  concentrations will also be variable, since it is unlikely that the interfering radionuclide has the same half-life as  $^{95}\text{Nb}$ . The p.o. tracer data of Zr.01.03 and Zr.25.16, shown in Figure 6.3, further strengthens this assumption. Although the relative uncertainties of the p.o. tracer concentrations are larger and the correlation between PNA and TIMS is small, the concentration ratios themselves are centred on  $\sim 1$ , in contrast to the biased i.v. results. Taking into account the good correlation of T-90 data from Zr.01.03 and the change in detectors between PSI and GSF, it is likely that the main cause for the biased results is inherent in gamma spectrometry, and not in irradiation conditions or TIMS measurement.

The information available for comparison of urinary data is limited to 9 pairs of tracer combinations in 8 samples, because both methods are not capable of detecting the tracers in many urine samples due to their respective detection limits. A tendency of larger values from PNA as compared to TIMS can be derived from those samples for which results are available from both methods.

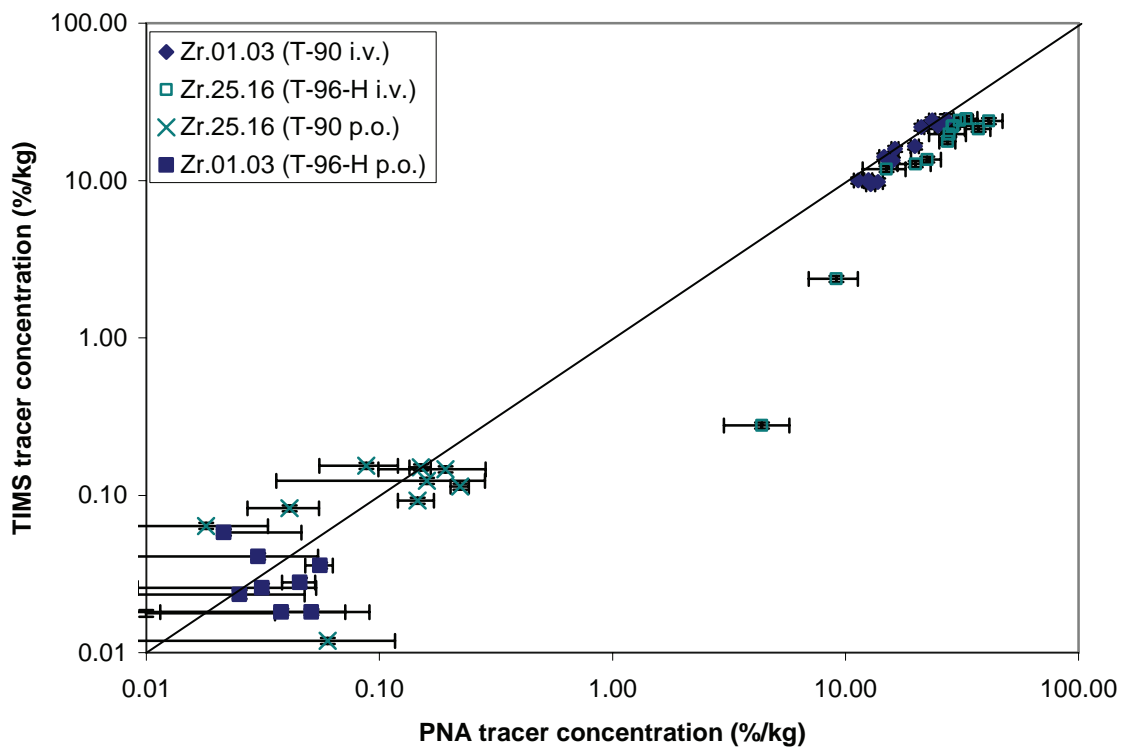


**Figure 6.3:** TIMS vs. PNA measured values of Zr.25.16. The diagonal line indicates identical values for both methods.

#### 6.2.4 Measured data

The measurement results of investigation samples are shown in Figures 6.4 – 6.9 on the following pages. For the sake of clarity, only TIMS results are shown in these figures; the agreement between TIMS and PNA results is discussed in section 6.2.3 above.

In order to establish a comparison between experiments with different amounts of tracer, the tracer concentration values in plasma are given as % of the administered tracer per kg plasma. Concentrations in urine are converted to tracer excretion rates in  $\% \cdot d^{-1}$ .

All values are shown with their combined uncertainties as discussed in section 4, which were also used as input for modelling. For most plasma samples, the relative uncertainty is 4 – 5 % according to Table 6.4 above. The uncertainty for urine samples encompasses the combined measurement uncertainty, as stated in Table 6.4, and the uncertainty inherent in the 24 h-sampling scheme, hence the relative uncertainties of most samples are  $\sim 18\%$ .

Measurement results below detection limits were omitted. The respective range of detection limits is indicated in each figure as shaded area. This is necessary because the detection limits are determined according to section 6.2.1 as mass per sample, yet the data in their presented form as percentages are scaled by the amount of administered tracer. Since the amounts of administered tracers were different in each investigation, the detection limits are also investigation-specific. Furthermore, urinary excretion rates are dependent on the daily excreted amount of urine, i.e. the excreted amount of tracer is diluted differently on each day.

It can be seen from Figures 6.4 and 6.5 that the information provided by urine samples is severely limited due to method detection limits. The variation of measured tracer excretion rates in urine both within and between investigations is of the same order of magnitude as the measured values. For the oral tracer, excretion data is incomplete in most experiments beyond the first day. Due to these results, the evaluation of fractional absorption in section 6.3.1 is restricted to plasma data.

The variability is large in plasma samples, too. However, most investigation data feature discernible trends over time, hence the data allows for modelling, which is discussed in the following section 6.3. The concentrations of the intravenous tracer are well above the detection limits for up to 30 d, and in reasonable accordance between all investigations. The oral tracer concentrations show a larger variability, and several long-term values are not detectable. Despite this limitation, the general pattern of absorption into and clearance from plasma is discernible in all investigations by an increase of tracer concentrations up to a few hours, followed by a continuous decline similar to the intravenous tracer concentrations.

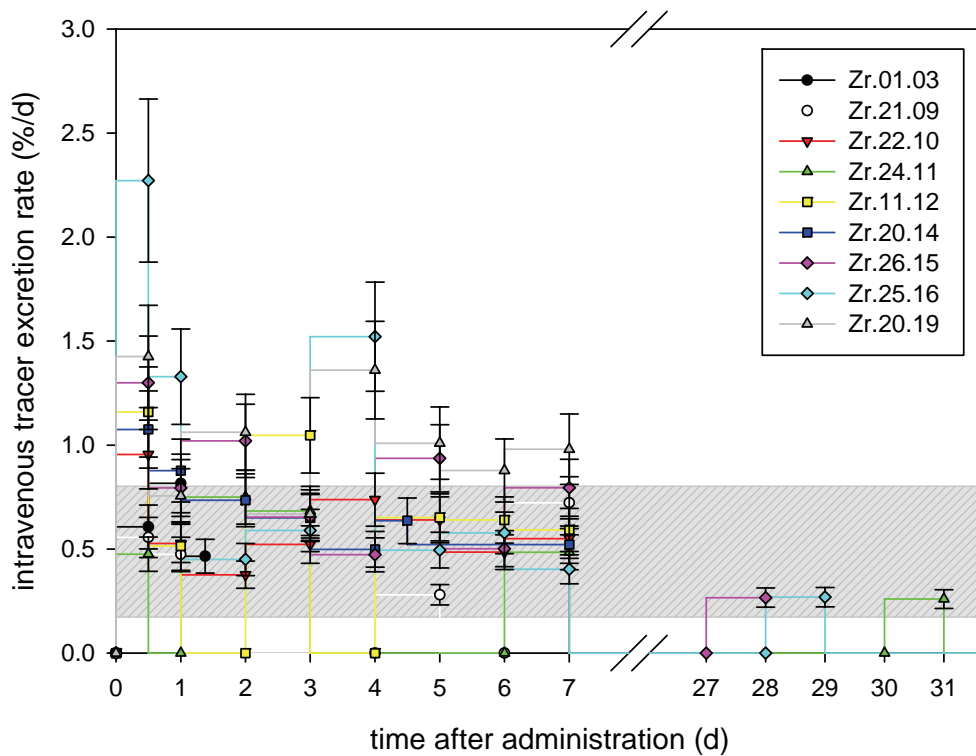


**Figure 6.4:** Excretion rates of intravenous tracer in urine. Out of 77 measurements, 16 values were below detection limit and are therefore omitted here.

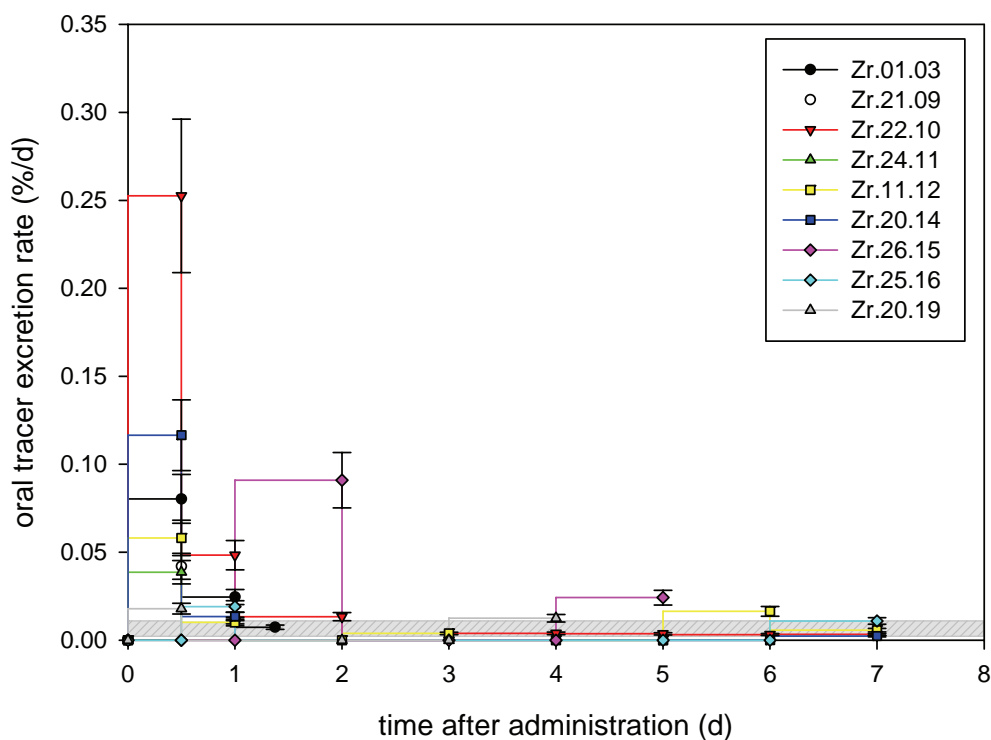


**Figure 6.5:** Excretion rate of oral tracer in urine. Out of 78 measurements, 51 values were below detection limit and are therefore omitted here.

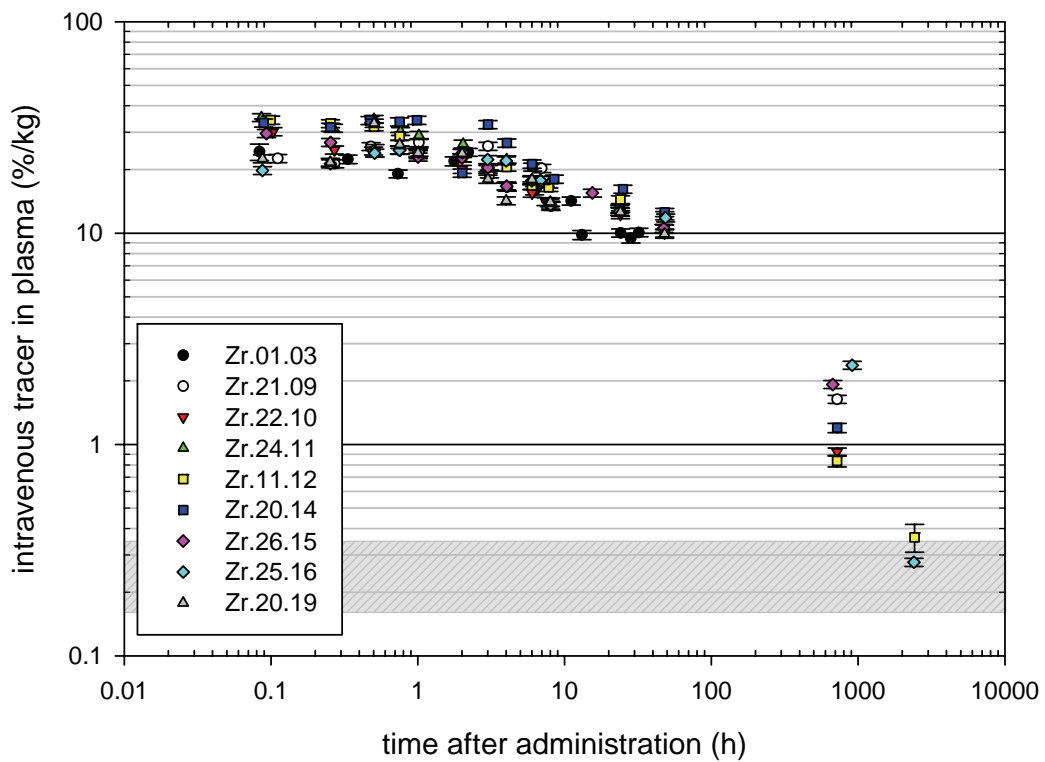


**Figure 6.6:** Concentration of intravenous tracer in plasma up to 100 d. Out of 115 measurements, 4 values were below detection limit and are therefore omitted here.

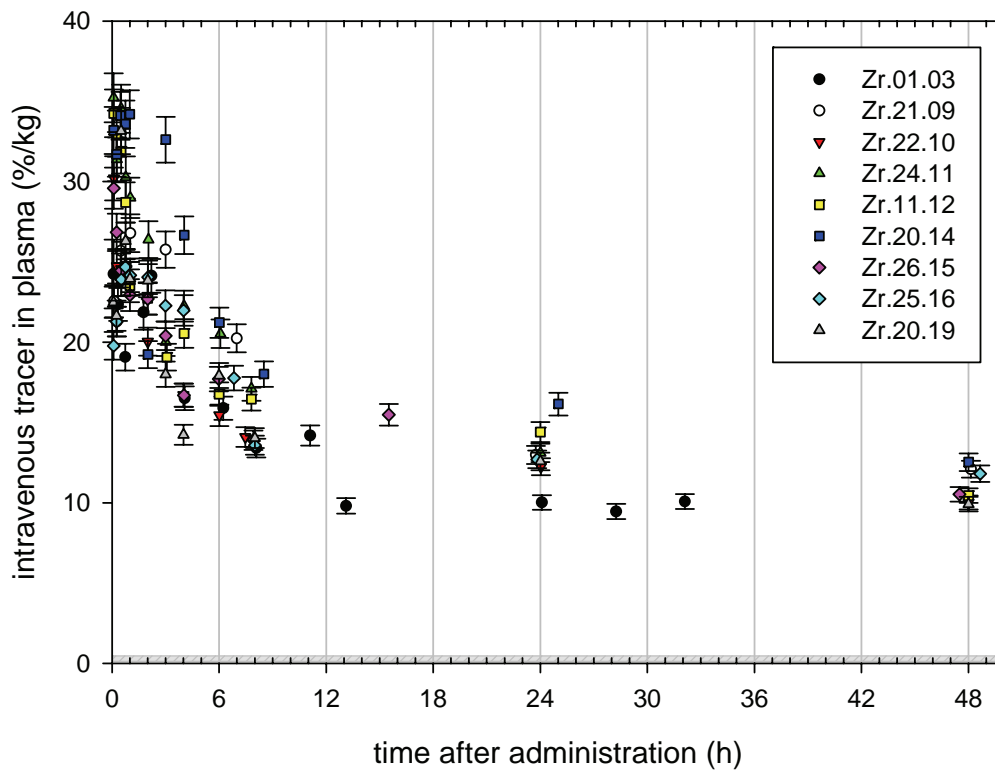


**Figure 6.7:** Concentration of intravenous tracer in plasma within the first 2 d after injection.

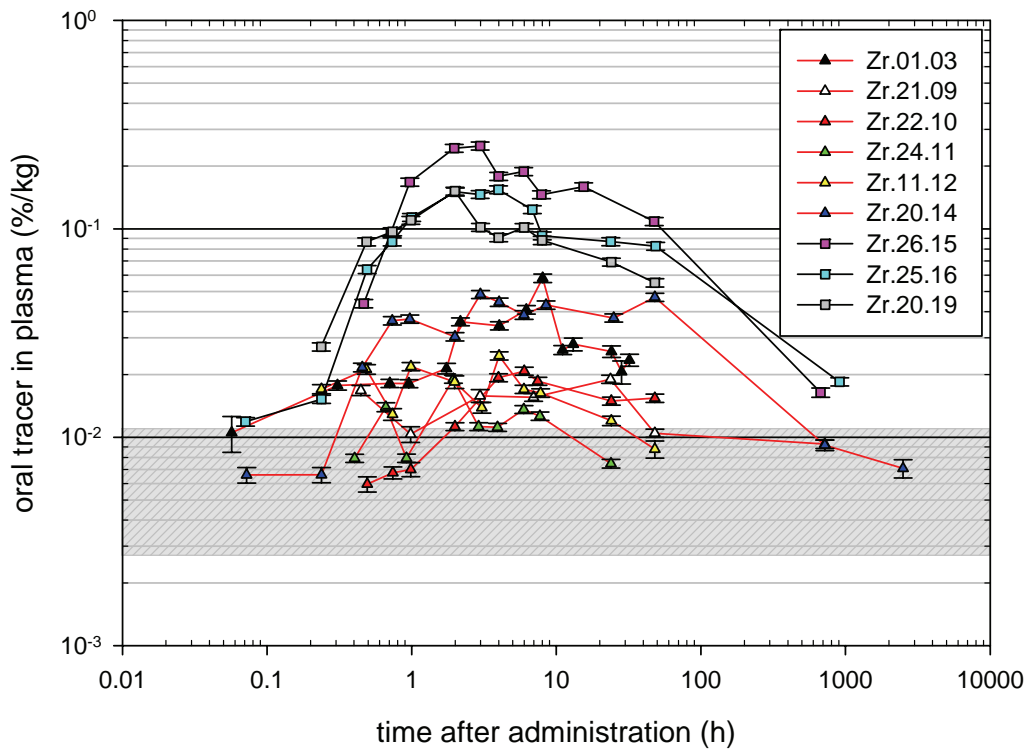


**Figure 6.8:** Concentration of oral tracer in plasma up to 100 d. Red lines indicate citrate investigations, black lines indicate oxalate investigations. Out of 112 measurements, 13 values were below detection limit and are therefore omitted here.

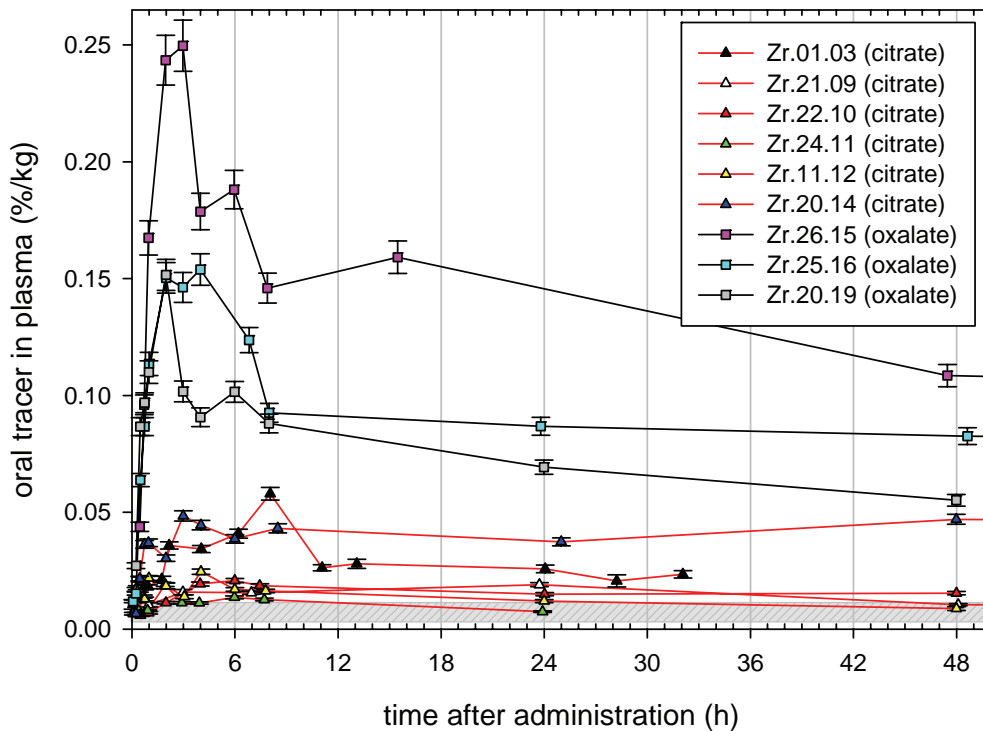


**Figure 6.9:** Concentration of oral tracer in plasma within the first 2 d after ingestion. Red lines indicate citrate investigations, black lines indicate oxalate investigations.

## **6.3 Model development**

It is worth mentioning that the uncertainties of measurement demonstrated in the last section are not as large as the variability observed within most investigations. Even if no specific compartmental model structure is assumed, a certain smoothness of tracer concentrations might be expected from consecutive measurements within an investigation, because zirconium has no known biological function and is thus expected to be subject to unspecific ion transport processes in the human metabolism. If such smoothness is not found in the data, two explanations, either errors in measurement, or biological variability, are suggestive.

Care has been taken to avoid the former, although they will still occur. Errors are likely not recognisable, since usually only one measurement per sample is available, thus precluding method comparison as in the example of Zr.01.03 shown in Figures 6.1 and 6.2 above.

Biological processes on different time scales, e.g. diurnal rhythm or weak spells, have been reported to have influence on measurement results (Lindsey, Jones et al. 2001). Variations in certain substance concentrations seem plausible due to the richness of transportation and regulation mechanisms in human metabolism, as well as due to the behaviour of test persons, e.g. the influence of dietary habits.

With the current experimental design, it is not possible to exclude, control or correct such influencing factors, thus the variation in the experimental data is considered as random uncertainty specific to tracer and sample type. Such previously not quantifiable components of uncertainty are accounted for by the software package used for modelling, SAAM II, as weights on the measurement uncertainties as described in section 5, and are thus included in the uncertainty estimates of the compartment models' parameters. In section 6.3.1, uncertainty of data is neglected for fitting. Fitting is used in this section only to smooth data, not to extrapolate by using a model.

### **6.3.1 Fractional absorption without compartment models**

#### **Double tracer technique**

Ratios of oral tracer concentration over intravenous tracer concentration, each in  $\% \cdot \text{kg}^{-1}$ , are calculated from the plasma samples in the range of  $\sim 7 - 48$  h as described in section 5.1.1. The resulting values are shown in Table 6.5 together with those from the convolution integral technique.

The assumption that both tracers have the same metabolic characteristics and are cleared similarly from blood plasma is strengthened by the small variation in tracer concentration ratios within each experiment. Ratios in samples from 30 d and 100 d after tracer administration often show larger ratios. However, if available, these ratios are not very reliable, since tracer concentrations are near detection limit and have large uncertainties.

#### **Convolution integral technique**

Fitted functions, rather than stepwise linearly interpolated functions, were used for the description of tracer concentration data needed for the convolution integral technique. The reason for this was the noise in many data sets; large variation in oral and intravenous concentrations would likely yield absorption rate functions with several local maxima and minima, thus possibly obscuring the underlying trend of oral tracer absorption into and clearance from plasma. In contrast, short-term variations have little influence on fitted functions and correspondingly also on the calculated absorption rate.

The number of data points available for fitting a clearance curve to plasma data was limited to 10 – 14 due to values below detection limit, outliers identified by PNA analysis, and blank samples being disregarded for intravenous tracers. Fit functions therefore should need only few parameters to avoid overfitting.

The fit functions used for intravenous tracer data were single and double exponential decay functions, as shown in equations 6.2 and 6.3, with 2 and 4 parameters, respectively. Except for Zr.01.03, the best fit was obtained with the latter option.

Oral tracer data were more difficult to fit, since the fitting function had to allow for an asymmetric peak. Options tested include a lognormal distribution function with 3 parameters (Equation 6.4), piecewise functions combined of a lognormal distribution with exponential decay functions with 4 or 6 parameters (equations 6.6 and 6.7), and products of an exponential rising function with exponential decays with 3 or 5 parameters (equations 6.8 and 6.9). For the calculation of fractional absorption, Zr.01.03 and Zr.22.10 oral tracer concentrations in plasma were fitted with  $f_{LN-SE}$ , while  $f_{LN-DE}$  was used for Zr.24.11, Zr.20.14, and Zr.26.15. The remaining 4 investigation data sets were best fitted with  $f_{ER-DE}$ .

$$f_{SE}(t) = a \cdot e^{-bt} \quad (6.2)$$

$$f_{DE}(t) = a \cdot e^{-bt} + c \cdot e^{-dt} \quad (6.3)$$

$$f_{LN}(t) = g \cdot e^{-\frac{1}{2} \left( \frac{\ln(t/T)}{h} \right)^2} \quad (6.4)$$

$$f_{ER}(t) = 1 - e^{-gt} \quad (6.5)$$

$$f_{LN-SE}(t) = \begin{cases} f_{LN}(t) & t \leq T \\ f_{SE}(t-T) & t > T; a = g \end{cases} \quad (6.6)$$

$$f_{LN-DE}(t) = \begin{cases} f_{LN}(t) & t \leq T \\ f_{DE}(t-T) & t > T; a + c = g \end{cases} \quad (6.7)$$

$$f_{ER-SE}(t) = f_{ER}(t) \cdot f_{SE}(t) \quad (6.8)$$

$$f_{ER-DE}(t) = f_{ER}(t) \cdot f_{DE}(t) \quad (6.9)$$

Although the use of exponential decay functions bears resemblance to first-order kinetic compartment models, the approach is different and model-independent for the convolution integral technique:

- Functions are selected based on their number of free parameters and their ability to fit to the data, rather than according to a specified (compartmental) model structure.
- In the case of piecewise functions, the clearance from plasma starts at the fitted peak time, not beginning with ingestion.
- Parameters of i.v. and p.o. functions are not linked, thus negative absorption is possible. However, its effect on cumulative fractional absorption is limited, since tracer concentrations are not extrapolated beyond 50 h.

Fractional absorption values, as well as absorption rates, were calculated from the fitted functions as explained in section 5. Figure 6.10 shows the time course of the resulting absorption rates. Due to the large variation in total absorption within the nine investigations, the shown absorption rates are normalised to the cumulative absorbed fraction of the oral tracer for each investigation. This normalisation allows for a visual comparison of peak times, peak heights, and progression of absorption rate with time.

It can be seen that most of the total absorption takes place within the first two hours after ingestion, although the peak time of absorption rate is highly variable in a range from ~ 15 – 70 min. There seems to be no difference in normalised absorption rate between dissolved zirconium administered as oxalate (dotted graphs) or in citrate-buffered solution (solid lines). Female test persons (11, 20, 21, and 24) have earlier peaks in absorption rate ( $p \sim 0.002$  in a two-tailed t-test). However, it is not clear whether the difference is due to gender or weight, since the male test persons are also heavier on average. No difference is discernable in relative peak height.

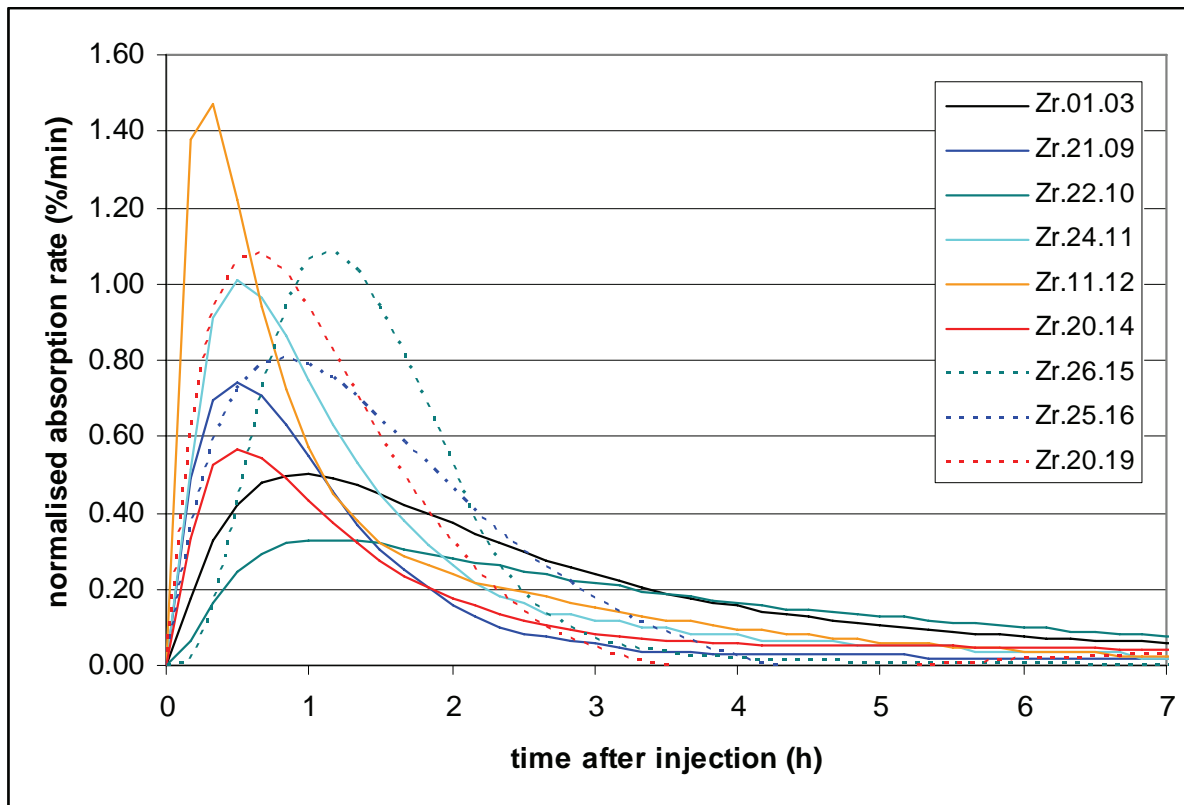


**Figure 6.10:** Absorption rates of zirconium tracers. The rates were normalised to cumulative fractional absorption, i.e. area under curve.

The results on fractional absorption are listed in Table 6.5 and compare well with the results from the double tracer evaluation. The mean fractional absorption of zirconium oxalate is higher by a factor of ~ 5 than the fractional absorption of zirconium in citrate-buffered solution. This is in accordance with the known insolubility and thus low bioavailability of many inorganic zirconium salts. However, the fractional absorption of zirconium oxalate is exceeding the values found in sources evaluated by the ICRP (Fletcher 1969; Shiraishi and Ichikawa 1972).

**Table 6.5:** Total fractional absorption of zirconium, determined by double tracer technique and convolution integral technique.

Investigation (chemical form)	Absorbed fraction, double tracer technique	Absorbed fraction, convolution integral technique
Zr.01.03 (citrate)	$2.4 \cdot 10^{-3}$	$2.3 \cdot 10^{-3}$
Zr.21.09 (citrate)	$1.0 \cdot 10^{-3}$	$1.1 \cdot 10^{-3}$
Zr.22.10 (citrate)	$1.4 \cdot 10^{-3}$	$1.4 \cdot 10^{-3}$
Zr.24.11 (citrate)	$0.7 \cdot 10^{-3}$	$0.6 \cdot 10^{-3}$
Zr.11.12 (citrate)	$0.9 \cdot 10^{-3}$	$0.8 \cdot 10^{-3}$
Zr.20.14 (citrate)	$2.8 \cdot 10^{-3}$	$2.8 \cdot 10^{-3}$
Zr.26.15 (oxalate)	$10.4 \cdot 10^{-3}$	$10.2 \cdot 10^{-3}$
Zr.25.16 (oxalate)	$6.9 \cdot 10^{-3}$	$6.9 \cdot 10^{-3}$
Zr.20.19 (oxalate)	$5.8 \cdot 10^{-3}$	$5.4 \cdot 10^{-3}$
Mean, citrate form	$1.5 \cdot 10^{-3}$	$1.5 \cdot 10^{-3}$
Mean, oxalate form	$7.7 \cdot 10^{-3}$	$7.5 \cdot 10^{-3}$

### 6.3.2 Tracer kinetics and compartment model structure

This section is divided into subsections explaining the motivation for various intermediate model proposals. It is concluded by a short summary of considerations leading to the final new proposed model, which is addressed in the next section.

#### Intravenous tracer in plasma and bidirectional flux

According to section 6.2.4, measured concentration values of intravenous tracer in plasma are usually well above the respective detection limits, and show relatively little variability in comparison with the remaining three data sets, i.e. oral tracer in plasma, and both tracers in urine. Therefore it seemed reasonable to initiate the modelling process with a comparison of the current ICRP model (cf. section 1.4) to intravenous tracer concentration data in plasma, as the most reliable data set available.

As presented in the previous section, intravenous tracer concentrations in plasma are described well by a double exponential decay for most investigations. Data and fits of Zr.26.15 are presented as an example in Figure 6.11. Data from this investigation is optimal in that it features a relatively smooth trend in comparison with other investigations. However, the general pattern is similar in the other investigations.

It can be seen that the plasma clearance predicted by the current ICRP systemic model structure and plasma clearance half-life (dotted curve) is in good accordance with the data until  $\sim 5$  h after tracer injection, but severely underestimates the data afterwards. The initial distribution volume  $V_D$  of 3.4 l can be estimated from the extrapolated tracer concentration  $c_{p,iv}$  at the time of injection and the plasma density  $\rho_{plasma}$ :

$$V_D = \frac{100}{c_{p,iv} \cdot \rho_{plasma}} \quad (6.10)$$

In maintaining the ICRP model structure and adjusting the clearance half-life (dashed curve), the estimated distribution volume is increased contradictory to the data. For later times, data is still underestimated. In contrast, the use of a double exponential decay function similar to  $f_{DE}$  (Equation 6.3) results in a good fit for 0 – 48 h and an estimate of  $V_D$  in consistence with the data at early times.

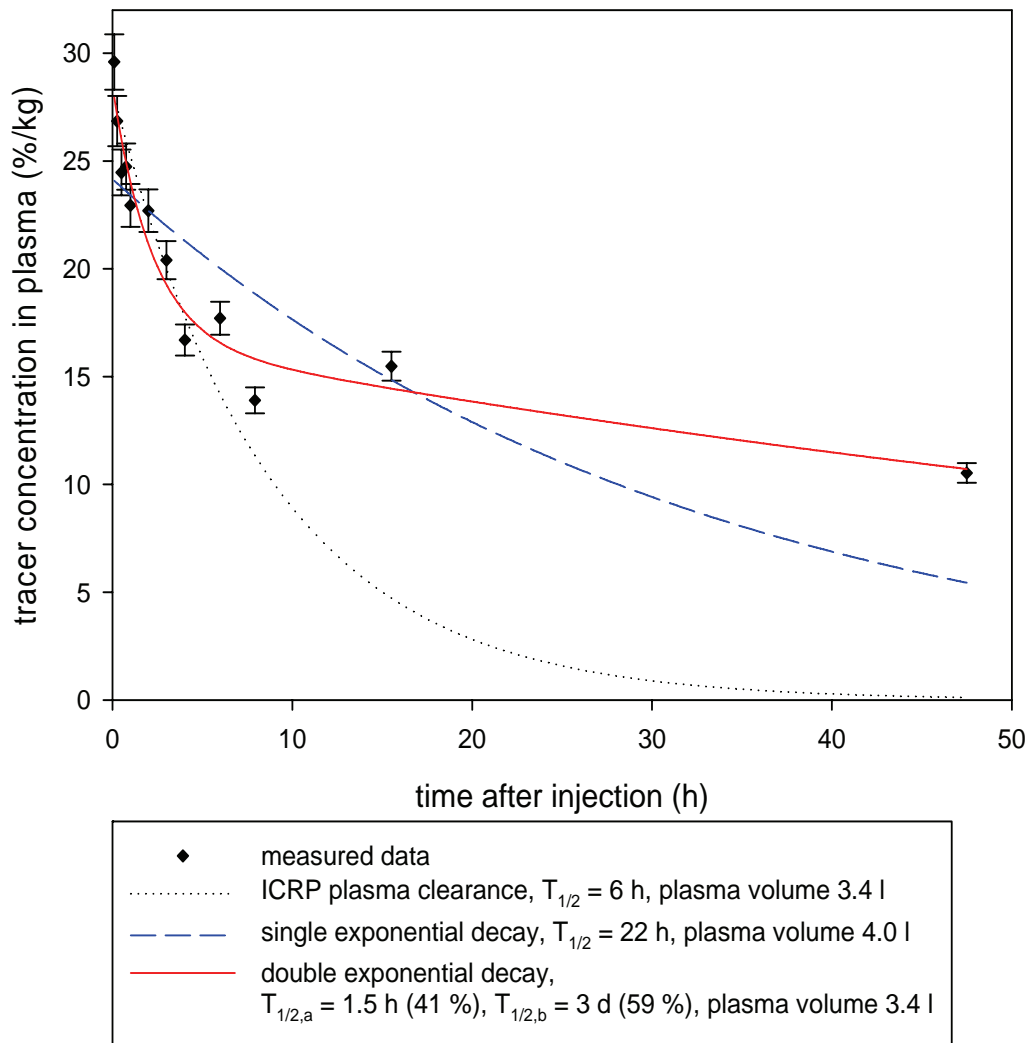


**Figure 6.11:** Data and various fits of plasma concentration of the intravenous tracer in Zr.26.15

In order to model this clearance, it is necessary to change the structure of the systemic model. This can be accomplished by adding at least one flux from the distribution compartments back to the transfer compartment.

In an initial modelling attempt, three systemic models were proposed as modifications to the current ICRP model presented in section 1.4. Their structures are depicted in Figures 6.12 – 6.14 below and the intention of the individual changes is explained briefly. Black arrows symbolise transfers adopted from the ICRP model; blue bold arrows indicate new transfers. All of these models were coupled to the new HAT model, which was introduced in ICRP publication 100 (ICRP 2006), by a direct transfer from small intestine to the transfer compartment.

In general, the two compartments ‘bone’ and ‘other tissues’ of the ICRP zirconium model were deprived of their attribution and assigned to abstract turnover compartments, since all transfer parameters should be available for variation. A further generalisation is the distribution of excretion into urinary excretion and any other pathways. The latter is termed ‘miscellaneous excretion’ and comprises all excreta which were not measured, e.g. faeces, sweat, and hair.

All prospect models were checked for theoretical a priori identifiability, based on an experimental scheme with two different tracers and concentration measurements in the transfer compartment (with unknown mass) and urine (known mass). Any necessary constraints are noted in the figure captions. The link between HAT model and the systemic model is not shown in the figures below, yet the identifiability tests were performed for the complete structure including the HAT model.

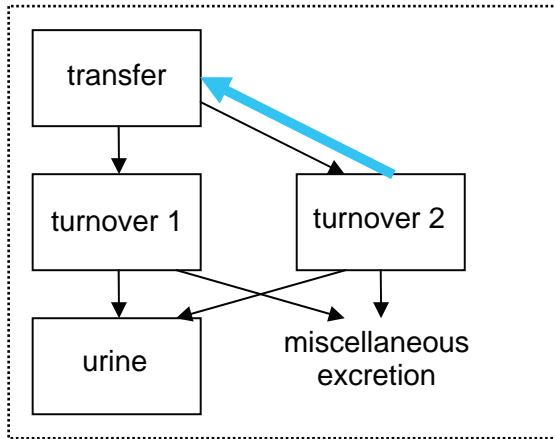


**Figure 6.13, 'Reflux' model:** Intending the least possible change as compared to the ICRP systemic model, a flux of zirconium from one turnover compartment back to the transfer compartment is added. The model is theoretically identifiable if the ratio of a pair of parameters is known, either between transfer and turnover 2, or for excretion from one of the turnover compartments. It is uniquely identifiable in the latter case.

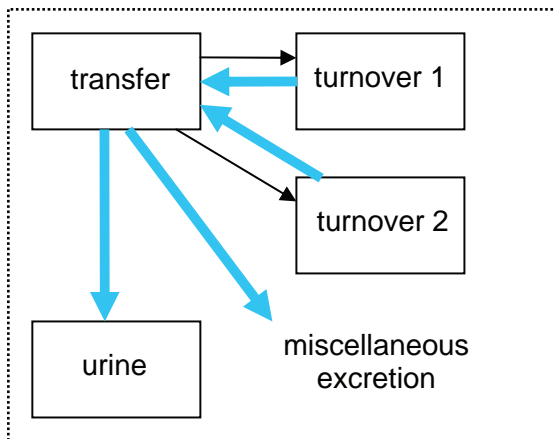


**Figure 6.12, 'Restructured' model:** Physiologically motivated, this model features direct excretion from the transfer compartment. As a side-effect, only two parameters instead of four are necessary to describe excretion. The model is theoretically identifiable without constraints. Unique identifiability can be attained by distinguishing between the two turnover compartments.

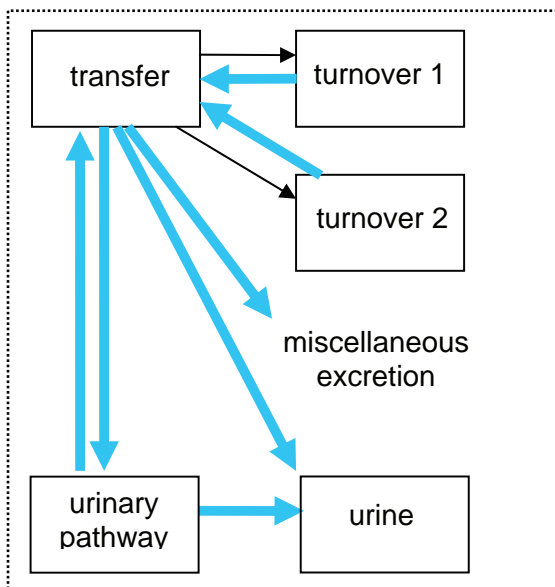


**Figure 6.14, 'Complex excretion' model:** Based on the restructured model, this model adopts a detailed urinary excretion pathway structure, motivated by (Guyton and Hall 2006). The model is theoretically identifiable with the same constraints as the restructured model.

All of the above models, as well as the ICRP model presented in section 1.4, were fitted individually to the data sets of the nine investigations evaluated in section 6.3.1 using the ‘data relative’ variance model (cf. section 5.2.2). Apart from the subjective, optical comparison of fitted curve to data, the resulting values of objective function, Akaike information criterion (AIC) and Schwarz-Bayesian information criterion (BIC) were compared.

Based on these comparisons, the following main results were obtained:

- (a) The modelled absorption of oral tracer into plasma was too slow. The reason for this was later attributed to the choice of variable parameters modelling absorption, i.e.  $\lambda_{\text{stomach} \rightarrow \text{small intestine (SI)}}$ ,  $\lambda_{\text{SI} \rightarrow \text{colon}}$ , and  $\lambda_{\text{SI} \rightarrow \text{transfer}}$ . One of these parameters must be kept fixed if the model shall be uniquely theoretically identifiable. The effect of the choice of variable parameters can be seen in Figure 6.15 and is discussed below.  
 The transfer parameters  $\lambda_{\text{SI} \rightarrow \text{colon}}$  (from small intestine (SI) to right colon or upper large intestine) and  $\lambda_{\text{SI} \rightarrow \text{transfer}}$  (from SI to the transfer compartment) are linked by the fractional absorption according to Equation 1.5. The fractional absorption is in turn influenced by the fitted ratio of oral to intravenous plasma concentration, which is quite well-defined by a long period of investigation.  
 The conflict between data and model arises because the fractional absorption is low, and the accordingly small value of  $\lambda_{\text{SI} \rightarrow \text{transfer}}$  causes a slow transfer of oral tracer into the transfer compartment. As a consequence, the transfer parameter from stomach to SI is increased during fitting to unreasonably high values to speed up the absorption, yet having little effect (Figure 6.15, fit (1)). This problem can be overcome to a large extent by fixing  $\lambda_{\text{stomach} \rightarrow \text{SI}}$ , varying  $\lambda_{\text{SI} \rightarrow \text{colon}}$  instead, which is related to  $\lambda_{\text{SI} \rightarrow \text{transfer}}$  by Equation 1.5, and thus allowing for substantial variation of  $\lambda_{\text{SI} \rightarrow \text{transfer}}$  (Figure 6.15, fit (2)).  
 As an alternative, the possibility of substance transfers from other compartments of the alimentary tract to the transfer compartment, as implemented in the HAT model, could be used. This option was tested for Zr.21.09 and Zr.26.15 by introducing additional transfers from oral cavity and stomach. The resulting fit for Zr.21.09 was acceptable, but the approach failed for Zr.26.15. As can be seen in Figure 6.15 (3), no satisfactory fit to oral tracer data could be obtained for the latter investigation, i.e. absorption was too slow and the data-typical absorption peak was too flat.
- (b) According to the minimised objective function, the best fit is usually obtained by the ‘complex excretion’ model. The two information criteria favour either the same model or the ‘restructured’ model due to the weighting of number of parameters. The fitted curves of the two preferred models are often similar in comparison with the other models, thus the additional complexity of the urinary pathway is unnecessary. Subsequently, the complex excretion model is excluded from further modelling. The ICRP model generally offers the worst fit to the data as expected from the above considerations on tracer clearance from plasma.
- (c) Similar to the fit results in section 6.3.1, the initial distribution volume is estimated by all models to be in the range of 1.7 – 4.3 l. This is consistent with the normal plasma volume of 3.0 l for a 70 kg adult person (Guyton and Hall 2006), scaled to the test persons’ variation in body weight and haematocrit, i.e. the fraction of blood volume composed of red blood cells. Thus, the transfer compartment can likely be identified with blood plasma; henceforth both being treated as synonyms.
- (d) Urinary excretion, especially of the oral tracer, was severely underestimated by all fitted models.

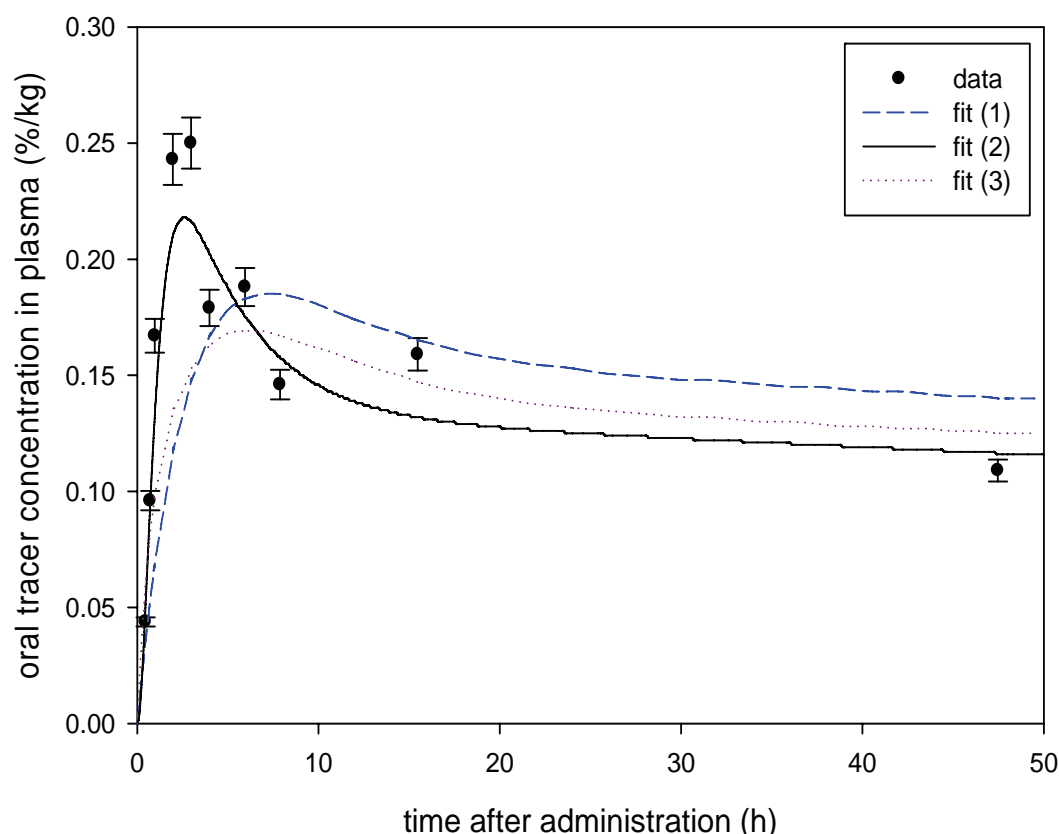


**Figure 6.15:** Various fits of the oral tracer concentration data in Zr.026.15 illustrating the discussion in (a) above. The fit options include: (1) absorption from small intestine, variation of  $\lambda_{\text{stomach} \rightarrow \text{SI}}$ ; (2) absorption from small intestine, variation of  $\lambda_{\text{SI} \rightarrow \text{colon}}$ ; (3) absorption from oral cavity, stomach and small intestine, with fixed default values of the HAT model parameters.

## An excursion into chemical speciation

Since during the first modelling cycle the absorption kinetic was modelled too slow as illustrated above in (a) and Figure 6.15 (fit 1), and especially urinary excretion of the oral tracer was severely underestimated (d), it was considered whether the biological behaviour of the two tracers might be different, contrary to the basic assumption of the double tracer methodology. The exact processes during transfer from the gut into the systemic circulation are unknown, and even the speciation of zirconium in plasma is unclear, thus the possibility of various slowly-exchanging, chemically different pools of zirconium cannot be neglected a priori.

Under the assumption that the different pools of zirconium, if existent, are connected by metabolic processes, two models were selected for further tests. The structure of both models is discussed below. Both models are based on the ‘restructured’ model preferred so far.

The first alternative, depicted in Figure 6.16 and termed ‘split transfer’ model, divides the transfer compartment, which is identified with plasma, into two compartments. Both divisions of the transfer compartment are individually connected to the turnover and excretion compartments of the ‘restructured’ model. The two transfer compartment divisions are

attributed to *different chemical form with similar stability*. These chemical forms are assumed to be generated initially from injected zirconium oxalate and by absorption processes from the gut, independent of the chemical form in which the oral tracer is administered. Over time, both tracers can be found in any compartment.

The second alternative (Figure 6.17, ‘transitory’ model) is based on the assumption of a common *stable, or chemically preferred, speciation of zirconium* within human metabolism, which *differs from the administered chemical forms*. The tracers are introduced into metabolism in initial transitory states, which may be excreted differently from the preferred common form, but are eventually converted to the preferred common form. Only the latter is distributed within the metabolism as previously described by the ‘restructured’ model. Each transitory compartment is exclusive to the respective administered tracer (i.v. or p.o.), whereas both tracers are distributed to all other compartments in the course of time.

In both alternatives, the plasma, or transfer compartment, includes multiple sub-compartments. Tracer concentrations in plasma are attributed to the total amount of tracer in all transfer sub-compartments, divided by the common plasma mass. The respective transfer compartment is indicated in Figures 6.16 and 6.17 by the dotted frames encompassing its divisions.

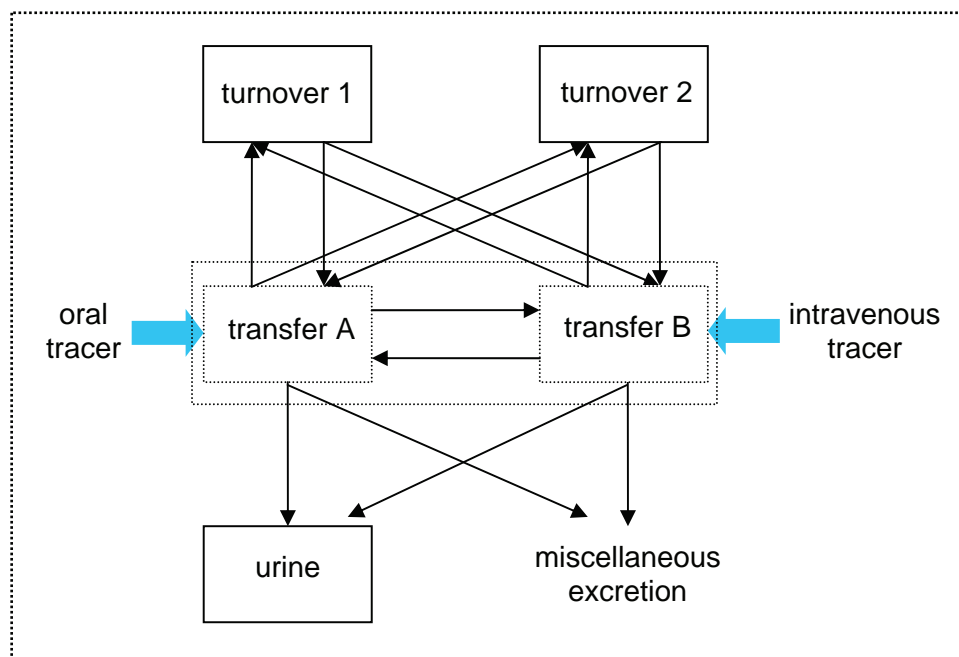


**Figure 6.16,** ‘Split transfer’ model:

The split transfer model is theoretically identifiable if and only if each of the two different tracers is initially introduced into its own distinct division of the transfer compartment. The model is uniquely identifiable if the two turnover compartments can be distinguished by additional information.

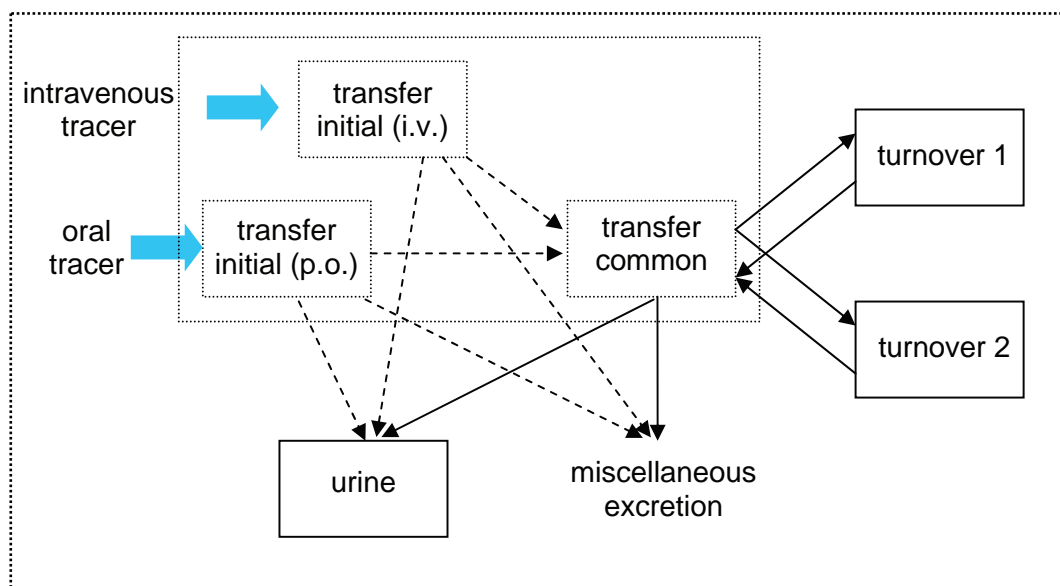


**Figure 6.17:** ‘Transitory’ model:

Dashed arrows indicate tracer-specific transfer rates. The dotted part represents the transfer compartment, consisting of three divisions, each representing a distinct chemical form of zirconium. This model is theoretically identifiable without further constraints. It is uniquely identifiable if the two turnover compartments can be distinguished by additional information.

Although the fitted curves of both models are usually better aligned to oral tracer data in plasma than the previously evaluated models, the following critical issues have to be pointed out:

- (e) The problem of underestimation of oral tracer data in urine is resolved at the cost of unreasonably high estimates of fractional absorption. Values of up to 10 % are found, which are in severe disagreement with both previous estimations as well as with the literature data referred to in section 6.3.1. In some investigations, urinary excretion of the oral tracer is now overestimated.
- (f) For many investigations, parameter estimates of fits with the ‘data relative’ variance model differ substantially from those with the ‘data absolute’ variance model. Parameter estimates therefore effectively depend more on the variance associated with a data set than on the data values themselves. In some cases, single values with different weighting according to the variance model have a large influence on the parameter estimates. A practically feasible model should in contrast be resistant to changes in data, or data variance, in order to give reproducible estimates for repeated experiments with slightly changed data sets.
- (g) Various parameters were frequently estimated to have zero value. For some parameters, e.g.  $\lambda_{\text{transfer\_A} \rightarrow \text{transfer\_B}}$ , this estimate was consistent for different experiments and variance models, indicating that such parameters are unnecessary to fit the data. Other parameter estimates were highly variable or alternatively estimated as zero between investigations.

Observations (f) and (g) indicate that the models with divided transfer compartments, although theoretically identifiable with the current experimental design, are practically not identifiable with the available data. The occasional dependence of parameter estimates on single measured values suggests that this problem is due to overfitting the data with too many free parameters, which are necessary to a certain degree for modelling tracers individually. For this reason, the implementation of individual tracer behaviour was suspended.

In order to find out whether the tracers actually have different biokinetic behaviours, it would be necessary to perform speciation measurements, i.e. to determine the chemical forms of the tracers in plasma and urine samples. For these measurements, a completely different measurement technique would be necessary, shifting them outside of the scope of the current study.

## Data bias

As stated above, the individual modelling of intravenous and oral tracers was based on two observations, namely slow absorption from the gut and substantial underestimation of oral tracer urinary excretion. Since no appropriate models were found to describe individual behaviour of tracers, these two issues were reinvestigated.

The first problem, slow absorption, was solved by changing the absorption-related modelled parameters, as described in (a) above, from  $\lambda_{ST \rightarrow SI}$  and  $\lambda_{SI \rightarrow transfer}$  to  $\lambda_{SI \rightarrow colon}$  and  $\lambda_{SI \rightarrow transfer}$ .

The second issue, underestimation of tracer excretion, was investigated prior to further modelling by calculation of the ratio of oral tracer excretion data over the respective fitted values. Median values of these ratios are in the range of 5 – 35 for investigations with citrate-buffered oral tracer solution, and 0.8 – 1.6 for zirconium oxalate administered in solution. Since the absorbed amount of tracer is smaller in the former investigations, and the concentrations measured in urine are correspondingly lower on average, the discrepancy between data and fitted curves could also be caused by positively biased concentration measurements for low concentrations. In this context, it is not important whether values below detection limit are simply omitted or replaced as described in section 5.2.2; the median of data-to-fit ratios of individual investigations changes, but the general difference between citrate and oxalate investigations still applies.

Another argument for the appropriateness of the initial ‘restructured’ and ‘reflux’ models is the scaled data variance of the oral tracer data in plasma. For data sets with similar uncertainties, a smaller scaling factor indicates a better consistency of data and model. In fits with a modified ‘restructured’ model, the scaling factors of citrate investigations were 15, 48, 49, 52, 54, and 114 for the oral tracer concentration in plasma, while the scaling factors of the three oxalate investigations were 8, 10, and 38. The range of further scaling factors is 1.5 – 13 for intravenous tracer concentrations in plasma, 2.4 – 15 for intravenous tracer in urine, and 4.6 – 37 for oral tracer in urine. The lowest three values of the latter are obtained for the oxalate investigations, similar to the plasma data results. Therefore, it is supposable that the increased variance in low-concentration measured data is a reason for deviation from principally appropriate models.

Consequently, the earlier fits of the ‘restructured’ and ‘reflux’ models were complemented by fits with the ‘data absolute’ variance model to check for deviations similar to those observed with the ‘split transfer’ and ‘transitory’ models and described in (f) above.

It was observed that the ‘reflux’ model is more stable concerning the variation of long-term single data values, which are very influential for fit results using the absolute variance model, since the variances are generally smaller. Except for Zr.24.11, parameter estimates from fits with absolute and relative variance models are in better agreement for the ‘restructured’ model. In general, also the parameter uncertainty estimates are smaller, thus the ‘restructured’ model is preferred for further analysis.

For five investigations, the parameter estimates of one turnover compartment are very small or zero in both models, yet have large uncertainties, indicating that one turnover compartment is redundant, and the model is practically not identifiable from the available data.

Since the estimated retention times of the turnover compartments are in the range of 0.6 min to ~200 d except for Zr.25.16, retention in bone seems to be neglected if the ICRP estimate of a biological half-life of 10,000 d in bone is assumed to be correct within its order of magnitude. To be consistent with the literature data on deposition of zirconium on bone on in animals (Hamilton 1947; Fletcher 1969) and the retention-time estimate of the ICRP (ICRP 1993), as well as to reduce the apparently too great number of free parameters, the retention half-life of one turnover compartment was fixed to 10,000 d as in the ICRP 67 model, thus associating this compartment with mineral bone.

The resulting modified ‘restructured’ model yields a better agreement between fits with the two variance models. However, one parameter still seems to be redundant, since in all but three fits, the transfer rate from plasma to non-urine excretion is estimated as zero. In the three remaining fits,  $\lambda_{\text{plasma} \rightarrow \text{bone}}$  is zero instead. Obviously no additional excretion beyond urine formation is necessary to describe the data, at least not within the duration of the investigations of up to 100 d. Owing to the long retention half-time of zirconium in bone, the immobilisation of zirconium in bone may substitute for additional slow excretion processes within the design of the investigations. Since a comparison with the ICRP model showed that retention in bone is not excessively increased by neglecting faecal excretion, the latter process was removed from the ‘restructured’ model. This may be a biologically questionable decision, but there seems to be no contradictory evidence on the excretion of previously absorbed zirconium in faeces, and the simplified model still provides a good description of the available data.

## Summary of model development

The following issues are essential for the model proposed in the current work:

- The measured concentrations of the intravenously injected tracer cannot satisfactorily be modelled with the current ICRP biokinetic model of zirconium. This issue can be solved by introducing bidirectional transfers between the transfer compartment and turnover compartments.
- The selection of parameters for variation is crucial for successful fitting of absorption processes from the alimentary tract. There is no evidence on absorption from compartments or organs other than the small intestine.
- The estimated transfer compartment volume suggests exclusive initial distribution in plasma.
- Data on urinary excretion of the oral tracer may either be biased, or indicate different biological behaviour of oral and intravenous tracer. The variance and scarcity of the available data prohibits practical identifiability of models accounting for the latter. In general, data loss due to non-detectable concentrations in measured samples substantially constrains the analysis of all long-term data, as well as of oral tracer excretion in urine.
- Due to the limited duration of investigations, long-term whole-body retention can only be covered by assumptions and is therefore based on the bone turnover rate adopted by the ICRP in its publication 67.

### 6.3.3 Proposed new model

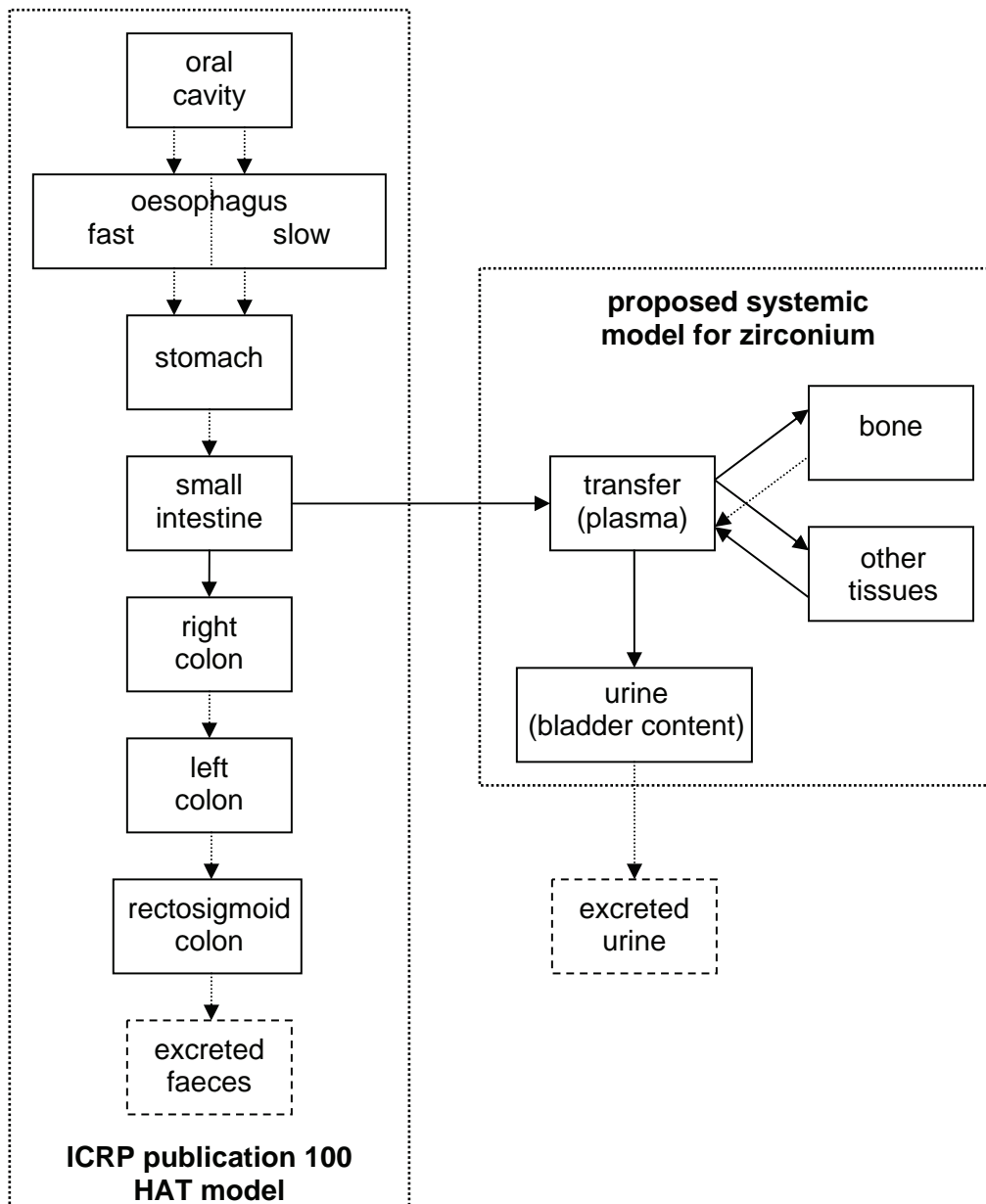


**Figure 6.18:** Proposed biokinetic model of zirconium, including the adopted human alimentary tract model from ICRP publication 100. Arrows indicate directional transfers between compartments. Solid arrows are associated with fitted parameters; ICRP default transfer rates were used for transfers with dotted arrows. Dashed compartment boundaries indicate that radionuclide transformations in these compartments do not contribute to the ingestion dose coefficients presented in section 6.4.

#### Evaluation of characteristic parameters

The final model presented in Figure 6.18 was fitted individually to the data of each of the nine studies, resulting in nine parameter sets. Since some of the parameter values reached their respective limits, thus preventing the calculation of parameter uncertainties by SAAM II, weighted mean values could not be given for all parameters in the first evaluation. The calculation of the arithmetic mean yields biased results, while the median is effectively only

dependent on the central values and is not affected by the magnitude of the deviation of extreme results.

To solve this problem, mean parameter values and standard deviations were calculated from the respective non-affected investigations for the relevant parameters. These population estimates were then used as input for a repetition of the fit process, including the Bayesian estimation option provided by SAAM II (cf. section 5.2.2) for the parameters at limit.

In the investigations Zr.20.09, Zr.24.11 and Zr.11.12, the clearance rate  $\lambda_{\text{SI} \rightarrow \text{RC}}$  from small intestine to right colon (RC) exceeded  $50 \text{ h}^{-1}$ . When compared with the information compiled in ICRP publication 100, this seems to be rather unphysiological. The reason for such high rates may be an artefact of the first-order kinetic model. If the model is fitted to p.o. tracer plasma data without a pronounced absorption peak, a very steep increase at the start of the investigation can result, with a slow decline of tracer concentration afterwards. This was the case for the three investigations named above, and could be avoided by using Bayesian estimation. The population (weighted) mean for  $\lambda_{\text{SI} \rightarrow \text{RC}}$  calculated from the rest of the nine studies was  $0.59 \text{ h}^{-1}$ , and the population standard deviation was  $2.8 \text{ h}^{-1}$ . With these characteristic values, the fit process was repeated. It provided more reasonable values for  $\lambda_{\text{SI} \rightarrow \text{RC}}$  as well as an estimate of parameter uncertainty, while changing little the values for the rest of the parameter sets.

A similar approach was followed for  $\lambda_{\text{transfer} \rightarrow \text{bone}}$  in Zr.01.03 and Zr.20.19. The reason why this transfer parameter was estimated to zero in the two experiments was likely that their duration was limited to 2 d, hence any estimate for long-term retention would at least have a large uncertainty, if it was not outright zero. The effect of unavailable long-term measurements can be seen in Figure 6.11; the ICRP curve is an adequate description of the data until  $\sim 8 \text{ h}$ , when the contribution of the second exponential decay function becomes clearly perceptible. The population values of  $\lambda_{\text{transfer} \rightarrow \text{bone}}$  were  $4.9 \cdot 10^{-3} \text{ h}^{-1}$  (weighted mean) and  $2.1 \cdot 10^{-3} \text{ h}^{-1}$  (standard deviation). Again, the fit process including Bayesian estimation yielded visually good fits and uncertainty estimates for  $\lambda_{\text{transfer} \rightarrow \text{bone}}$  with little change in the remaining parameters.

The estimates of fractional absorption, which were calculated from  $\lambda_{\text{SI} \rightarrow \text{colon}}$  and  $\lambda_{\text{SI} \rightarrow \text{transfer}}$  by Equation 1.5, are in good accordance with the results presented in section 6.3.1 above. Absolute deviations from the means of the values in Table 6.5 are below  $2.5 \cdot 10^{-4}$  within each investigation, except for Zr.20.14, which yields an estimate of  $f_A = 2.0 \cdot 10^{-3}$  from the model, in contrast to the earlier value of  $2.8 \cdot 10^{-3}$ . The mean relative deviation of model estimates from the values in Table 6.5 is -7 % including Zr.20.14, or -4 %, excluding Zr.20.14.

The final population estimates of all fitted parameters are calculated as weighted means from the individual studies. The systemic parameters  $\lambda_{\text{transfer} \rightarrow \text{other tissue}}$ ,  $\lambda_{\text{OT} \rightarrow \text{transfer}}$ ,  $\lambda_{\text{transfer} \rightarrow \text{bone}}$ ,  $\lambda_{\text{transfer} \rightarrow \text{urine}}$ , and plasma mass show little difference between citrate and oxalate tracer investigations, whereas  $\lambda_{\text{SI} \rightarrow \text{transfer}}$  is clearly dependent on tracer speciation.  $\lambda_{\text{SI} \rightarrow \text{colon}}$  is highly variable, but the difference between the weighted mean values of citrate and oxalate investigations is comparatively small, given the large uncertainty within both groups.  $\lambda_{\text{SI} \rightarrow \text{colon}}$  can therefore be assumed to be independent of tracer speciation, at least for the two administered non-caloric tracer solutions.

Fractional absorption coefficients  $f_A$  can either be calculated as weighted mean from the individual investigations, or from the expected values of the parameters  $\lambda_{\text{SI} \rightarrow \text{colon}}$  and  $\lambda_{\text{SI} \rightarrow \text{transfer}}$ . The former alternative is preferred, since in the latter case, the resulting  $f_A$  values are not consistent with the individual investigation results. Furthermore, the time-invariant  $f_A$  values have a greater significance than the above transfer rates for bioassay measurements of urine excretion, as well as for zirconium retention in the body beyond a few days and its

consequences for dosimetry. The consistency of  $f_A$  values within the two speciation groups in comparison with large uncertainties estimates for  $\lambda_{SI \rightarrow colon}$  and  $\lambda_{SI \rightarrow transfer}$  suggests that speciation-specific estimates for  $\lambda_{SI \rightarrow transfer}$  should not be calculated as weighted means from the individual investigations, but should instead be derived from the speciation-specific weighted means of  $f_A$  and the general weighted mean of  $\lambda_{SI \rightarrow colon}$  from all nine investigations. The resulting parameters are listed in Table 6.6. The uncertainties given are standard deviations of the mean, with  $n = 9, 6,$  and  $3$  for all investigations, citrate investigations, and oxalate investigations, respectively.

**Table 6.6:** Parameter estimates from fitted data for nine investigations. Fixed parameters are not included.

<b>Parameter, all investigations</b>	<b>Expected value (h<sup>-1</sup>)</b>	<b>Uncertainty, absolute (h<sup>-1</sup>)</b>
$\lambda_{SI \rightarrow colon}$	0.6	0.7
$\lambda_{other\ tissue \rightarrow transfer}$	$9.0 \cdot 10^{-2}$	$1.4 \cdot 10^{-2}$
$\lambda_{transfer \rightarrow other\ tissue}$	$8.9 \cdot 10^{-2}$	$1.8 \cdot 10^{-2}$
$\lambda_{transfer \rightarrow bone}$	$4.9 \cdot 10^{-3}$	$0.7 \cdot 10^{-3}$
$\lambda_{transfer \rightarrow urine}$	$5.1 \cdot 10^{-4}$	$0.7 \cdot 10^{-4}$
Plasma mass (kg)	3.39	0.19
<b>citrate investigations</b>		
$\lambda_{SI \rightarrow transfer}$	$6.3 \cdot 10^{-4}$	$7.8 \cdot 10^{-4}$
$f_A$	$1.0 \cdot 10^{-3}$	$0.3 \cdot 10^{-3}$
<b>oxalate investigations</b>		
$\lambda_{SI \rightarrow transfer}$	$4.7 \cdot 10^{-3}$	$5.8 \cdot 10^{-3}$
$f_A$	$7.7 \cdot 10^{-3}$	$1.3 \cdot 10^{-3}$

Even though the standard deviation of the mean of  $\lambda_{SI \rightarrow colon}$  is greater than the parameter value, negative parameter values are impossible in first-order kinetic compartment models. The same holds true for the propagated uncertainty of  $\lambda_{SI \rightarrow transfer}$ , because this parameter is derived from  $\lambda_{SI \rightarrow colon}$ . The low value of  $\lambda_{SI \rightarrow colon}$  is a result of weighting in the calculation of the weighted mean, which in this case favours small measured values.

Although some bias is introduced by this calculation, which is also visible in the delayed rise of the modelled concentration curve in Figure 6.20, the low parameter value is more consistent with the ICRP value of  $0.25\text{ h}^{-1}$  (ICRP 2006) than are either the arithmetic mean ( $3.0\text{ h}^{-1}$ ) or the median ( $3.1\text{ h}^{-1}$ ). The large individual estimates of  $\lambda_{SI \rightarrow colon}$  are in turn caused by the formulation of the model with first-order kinetics, combined with low fractional absorption and a relatively fast rise in tracer concentration. Since absorption from other compartments of the alimentary tract does not resolve this problem as was discussed above, the discrepancy between literature data and fit results is an indication that first-order kinetics may not be appropriate for the description of absorption processes of zirconium. However, since the current purpose of this model is the calculation of ingestion dose coefficients, which have a large inherent uncertainty due to individual differences of persons from the reference man, the bias introduced by first-order kinetics is considered acceptable in this case.

Figures 6.19 – 6.21 below illustrate the variation of measured data, and in some cases individual fits, from the modelled zirconium concentration after intravenous injection or ingestion. The shown uncertainties are the uncertainties discussed in section 4, scaled according to the investigation-specific variance parameters evaluated with the ‘data relative’ variance model by the modelling software SAAM II. Table 6.7 gives an overview on the respective scaling factors.

**Table 6.7:** Uncertainty scaling factors derived from SAAM II fit results.

Please remember that the mean urine uncertainties are estimated to be ~ 4 times larger than plasma uncertainties prior to scaling due to the sampling behaviour.

Investigation	Plasma		Urine	
	i.v. tracer	oral tracer	i.v. tracer	oral tracer
Zr.01.03	2.2	6.2	1.5	5.4
Zr.21.09	2.1	9.3	1.5	4.7
Zr.22.10	1.1	3.5	1.6	4.7
Zr.24.11	1.6	6.6	2.6	4.3
Zr.11.12	2.5	6.4	3.6	4.3
Zr.20.14	1.7	6.6	1.4	3.1
Zr.26.15	1.7	2.9	1.7	3.0
Zr.25.16	2.6	5.7	2.7	2.0
Zr.20.19	3.3	2.5	1.4	2.3
Range	1.1 – 3.3	2.5 – 9.3	1.4 – 3.6	2.0 – 5.4

In general, the scaling factors are greater than unity, which could be caused by a combination of several reasons.

First, the model may not be completely appropriate to fit the data. With its simple compartmental structure, the model is likely only an approximation of more complex metabolic processes; however, the fitted model curves are generally in good accordance with the data. As a consequence, the scaling factors can be expected to be greater than, but close to unity.

A second reason can be that some components of the measurement uncertainties are larger than assessed in section 4. This is especially likely for estimated type B uncertainties. Type A uncertainties can principally also be underestimated, especially if changes in experimental conditions occurred, yet were not recognised.

Finally, additional components of uncertainty could affect the results. Possible further components of uncertainty which were not or could not be quantified include:

- urine loss during collection;
- total fluid balance, e.g. losses by sweat, diarrhoea, or vomiting;
- ingested volume of liquids;
- effect of food and beverage contents on urine production.

The scaling factors are greater for oral tracer data than for intravenous tracer data, but their range is similar for plasma and urine data of each tracer. The difference between tracers might be expected for measurement uncertainty values due to the generally lower oral tracer concentrations. This was not observed; the range and median of measurement uncertainties of T-91 and T-96-L in plasma, which were exclusively used as oral tracers in citrate investigations with low absorption, are similar to those of T-90 and T-96-H, which were used both as oral and intravenous tracers. Furthermore, the greater scaling factors are not attributable to test person behaviour, like e.g. drinking speed or prolonged retention within the mouth, since such effects would cause systematic biases, but not increased variance.

The large deviations for oral data, combined with similarities in plasma and urine, might be caused by different tracer behaviour as discussed in section 6.3.2. However, the number of measurements and the relative uncertainties are similar for the two tracers in plasma, hence both tracers should be treated similarly by the modelling software. In the case of different tracer behaviour, the scaling factors of plasma data would also be expected to be similarly large for both tracers, indicating that the model parameters are not correct for either of the tracers.

With a closer look at individual investigations, the worse fit of oral tracer data compared to i.v. tracer data can be attributed to noise in the oral tracer data and thus disagreement between data and modelled curves. For Zr.22.10, Zr.26.15, and Zr.20.19, the scaling factors of oral tracer data in plasma are relatively low. This coincides with clearly perceptible absorption peaks and relatively little noise, as can be seen in Figures 6.19 and 6.20. Other experiments either lack pronounced absorption peaks due to large noise or single outlying values, resulting in a poor fit of the smooth curve determined by the model.

Oral tracer data in urine and, for very short or long times after tracer administration also in plasma, further suffer from high measurement detection limits. Whereas only 4 of 115 measured values of intravenous tracer concentration in plasma were below the respective detection limits, 13 of 112 concentration values of oral tracer in plasma and 51 of 77 in urine were not detectable. Of these, 5 values of oral tracer in plasma and 26 in urine were substituted according to the approach described in section 5.2.2. Thus, the large scaling factors of oral tracer in urine may well be caused by a severe lack of data.

The comparison of model and data for intravenously injected zirconium in Figure 6.19 shows that the set of mean parameters presented in Table 6.6 yields an appropriate fit to the collected data. The predicted zirconium concentration in plasma can be described by a triple exponential decay function, with clearance half-lives of 3.8 h, 10.8 d, and  $\sim 280$  y for fractions of 51 %, 49 %, and  $< 1$  % of injected zirconium, respectively. The slowest clearance term is obviously a consequence of the implementation of the ICRP value of bone turnover rate and accounts for differences from a double exponential decay starting to be discernible at  $\sim 75$  d. Its contribution should not be weighted too much, as even the longest investigations are limited to 100 d; yet it is not negligible for medium- to long-lived radioisotopes of zirconium, i.e.  $^{93}\text{Zr}$  with its half-life of  $1.5 \cdot 10^6$  y and  $^{95}\text{Zr}$  (64 d), since this term accounts for continued excretion from plasma to urine.

However, the distribution between the different plasma clearance processes is not optimal; starting at  $\sim 10$  h, the model overestimates the data, yet all measured values at 100 d after tracer administration are larger than the model prediction. The same holds true for oral tracer data presented below, although less oral data is available due to the TIMS detection limit.

If the prediction is compared to model fits of individual investigations, which are not shown for sake of clarity except in Figure 6.21, it is perceptible that the model in its current state has limitations in fitting long-term data.

In recall of the considerations in the previous section, many structural options are possible to improve the proposed first-order kinetic model, but these are practically not identifiable with the currently available data.

Important enhancements of double tracer investigations in this context would therefore be additional sampling times between 2 d and 30 d, and improvements to the measurement technique(s) in order to lower the detection limit, especially for the oral tracer, to enable reliable measurements of samples beyond 100 d.

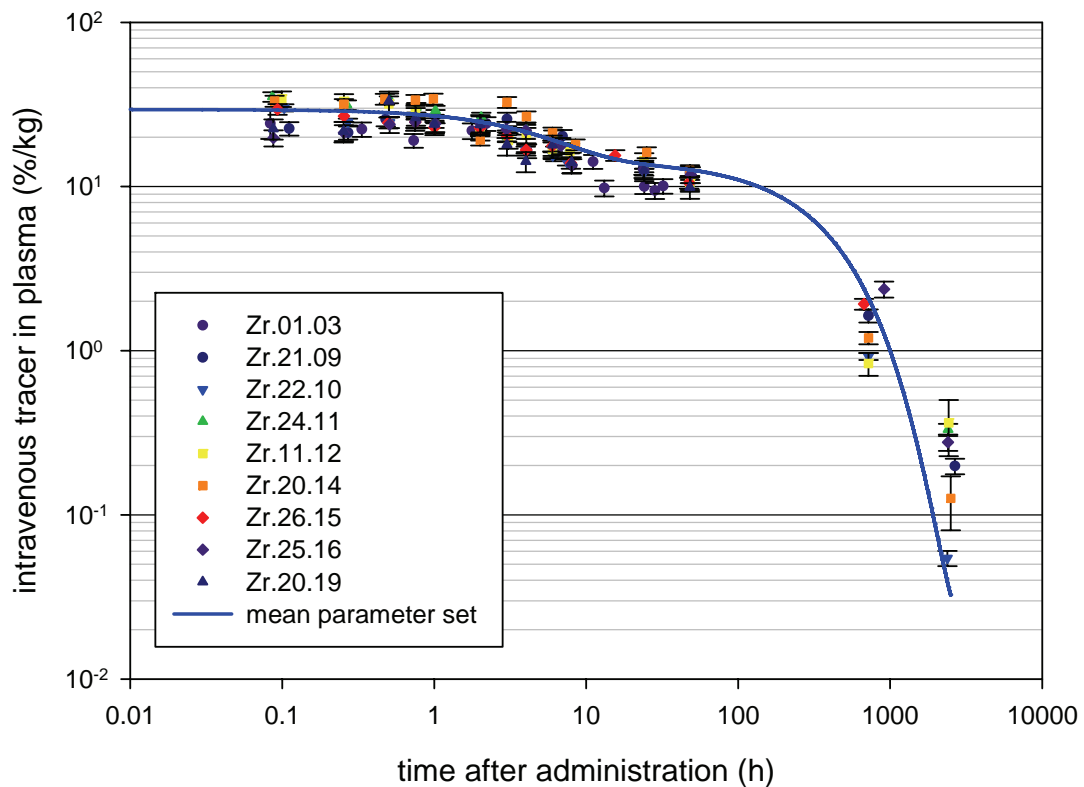
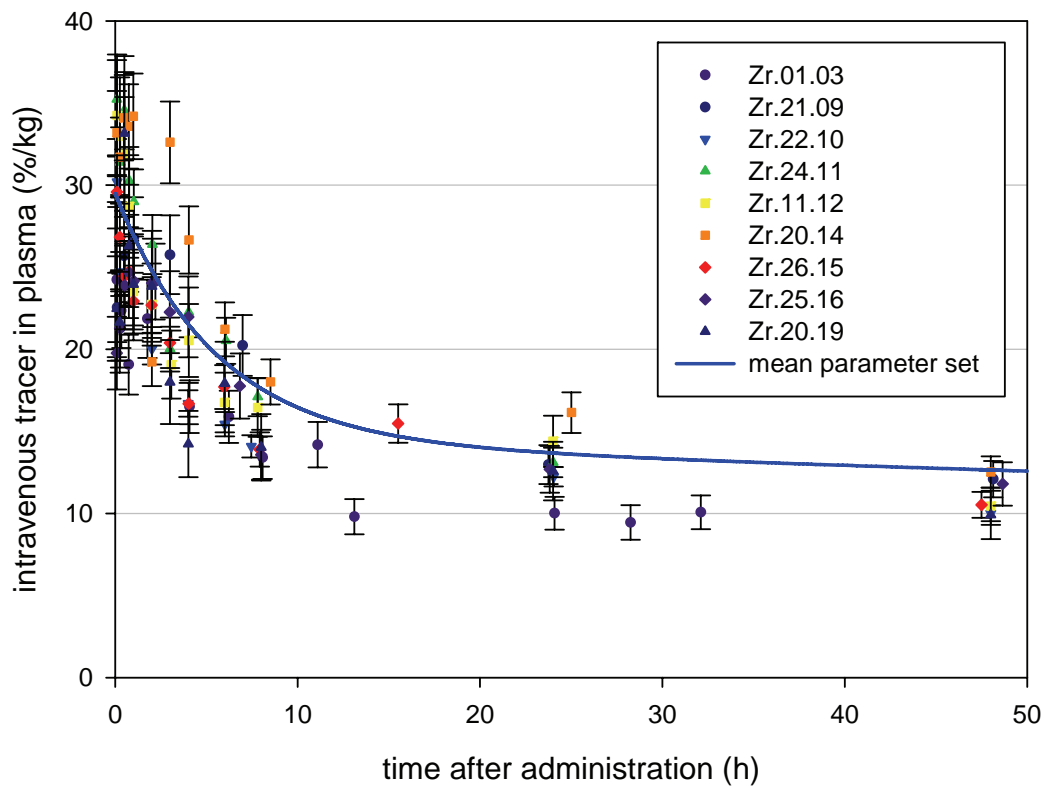


**Figure 6.19:** Intravenous tracer concentration data in plasma and the respective estimate of the proposed model with the set of mean parameters presented in Table 6.6.

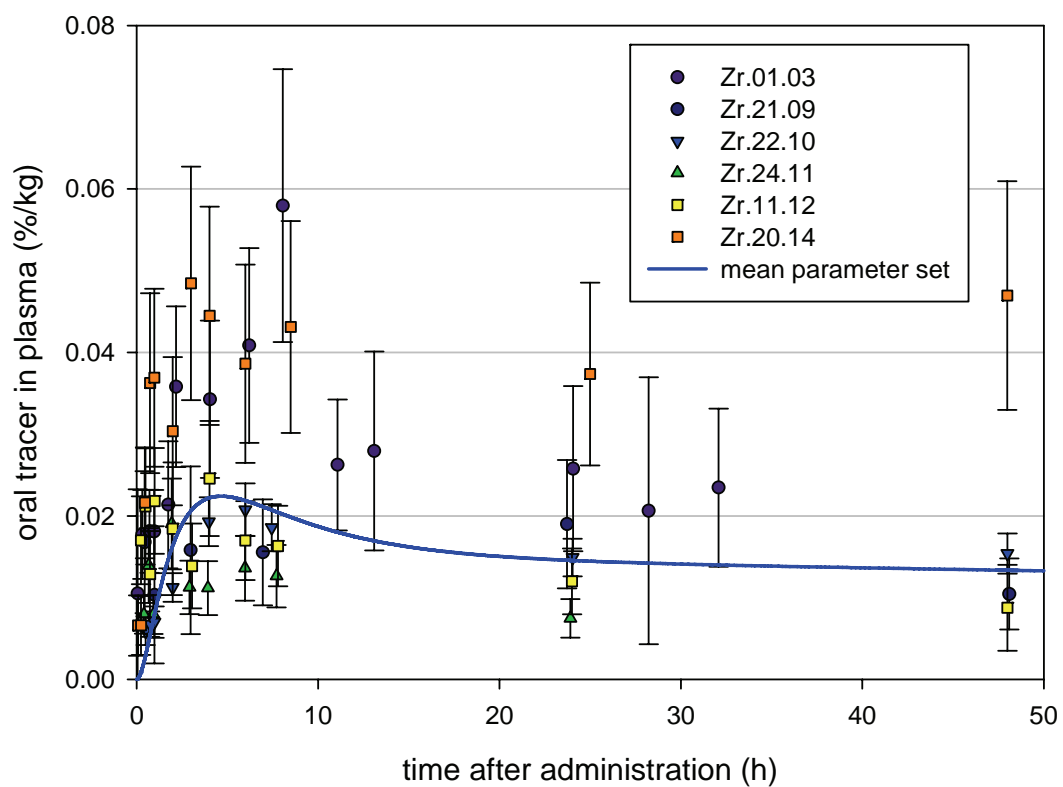


**Figure 6.20:** Oral tracer concentration data in plasma from citrate investigations and the respective estimate of the proposed model.

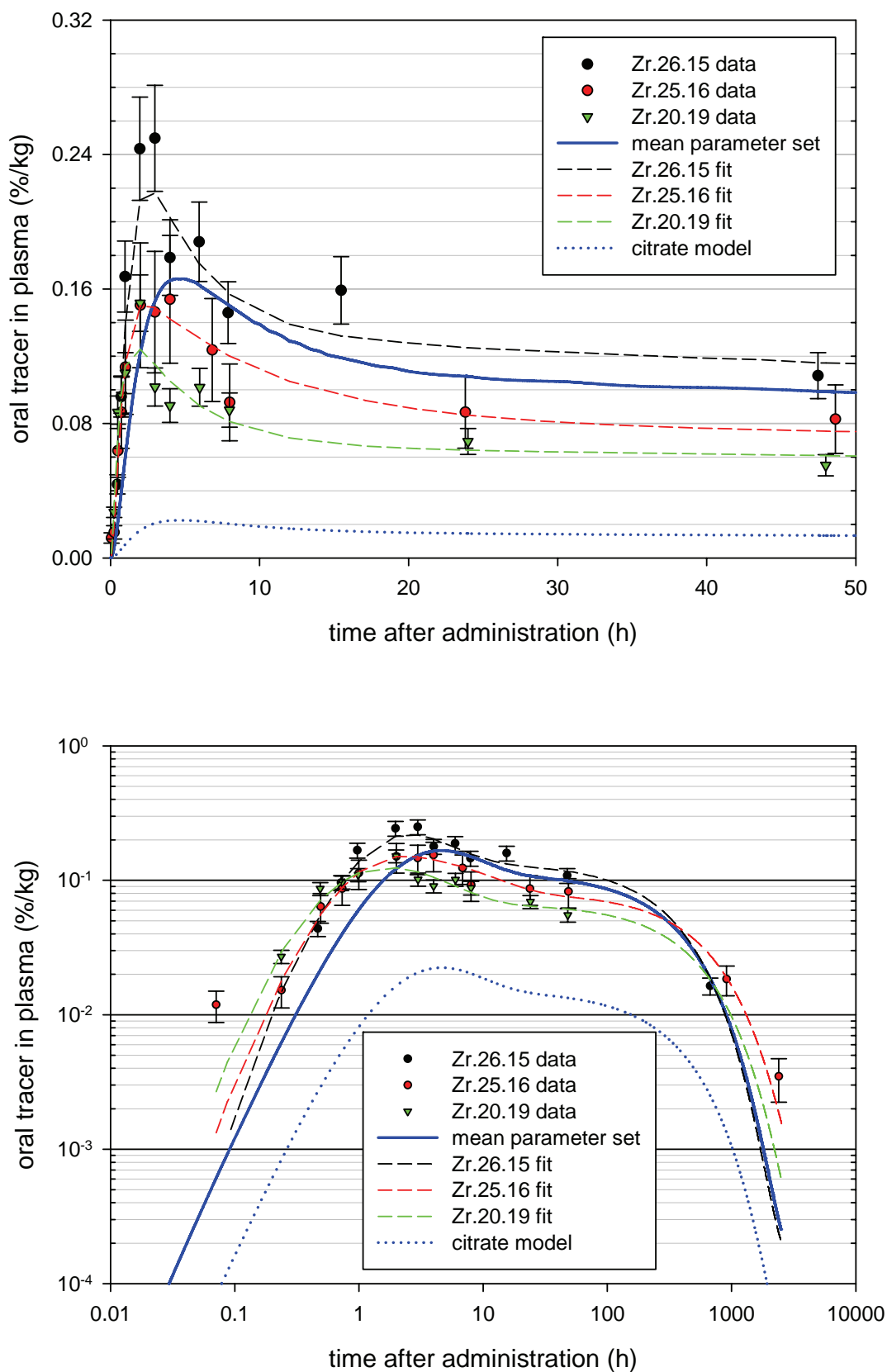


**Figure 6.21:** Oral tracer concentration data in plasma from oxalate investigations, individual fits to the oxalate investigation data, and the estimate of the proposed model. The estimated concentration curve of zirconium ingested in citrate-buffered solution is given for comparison as dotted curve (cf. Figure 6.20).

## 6.4 Dosimetry

The new biokinetic model proposed in the previous section differs from the current ICRP model (cf. section 1.4) in three essential ways:

- The structure of the systemic model has been altered to include recycling by bidirectional transfers, giving rise to increased zirconium concentrations in the blood plasma. Radioisotopes of zirconium will therefore be continually redistributed over the whole body, resulting in a shift in the number of transformations between the source regions ‘other tissues’ and ‘bone’.
- The new systemic model is coupled to the human alimentary tract model (HATM) of ICRP publication 100 (ICRP 2006), while the ingestion dose coefficients of ICRP publication 67 (ICRP 1993) were calculated using the older GI tract model. This change implies two new source organs (oral cavity and oesophagus) for dose calculation, as well as slightly different residence times within the lower sections of the alimentary tract.
- The current ingestion dose coefficients for  $^{95}\text{Zr}$  were calculated for the ICRP reference man, neglecting gender differences. Since the HATM includes some gender-specific transfer rates, and sets of *SEE* values exist for both male and female reference persons, the dose coefficients of the new model were calculated gender-specific.

### 6.4.1 Reproducibility of ICRP ingestion dose coefficients

The modelling procedure was tested by using the ICRP model as presented in section 1.4 to recalculate the current ingestion dose coefficients from ICRP publication 67 (ICRP 1993), to ensure correct calculation procedures.

In publication 56 (ICRP 1990), the ICRP states that “if a radionuclide has radioactive decay products, the contribution to dose from their build-up in the body is included [in the dose coefficient calculation]. However, specific biokinetic data are given for these [decay products] only when experimental evidence is available on their biological behaviour. In all other cases the biokinetic behaviour of the radioactive decay products is assumed to be the same as that of the parent radionuclide taken into the body.”

The ICRP provides a specific model for niobium, hence it can be assumed that the distribution of its isotopes should be modelled according to their own biokinetic characteristics. Niobium transformed from zirconium in unspecified ‘other tissues’ (other than bone) is then distributed within the three niobium compartments ‘liver’, ‘kidneys’ and ‘other tissues’ (other than bone, liver and kidneys), according to their mass fractions, under the premise of an even distribution within the tissues of each compartment.

The resulting ingestion dose coefficients disprove this assumption; apparently the ingestion dose coefficients in ICRP publication 67 (ICRP 1993) were calculated with niobium following the zirconium distribution and biokinetic model. The published and modelled dose coefficients are shown in Table 6.8.

The small deviations between the dose coefficients from ICRP publication 67 and the zirconium biokinetic model results (‘Zr biokinetics’) are likely due to rounding uncertainties either in parameters or during the numerical computation of the number of transformations in 50 y with SAAM II. Tentatively setting the model parameters to 2-digit instead of 4-digit accuracy changes dose coefficients by up to ~ 1 %. A second, independent recalculation with the same software and parameters was performed by Dr. Weibo Li (GSF), who used a different numerical approach to calculate the number of transformations in 50 y, but the same

SEE values. The resulting dose coefficients showed slightly changed deviations from the ICRP dose coefficients of up to 6.7 %.

As a consequence of this comparison, the general modelling and calculation procedure is assumed to be correct due to the reproducibility of the published ingestion dose coefficients. The relative uncertainty of the numeric calculation is estimated as ~ 2 %, based on the distribution of relative deviations presented in Table 6.8 (column ‘Zr biokinetics’).

**Table 6.8:** Comparison of ingestion dose coefficients ( $\text{Sv}\cdot\text{Bq}^{-1}$ ), calculated according to ICRP recommendations as of publication 67. Both sets of modelled results include the dose contribution from  $^{95}\text{Nb-m}$  and  $^{95}\text{Nb}$ , but niobium was distributed either according to the zirconium biokinetic model (‘Zr biokinetics’) or according to its own model (‘Nb biokinetics’).

Target region	Published ICRP 67	Modelled Zr biokinetics	Modelled Nb biokinetics	Deviation (% of ICRP 67)	
				Zr biokinetics	Nb biokinetics
Adrenals	$1.3\cdot 10^{-10}$	$1.3\cdot 10^{-10}$	$1.1\cdot 10^{-10}$	3	-12
Bladder wall	$2.9\cdot 10^{-10}$	$2.9\cdot 10^{-10}$	$2.8\cdot 10^{-10}$	-2	-3
Bone Surface	$2.3\cdot 10^{-9}$	$2.2\cdot 10^{-9}$	$1.9\cdot 10^{-9}$	-2	-16
Brain	$5.3\cdot 10^{-11}$	$5.3\cdot 10^{-11}$	$4.2\cdot 10^{-11}$	1	-21
Breast	$3.7\cdot 10^{-11}$	$3.7\cdot 10^{-11}$	$3.2\cdot 10^{-11}$	0	-14
ST wall	$3.9\cdot 10^{-10}$	$3.8\cdot 10^{-10}$	$3.8\cdot 10^{-10}$	-2	-4
SI wall	$1.1\cdot 10^{-9}$	$1.1\cdot 10^{-9}$	$1.1\cdot 10^{-9}$	-3	-4
ULI wall	$3.1\cdot 10^{-9}$	$3.0\cdot 10^{-9}$	$3.0\cdot 10^{-9}$	-2	-2
LLI wall	$7.8\cdot 10^{-9}$	$7.8\cdot 10^{-9}$	$7.8\cdot 10^{-9}$	0	0
Kidneys	$1.7\cdot 10^{-10}$	$1.6\cdot 10^{-10}$	$1.5\cdot 10^{-10}$	-3	-10
Liver	$1.1\cdot 10^{-10}$	$1.1\cdot 10^{-10}$	$1.0\cdot 10^{-10}$	-3	-8
Lungs	$6.0\cdot 10^{-11}$	$6.0\cdot 10^{-11}$	$5.1\cdot 10^{-11}$	0	-16
Muscle	$1.4\cdot 10^{-10}$	$1.4\cdot 10^{-10}$	$1.3\cdot 10^{-10}$	-3	-9
Ovaries	$8.8\cdot 10^{-10}$	$8.7\cdot 10^{-10}$	$8.6\cdot 10^{-10}$	-1	-2
Pancreas	$1.5\cdot 10^{-10}$	$1.5\cdot 10^{-10}$	$1.4\cdot 10^{-10}$	-2	-9
Red marrow	$4.8\cdot 10^{-10}$	$4.8\cdot 10^{-10}$	$4.2\cdot 10^{-10}$	0	-13
Skin	$6.3\cdot 10^{-11}$	$6.3\cdot 10^{-11}$	$5.7\cdot 10^{-11}$	0	-9
Spleen	$1.1\cdot 10^{-10}$	$1.1\cdot 10^{-10}$	$1.0\cdot 10^{-10}$	1	-5
Testes	$1.0\cdot 10^{-10}$	$1.0\cdot 10^{-10}$	$1.0\cdot 10^{-10}$	4	1
Thymus	$4.3\cdot 10^{-11}$	$4.3\cdot 10^{-11}$	$3.6\cdot 10^{-11}$	1	-15
Thyroid	$4.3\cdot 10^{-11}$	$4.2\cdot 10^{-11}$	$3.4\cdot 10^{-11}$	-1	-20
Uterus	$4.0\cdot 10^{-10}$	$4.0\cdot 10^{-10}$	$3.9\cdot 10^{-10}$	0	-2
Remainder	$1.5\cdot 10^{-10}$	$1.5\cdot 10^{-10}$	$1.4\cdot 10^{-10}$	1	-5
Effective dose	$9.6\cdot 10^{-10}$	$9.7\cdot 10^{-10}$	$9.5\cdot 10^{-10}$	1	-1

#### 6.4.2 Influence of daughter radionuclide modelling on dose coefficients

The relative deviations between ICRP dose coefficients and the dose coefficients obtained from modelling daughter products with their own biokinetic model (‘Nb biokinetics’ in Table 6.8) are clearly higher than those associated with the previous approach; their range is -21 % to +1 %, in contrast to -3 % to +4 %.

The main difference in model parameters is the shorter retention time in mineral bone for niobium (50 % retained for 6 d and 50 % for 200 d) as compared to zirconium (10,000 d). Therefore, substantially more transformations of niobium occur in bone surfaces if the zirconium biokinetic model is used for niobium, and all target tissues close to bone surfaces (e.g. the brain in the cranial cavity) accordingly receive a higher dose. Doses to kidneys and

liver, although both being source compartments subject to beta radiation in the niobium model, are not increased by using the niobium model. The reason is likely that the major fraction of absorbed zirconium is excreted from ‘other tissues’ before a substantial amount is transformed to niobium, since the biological half-time in ‘other tissues’ is set to 7 d and the radioactive half-life is 64 d.

It is not clear why the ICRP did not use the niobium model for  $^{95}\text{Nb}$ . The niobium model was even changed from publication 30 to 56 due to additional data, thus evidence is indeed available on the biological behaviour of this element. In the further discussion, the biokinetic model of niobium is used to model niobium distribution for the determination of dose coefficients, in consistency with the above-cited statement in ICRP publication 56 (ICRP 1990). Unless otherwise stated, all further comparisons concerning the proposed new zirconium model refer to the dose coefficients calculated with the distribution of  $^{95}\text{Nb}$  according to the niobium model.

### 6.4.3 Gender differences due to SEE values

The SEECAL software (Eckerman 1993), which provides the standard reference man *SEE* values for the calculation of dose coefficients, includes also *SEE* values for a female standard person. In order to be able to distinguish between *SEE*-related and model-related differences in dose coefficients, it is suggestive to evaluate what differences in dose coefficients result from the use of these two sets of *SEE* values.

Table 6.9 lists the dose coefficients for both male and female persons, calculated from identical numbers of transformations, which were obtained from the ICRP zirconium model (cf. section 1.4) and with niobium kinetics for transformation products.

**Table 6.9:** Dose coefficients ( $\text{Sv}\cdot\text{Bq}^{-1}$ ) for male and female reference persons calculated from the ICRP publication 67 zirconium model with niobium daughter kinetics.

Target region	Dose coefficients with male SEEs	Dose coefficients with female SEEs	Deviation of female from male (%)
Adrenals	$1.14\cdot 10^{-10}$	$1.45\cdot 10^{-10}$	+27
Bladder wall	$2.82\cdot 10^{-10}$	$3.35\cdot 10^{-10}$	+19
Bone Surface	$1.93\cdot 10^{-9}$	$2.56\cdot 10^{-9}$	+32
Brain	$4.16\cdot 10^{-11}$	$4.87\cdot 10^{-11}$	+17
Breast	$3.19\cdot 10^{-11}$	$3.79\cdot 10^{-11}$	+19
ST wall	$3.76\cdot 10^{-10}$	$4.43\cdot 10^{-10}$	+18
SI wall	$1.06\cdot 10^{-9}$	$1.26\cdot 10^{-9}$	+19
ULI wall	$3.03\cdot 10^{-9}$	$3.35\cdot 10^{-9}$	+11
LLI wall	$7.81\cdot 10^{-9}$	$8.20\cdot 10^{-9}$	+5
Kidneys	$1.53\cdot 10^{-10}$	$1.85\cdot 10^{-10}$	+21
Liver	$1.01\cdot 10^{-10}$	$1.26\cdot 10^{-10}$	+24
Lungs	$5.07\cdot 10^{-11}$	$6.39\cdot 10^{-11}$	+26
Muscle	$1.27\cdot 10^{-10}$	$1.56\cdot 10^{-10}$	+23
Pancreas	$1.36\cdot 10^{-10}$	$1.68\cdot 10^{-10}$	+23
Red marrow	$4.16\cdot 10^{-10}$	$4.85\cdot 10^{-10}$	+16
Skin	$5.72\cdot 10^{-11}$	$6.88\cdot 10^{-11}$	+20
Spleen	$1.04\cdot 10^{-10}$	$1.30\cdot 10^{-10}$	+25
Thymus	$3.64\cdot 10^{-11}$	$4.37\cdot 10^{-11}$	+20
Thyroid	$3.43\cdot 10^{-11}$	$3.95\cdot 10^{-11}$	+15
Remainder	$1.43\cdot 10^{-10}$	$1.85\cdot 10^{-10}$	+29
Effective dose	$9.54\cdot 10^{-10}$	$1.09\cdot 10^{-9}$	+14

Dose coefficients calculated with female *SEEs* are increased by 5 – 32 % over their respective male equivalents. Although the masses of the most organs are lower in the female reference person, the *SEE* values do not simply scale with target organ mass as might be inferred from Equation 5.14.

#### 6.4.4 Differences due to alimentary tract models

One objective of the new zirconium biokinetic model proposal is to include the newest information on substance kinetics in the human alimentary tract (HAT) available inside the ICRP framework, i.e. ICRP publication 100 (ICRP 2006). This is especially important, since the double tracer investigations, as performed in the current study, do not yield detailed information about substance transfer within the alimentary tract. Thus, it is suggestive to use the revised, more detailed model and parameters from ICRP publication 100 instead of those in ICRP publication 30 (ICRP 1979) in order to better describe substance transfer through the alimentary tract.

Table 6.10 lists the dose coefficients calculated for the ICRP publication 67 biokinetic model with the alimentary tract models from ICRP publications 30 (GI) and 100 (HAT) for the male reference man. For the HAT model calculation, the default parameter values for non-caloric liquids in males were used.

**Table 6.10:** Dose coefficients ( $\text{Sv}\cdot\text{Bq}^{-1}$ ) for transformations over 50 y, modelled with different alimentary tract models.

Target region	ICRP 30 GI tract	ICRP 100 HAT	Deviation of HAT from GI (%)
Adrenals	$1.14\cdot 10^{-10}$	$1.10\cdot 10^{-10}$	-4
Bladder wall	$2.82\cdot 10^{-10}$	$2.78\cdot 10^{-10}$	-1
Bone Surface	$1.93\cdot 10^{-9}$	$1.93\cdot 10^{-9}$	0
Brain	$4.16\cdot 10^{-11}$	$3.84\cdot 10^{-11}$	-8
Breast	$3.19\cdot 10^{-11}$	$3.10\cdot 10^{-11}$	-3
ST wall	$3.76\cdot 10^{-10}$	$2.67\cdot 10^{-10}$	-29
SI wall	$1.06\cdot 10^{-9}$	$1.03\cdot 10^{-9}$	-2
ULI wall	$3.03\cdot 10^{-9}$	$2.81\cdot 10^{-9}$	-7
LLI wall	$7.81\cdot 10^{-9}$	$7.80\cdot 10^{-9}$	0
Kidneys	$1.53\cdot 10^{-10}$	$1.46\cdot 10^{-10}$	-4
Liver	$1.01\cdot 10^{-10}$	$9.59\cdot 10^{-11}$	-5
Lungs	$5.07\cdot 10^{-11}$	$4.92\cdot 10^{-11}$	-3
Muscle	$1.27\cdot 10^{-10}$	$1.24\cdot 10^{-10}$	-2
Oesophagus	$3.64\cdot 10^{-11}$	$4.24\cdot 10^{-11}$	17
Pancreas	$1.36\cdot 10^{-10}$	$1.23\cdot 10^{-10}$	-10
Red marrow	$4.16\cdot 10^{-10}$	$4.12\cdot 10^{-10}$	-1
Skin	$5.72\cdot 10^{-11}$	$5.60\cdot 10^{-11}$	-2
Spleen	$1.04\cdot 10^{-10}$	$9.59\cdot 10^{-11}$	-8
Testes	$1.01\cdot 10^{-10}$	$1.00\cdot 10^{-10}$	-1
Thymus	$3.64\cdot 10^{-11}$	$3.39\cdot 10^{-11}$	-7
Thyroid	$3.43\cdot 10^{-11}$	$3.42\cdot 10^{-11}$	0
Remainder	$1.43\cdot 10^{-10}$	$1.39\cdot 10^{-10}$	-3
Effective dose	$8.02\cdot 10^{-10}$	$7.73\cdot 10^{-10}$	-4

For radionuclides like zirconium and niobium, with short half-lives and small fractional absorption from intestine to the systemic circulation, the absorbed dose is primarily dependent on radionuclide transformations in the alimentary tract. The HAT model features a slightly faster substance transfer through the body; hence the calculated dose coefficients are generally lower than those associated to the older GI tract model. The most extreme target organ in this context is the stomach wall, which can be explained by the change in the transfer rate from stomach to small intestine in the HAT model as compared to the GI tract model. In the HAT model, the transfer rate is a factor of 2 higher than in the GI tract model, hence the energy absorbed in the stomach wall from radionuclide transformations in the stomach contents is substantially reduced in the HAT model.

The increased oesophagus dose coefficient is an exception to this general trend, because the oesophagus is a source organ only in the HAT model, and as such receives dose also from beta radiation (cf. section 5.3).

#### **6.4.5 Dose coefficients of $^{95}\text{Zr}$ for the proposed new zirconium biokinetic model**

In the following, various aspects of the dose coefficients resulting from the ICRP model and the proposed new model are presented. Published and calculated dose coefficients are listed in Table 6.11. Consecutively, gender-specific deviations are shown in Table 6.12, differences due to the chemical form of ingested zirconium are listed in Table 6.13, and the contribution of specific organs to the effective dose is presented for the different models in Figures 6.22 – 6.26. The section is concluded by a summary of the main differences between the ingestion dose coefficients resulting from the proposed new model and the current published ingestion dose coefficients.

The relative differences of committed equivalent doses in Table 6.11 are in the range of -87 % to +65 %, with a median of -3.3 % and a mean of -8.4 %. The relative differences of committed effective doses are -27 % to +42 %, with a mean and median of +7 %. Thus, the ingestion dose coefficients calculated for the proposed new model are significantly different from the published ICRP dose coefficients, considering the estimated uncertainty of the numerical modelling process of ~ 2 % (cf. Table 6.8 above).

Absolute equivalent dose coefficients lie in the range of  $7.0 \cdot 10^{-12} - 1.1 \cdot 10^{-8} \text{ Sv} \cdot \text{Bq}^{-1}$ , implying that the ingestion of ~ 0.1  $\mu\text{g}$  pure  $^{95}\text{Zr}$  with a specific activity of  $8.0 \cdot 10^{14} \text{ Bq} \cdot \text{g}^{-1}$  (ICRP 1983) imparts a collective equivalent dose of up to 1 Sv to each target region. The target regions with the largest equivalent dose coefficients are the sections of the colon wall, the small intestine wall, the bone surfaces, and the ovaries.

#### **6.4.6 Gender differences resulting from the use of the HAT model**

One new feature of the HAT model is that transfer rates between some compartments are material- and gender-specific. Within the current study, only non-caloric liquids, i.e. solutions of zirconium tracers, are used for investigations, thus no material-specific parameters are yet included in the proposed model. However, investigations of both genders are included and dose coefficients are derived for both genders individually by the use of gender-specific *SEEs* (cf. Table 6.9), and gender-specific parameters for transfers from large intestine compartments.

In the HAT model, the transfer rates  $\lambda_{\text{right colon} \rightarrow \text{left colon}}$ ,  $\lambda_{\text{left colon} \rightarrow \text{rectosigmoid colon}}$ , and  $\lambda_{\text{rectosigmoid colon} \rightarrow \text{excreted faeces}}$  are  $2 \text{ d}^{-1}$  for men and  $1.5 \text{ d}^{-1}$  for women. Therefore ingested radionuclides stay longer in the female colon than in the male colon, resulting in a calculated increase of the number of transformations in the colon compartments by  $\sim 33 \%$  in women.

Accordingly, the comparison in Table 6.12 shows that the dose coefficients for women are more elevated in the proposed new model than in the ICRP publication 67 model. In general, target regions in close proximity to the colon receive a clearly elevated dose in women, while the gender difference is smaller in remote target regions like the brain.

This effect is even more pronounced for the citrate model, since the fractional absorption  $f_A$  of zirconium is smaller in this model ( $1.0 \cdot 10^{-3}$ ) than in the oxalate model ( $7.7 \cdot 10^{-3}$ ). As a consequence, a larger fraction of the equivalent dose is caused by radionuclide transformations in the colon. The contribution of this effect is an additional increase of female dose coefficients by  $0.1 - 33 \%$  for the citrate model in comparison with the oxalate model.

**Table 6.11:** Dose coefficients ( $\text{Sv} \cdot \text{Bq}^{-1}$ ) published in ICRP publication 67 and calculated for various models. In contrast to the published dose coefficients, all modelled dose coefficients are based on the niobium biokinetic model for  $^{95}\text{Nb}$ .

Target region	ICRP 67		Oxalate model		Citrate model	
	published	modelled	male	female	male	female
Adrenals	$1.3 \cdot 10^{-10}$	$1.1 \cdot 10^{-10}$	$1.3 \cdot 10^{-10}$	$1.8 \cdot 10^{-10}$	$5.1 \cdot 10^{-11}$	$8.6 \cdot 10^{-11}$
Bladder wall	$2.9 \cdot 10^{-10}$	$2.8 \cdot 10^{-10}$	$2.8 \cdot 10^{-10}$	$4.2 \cdot 10^{-10}$	$2.5 \cdot 10^{-10}$	$3.8 \cdot 10^{-10}$
Bone Surface	$2.3 \cdot 10^{-9}$	$1.9 \cdot 10^{-9}$	$2.4 \cdot 10^{-9}$	$3.1 \cdot 10^{-9}$	$3.7 \cdot 10^{-10}$	$5.1 \cdot 10^{-10}$
Brain	$5.3 \cdot 10^{-11}$	$4.2 \cdot 10^{-11}$	$5.1 \cdot 10^{-11}$	$5.9 \cdot 10^{-11}$	$7.0 \cdot 10^{-12}$	$8.5 \cdot 10^{-12}$
Breast	$3.7 \cdot 10^{-11}$	$3.2 \cdot 10^{-11}$	$3.9 \cdot 10^{-11}$	$4.9 \cdot 10^{-11}$	$1.2 \cdot 10^{-11}$	$1.9 \cdot 10^{-11}$
ST wall	$3.9 \cdot 10^{-10}$	$3.8 \cdot 10^{-10}$	$2.7 \cdot 10^{-10}$	$3.7 \cdot 10^{-10}$	$2.4 \cdot 10^{-10}$	$3.4 \cdot 10^{-10}$
SI wall	$1.1 \cdot 10^{-9}$	$1.1 \cdot 10^{-9}$	$8.0 \cdot 10^{-10}$	$1.2 \cdot 10^{-9}$	$7.5 \cdot 10^{-10}$	$1.2 \cdot 10^{-9}$
ULI wall	$3.1 \cdot 10^{-9}$	$3.0 \cdot 10^{-9}$	$2.8 \cdot 10^{-9}$	$4.1 \cdot 10^{-9}$	$2.7 \cdot 10^{-9}$	$4.0 \cdot 10^{-9}$
LLI wall	$7.8 \cdot 10^{-9}$	$7.8 \cdot 10^{-9}$	$7.8 \cdot 10^{-9}$	$1.1 \cdot 10^{-8}$	$7.8 \cdot 10^{-9}$	$1.1 \cdot 10^{-8}$
Kidneys	$1.7 \cdot 10^{-10}$	$1.5 \cdot 10^{-10}$	$1.6 \cdot 10^{-10}$	$2.2 \cdot 10^{-10}$	$1.0 \cdot 10^{-10}$	$1.5 \cdot 10^{-10}$
Liver	$1.1 \cdot 10^{-10}$	$1.0 \cdot 10^{-10}$	$1.1 \cdot 10^{-10}$	$1.6 \cdot 10^{-10}$	$6.7 \cdot 10^{-11}$	$1.1 \cdot 10^{-10}$
Lungs	$6.0 \cdot 10^{-11}$	$5.1 \cdot 10^{-11}$	$6.1 \cdot 10^{-11}$	$8.1 \cdot 10^{-11}$	$1.9 \cdot 10^{-11}$	$3.1 \cdot 10^{-11}$
Muscle	$1.4 \cdot 10^{-10}$	$1.3 \cdot 10^{-10}$	$1.3 \cdot 10^{-10}$	$1.9 \cdot 10^{-10}$	$9.2 \cdot 10^{-11}$	$1.5 \cdot 10^{-10}$
Ovaries	$8.8 \cdot 10^{-10}$	$8.6 \cdot 10^{-10}$	-	$1.4 \cdot 10^{-9}$	-	$1.4 \cdot 10^{-9}$
Pancreas	$1.5 \cdot 10^{-10}$	$1.4 \cdot 10^{-10}$	$1.3 \cdot 10^{-10}$	$1.9 \cdot 10^{-10}$	$8.3 \cdot 10^{-11}$	$1.3 \cdot 10^{-10}$
Red marrow	$4.8 \cdot 10^{-10}$	$4.2 \cdot 10^{-10}$	$4.7 \cdot 10^{-10}$	$6.0 \cdot 10^{-10}$	$1.8 \cdot 10^{-10}$	$2.7 \cdot 10^{-10}$
Skin	$6.3 \cdot 10^{-11}$	$5.7 \cdot 10^{-11}$	$6.3 \cdot 10^{-11}$	$8.7 \cdot 10^{-11}$	$3.5 \cdot 10^{-11}$	$5.5 \cdot 10^{-11}$
Spleen	$1.1 \cdot 10^{-10}$	$1.0 \cdot 10^{-10}$	$1.0 \cdot 10^{-10}$	$1.5 \cdot 10^{-10}$	$6.7 \cdot 10^{-11}$	$1.1 \cdot 10^{-10}$
Testes	$1.0 \cdot 10^{-10}$	$1.0 \cdot 10^{-10}$	$1.1 \cdot 10^{-10}$	-	$8.3 \cdot 10^{-11}$	-
Thymus	$4.3 \cdot 10^{-11}$	$3.6 \cdot 10^{-11}$	$4.4 \cdot 10^{-11}$	$5.5 \cdot 10^{-11}$	$1.1 \cdot 10^{-11}$	$1.7 \cdot 10^{-11}$
Thyroid	$4.3 \cdot 10^{-11}$	$3.4 \cdot 10^{-11}$	$4.5 \cdot 10^{-11}$	$5.3 \cdot 10^{-11}$	$7.5 \cdot 10^{-12}$	$1.0 \cdot 10^{-11}$
Uterus	$4.0 \cdot 10^{-10}$	$3.9 \cdot 10^{-10}$	-	$6.0 \cdot 10^{-10}$	-	$5.5 \cdot 10^{-10}$
Remainder	$1.5 \cdot 10^{-10}$	$1.4 \cdot 10^{-10}$	$1.4 \cdot 10^{-10}$	$2.2 \cdot 10^{-10}$	$1.0 \cdot 10^{-10}$	$1.7 \cdot 10^{-10}$
Effective dose	$9.6 \cdot 10^{-10}$	$8.0 \cdot 10^{-10}$	$7.9 \cdot 10^{-10}$	$1.4 \cdot 10^{-9}$	$7.0 \cdot 10^{-10}$	$1.3 \cdot 10^{-9}$

**Table 6.12:** Deviations of female from male dose coefficients for the ICRP model, and the proposed model with oxalate or citrate-specific fractional absorption. The extreme deviation of effective doses is in part caused by the large variance in the contribution of the gonad dose, visible in Figures 6.22 – 6.26.

Target region	Deviation of female dose coefficients from male dose coefficients (%)		
	ICRP 67 model (GI)	Oxalate model (HAT)	Citrate model (HAT)
Adrenals	+27	+38	+67
Bladder wall	+19	+51	+57
Bone Surface	+32	+33	+37
Brain	+17	+17	+20
Breast	+19	+26	+50
ST wall	+18	+38	+41
SI wall	+19	+52	+54
ULI wall	+11	+46	+47
LLI wall	+5	+39	+40
Kidneys	+21	+42	+54
Liver	+24	+45	+61
Lungs	+26	+33	+66
Muscle	+23	+48	+60
Pancreas	+23	+42	+61
Red marrow	+16	+28	+49
Skin	+20	+39	+54
Spleen	+25	+46	+60
Thymus	+20	+25	+51
Thyroid	+15	+17	+34
Remainder	+29	+55	+68
Effective dose	+14	+73	+79

#### 6.4.7 Effect of fractional absorption on ingestion dose coefficients

Individual target tissues are even stronger affected by a variation in fractional absorption than are gender differences. The effect of such a variation is far more inhomogeneous, as is presented in Table 6.13. The ratios of dose coefficients of oxalate to citrate model vary between 1.0 and 7.2, with a tendency of slightly larger variances for the male models.

The lowest ratios are associated to the sections of the colon, in consistency with the small relative difference of zirconium passing through them, namely fractions of 0.999 and 0.9923 of the ingested amount of zirconium in the citrate and oxalate forms, respectively.

The largest ratios are associated with target tissues which receive dose from source tissues distant from the colon, and having a long retention time of zirconium and niobium; namely the bone surfaces, the brain in the cranial cavity, the thyroid between cranium and chest, and the lungs inside the chest.

**Table 6.13:** Ratio of ingestion dose coefficients of zirconium oxalate over inorganic zirconium in citrate-buffered solution

Target region	Oxalate/Citrate	
	male	female
Adrenals	2.5	2.0
Bladder wall	1.1	1.1
Bone Surface	6.4	6.2
Brain	7.2	7.0
Breast	3.1	2.6
ST wall	1.1	1.1
SI wall	1.1	1.0
ULI wall	1.0	1.0
LLI wall	1.0	1.0
Kidneys	1.6	1.4
Liver	1.6	1.4
Lungs	3.2	2.6
Muscle	1.4	1.3
Ovaries	-	1.0
Pancreas	1.6	1.4
Red marrow	2.6	2.2
Skin	1.8	1.6
Spleen	1.5	1.4
Testes	1.3	-
Thymus	3.9	3.2
Thyroid	6.1	5.3
Uterus	-	1.1
Remainder	1.4	1.3
Effective dose	1.1	1.1

#### 6.4.8 Contribution of individual target tissues to effective dose

In the figures below, the composition of effective dose is presented for the published ICRP ingestion dose coefficients of  $^{95}\text{Zr}$  (ICRP 1993) and the ingestion dose coefficients resulting from the proposed new biokinetic model of zirconium. The effective dose is calculated from the individual target tissue dose coefficients and the appropriate weighting factors as described in section 5.3. For each target tissue, the percentage contribution of the weighted individual dose coefficients to the effective dose is noted next to the tissue name.

The most striking observation is the contribution of the gonads, which is very different between genders due to the difference in *SEE* values for testes and ovaries. *SEE(ovaries←ULI)* and *SEE(ovaries←LLI)* are higher by approximately one order of magnitude, presumably because the ovaries are located closer to the large intestine than the testes.

It can also be observed that the dose to bone surfaces contributes little to the effective dose due to its weighting coefficient of 0.01, despite that it is the highest unweighted dose next to the colon dose. A change in the estimation of radiosensitivity and accordingly the weighing factor of this tissue type would therefore substantially change its relative contribution to the effective dose.

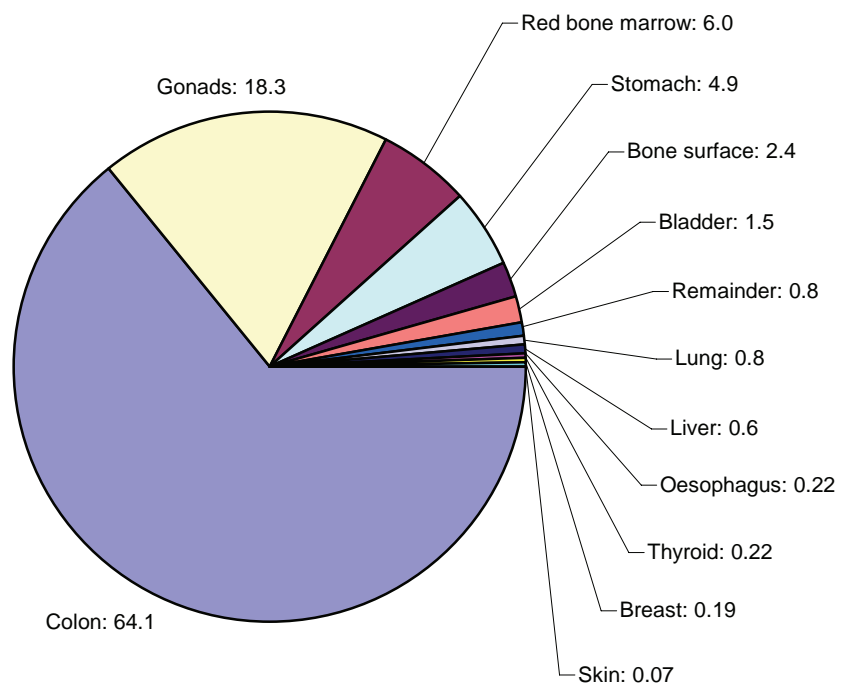


**Figure 6.22:** Composition of the effective dose calculated from ingestion dose coefficients in ICRP publication 67.

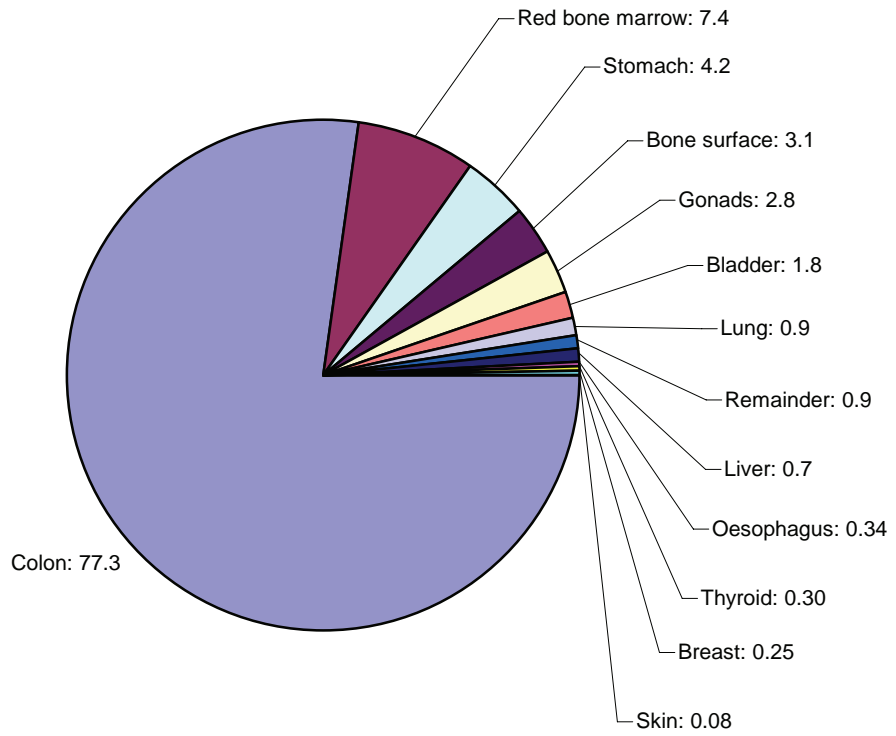


**Figure 6.23:** Composition of the effective dose calculated from ingestion dose coefficients of the proposed male oxalate model.

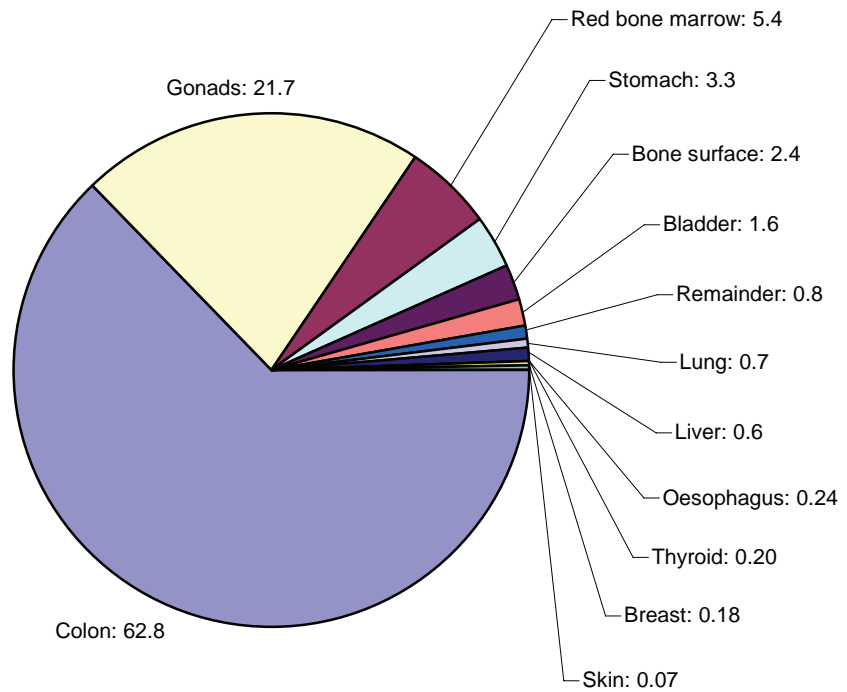


**Figure 6.24:** Composition of the effective dose calculated from ingestion dose coefficients of the proposed female oxalate model.

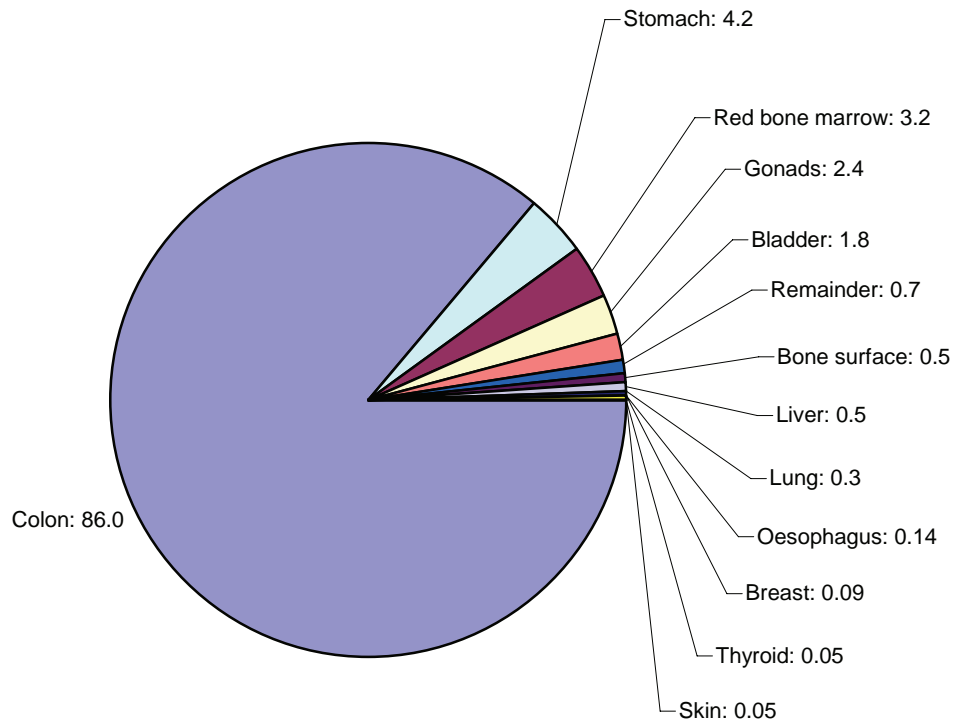


**Figure 6.25:** Composition of the effective dose calculated from ingestion dose coefficients of the proposed male citrate model.

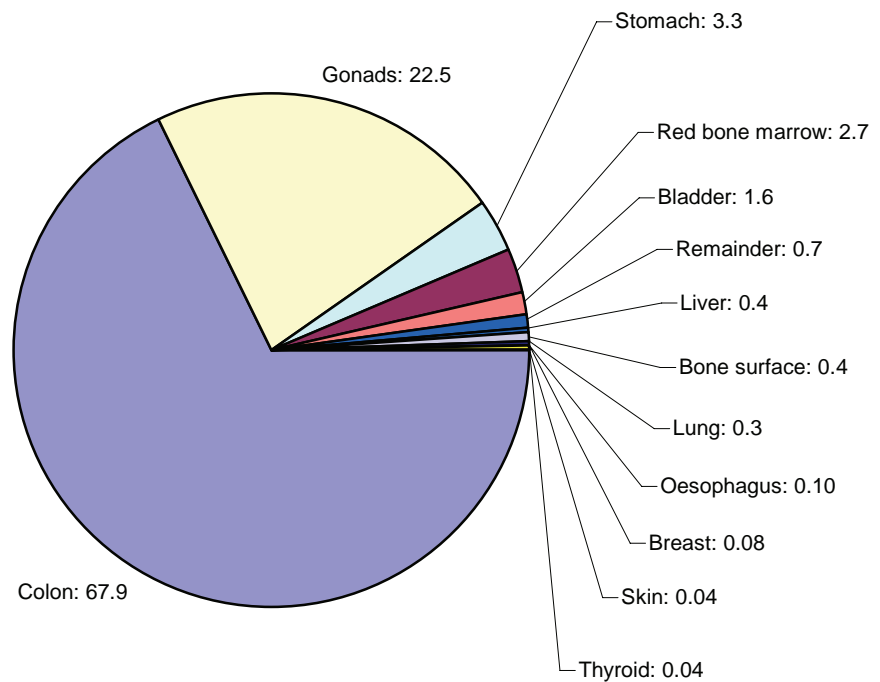


**Figure 6.26:** Composition of the effective dose calculated from ingestion dose coefficients of the proposed female citrate model.

#### 6.4.9 Summary of dosimetry

Ingestion dose coefficients were calculated from radionuclide transformations over 50 y with the proposed new model for male and female reference persons and for two different chemical forms of zirconium, namely inorganic zirconium ions in citrate-buffered solution, and dissolved zirconium oxalate.

- The deviation of individual equivalent dose coefficients from the current values published in ICRP publication 67 is in the range of -87 % to +65 %, with a median deviation of -3.3 %. Effective dose coefficients vary from the ICRP value by -27 % to +42 %.
- Ingestion equivalent dose coefficients are generally higher for women by 17 – 68 %, with a median increase over male dose coefficients of 52 % and 39 % for the citrate and the oxalate form, respectively. Female effective doses are increased over male effective doses by 79 % and 73 %, respectively.
- In accordance with the ratio of fractional absorption values of  $\sim 7.7$ , oxalate equivalent dose coefficients are increased over citrate dose coefficients by factors of up to  $\sim 7.2$ , with a median factor of 1.6 for men and 1.4 for women. The factors are substantially dependent on the target tissue. Oxalate-associated effective dose coefficients are higher than the citrate-associated doses by a factor of  $\sim 1.1$ .
- Weighted contributions of individual target tissues to the effective dose coefficient are dominated by the colon dose (63 – 86 %), the gonad dose ( $\sim 22$  % in women and 2 – 3 % in men), and doses to stomach, red bone marrow, urinary bladder wall, and bone surfaces (each exceeding 1 %, the latter only for the citrate model).

In consideration of potential dose estimates after accidents, it is important to stress that the substantial gender differences observed in modelling are a consequence of different SEE values and, to a large extent, the transfer rates between the sections of the colon introduced by the HAT model. Therefore it would be crucial for any individual dose estimate to accurately measure the zirconium clearance by faecal excretion and take into account the individual steric relations of radiosensitive tissues for the affected person.

## 7 Conclusions

The measurements performed within this study enabled the evaluation of two techniques for the analysis of isotope ratios of trace amounts of zirconium in biological samples. For the first time, a measurement method for thermal ionisation mass spectrometry (TIMS) of zirconium was optimised specifically for this purpose, enabling routine measurements. An established method for proton activation analysis (PNA) was adopted as a complementary technique, which is ideal to serve as quality control for the routine TIMS measurements.

The capabilities of both methods allowed to evaluate 9 tracer kinetic investigations of zirconium stable isotopes in humans, performed using a double tracer method with simultaneous oral and intravenous tracer administration. The results from these investigations significantly improve the data on the biokinetic behaviour of trace amounts of zirconium in humans.

As a consequence of the measured data, the biokinetic compartmental model of zirconium published by the International Commission on Radiological Protection (ICRP) was modified to include recycling processes and a physiologically motivated direct excretion from blood plasma to urine. Other paths of excretion were practically not identifiable and are not included in the model.

The ingestion dose coefficients calculated with the new proposed model are on average consistent with the current ingestion dose coefficients published in ICRP publication 67 (ICRP 1993), yet can vary significantly depending on gender and speciation of ingested zirconium.



## Acknowledgements

Many people have contributed to this work, and I am sincerely grateful for the time I was allowed to work for and with them.

First and foremost, I would like to thank Prof. Dr. Dr. Herwig G. Paretzke for giving me the possibility to begin and complete this work under his supervision.

My thanks go to the staff of the working group Medical Physics in the Institute of Radiation Protection of the GSF. Many colleagues at the working group and beyond were involved in this work, but some more than others, to whom my deepest gratitude is:

Dr. Augusto Giussani, for many fruitful discussions, explanations, nearly everything related to PNA, and ongoing scientific mentorship;

Felix Schöfer, for even more inspiring discussions, and his efforts for all PhD students at the GSF;

Dr. Wei Bo Li, Dr. Uwe Oeh, and Dr. Vera Höllriegl, for their joint involvement in the biokinetics project;

Beate Saath, Oleksandr Khagai, Alexander Wolf, and Florian Wagner for their efforts and assistance in sample gathering, preparation, and measurement;

Dr. Christoph Hoeschen, for his support as an excellent group leader, and his introduction in uncertainty judgement;

Maria Zankl, especially for her help and ideas in the joint implementation of a working-group wide bibliographic data base;

Janine Becker, for technical help, despite suffering many interruptions by me.

I wish to thank Dr. Udo Gerstmann, Almut Geisler, and Oliver Meisenberg, for the gamma spectrometric measurement at the GSF.

I am greatly indebted to all volunteers, without whom this work would not have been possible. Less painful for them, but nevertheless appreciated was the cooperation with Dr. N. Felgenhauer, Prof. Dr. T. Zilker, and Prof. Dr. Martin Göttlicher.

I am grateful for the friendly and supportive reception at the MLL. I am especially indebted to Dr. Ralf Hertenberger and his proton source, to Walter Carli and Dr. Ludwig Beck, to all operators, and to Prof. Dr. Reiner Krücken, for the support of PNA at the tandem accelerator laboratory.

My thanks go to Otmar Morath at the Paul Scherrer Institute, especially for rescuing the essential PNA setup parts from disposal.

I am deeply grateful for the support from my parents, my brother, and my friends, who helped me to keep up and finally finish this work.

The TRITON-related images in section 3.2.2 are courtesy of Thermo Fisher Scientific (Bremen) GmbH. I thank Ernst Schröder for the permission to use them in my presentation.

This work is a part of the project StSch 4471 and as such was funded by the Bundesministerium für Umwelt, Naturschutz und Reaktorsicherheit (BMU) through the Bundesamt für Strahlenschutz, Salzgitter.



## Bibliography

- (1994). Pschyrembel Klinisches Wörterbuch, de Gruyter.
- Adams, F., R. Gijbels, et al., Eds. (1988). Inorganic mass spectrometry. Chemical Analysis. New York, Chichester, Brisbane, Toronto, Singapore, Wiley-Interscience.
- Al-Jundi, J. (2000). "Determination of trace elements and heavy metals in the Zarka River sediments by instrumental neutron activation analysis." Nuclear Instruments and Methods in Physics Research B **170**: 180-186.
- Angerer, J. and K.-H. Schaller (1999). Anwendung der ICP-MS für das Humanbiomonitoring. Analytische Methoden zur Prüfung gesundheitsschädlicher Arbeitsstoffe - Analysen in biologischem Material. H. Greim, Wiley-VCH DFG. **2**: 156-203.
- Audoly, S., L. D'Angio, et al. (1997). Globi2 - software for GLOBAL Identifiability. Padova, Italy, Gruppo Biomed Mod.
- Baglan, N., C. Cossonnet, et al. (2001). "Determination of  $^{232}\text{Th}$  in urine by ICP-MS for individual monitoring purpose." Health Physics **81**(1): 76-81.
- Baler, G. R. (1966). "Granulomas from zirconium-containing ointments (Abstract and comment)." Food and Cosmetics Toxicology **4**: 120.
- Barrett, P. H. R., B. M. Bell, et al. (1998). "SAAM II: simulation, analysis, and modeling software for tracer and pharmacokinetic studies." Metabolism **47**: 484-492.
- Beal, S. L. (2001). "Ways to Fit a PK Model with Some Data Below the Quantification Limit." Journal of Pharmacokinetics and Pharmacodynamics **28**(5): 481-504.
- Beal, S. L. (2005). "Conditioning on Certain Random Events Associated with Statistical Variability in PK/PD." Journal of Pharmacokinetics and Pharmacodynamics **32**(2): 213-243.
- Becker, J. S. and H.-J. Dietze (1998). "Inorganic trace analysis by mass spectrometry." Spectrochimica Acta B **53**(11): 1475-1506.
- Becker, J. S. and H.-J. Dietze (1998). "Ultratrace and precise isotope analysis by double-focusing sector field inductively coupled plasma mass spectrometry." Journal of Analytical Atomic Spectrometry **13**(9): 1057-1063.
- Bianco, G. L. (1989). Programma ALPI: A program for the evaluation of peak areas from spectra (in Italian).
- Birchall, A. and A. C. James (1987). A general algorithm for solving compartmental models with constant coefficients and its implementation on a microcomputer. Chilton, Didcot, Oxon, UK, National Radiological Protection Board.
- Boswell, S. M. and H. Elderfield (1988). "The determination of zirconium and hafnium in natural waters by isotope dilution mass spectrometry." Marine Chemistry **25**(3): 197-209.
- Cantone, M. C., D. de Bartolo, et al. (1997). "CPAA for studying biokinetics with stable isotopes: A preliminary investigation on zirconium metabolism in animals." Journal of Radioanalytical and Nuclear Chemistry **217**(2): 279-282.
- Cantone, M. C., D. De Bartolo, et al. (1997). "A methodology for biokinetic studies using stable isotopes: Results of repeated molybdenum investigations on a healthy volunteer." Applied Radiation and Isotopes **48**: 333-338.
- Cantone, M. C., N. Molho, et al. (1982). "Trace elements analysis in biological samples by proton nuclear activation." Clinical Physics and Physiological Measurement **3**(1): 67-77.
- Carson, E., C. Cobelli, et al. (1983). The mathematical modelling of metabolic and endocrine systems. New York, Chichester, Brisbane, Toronto, Singapore, Wiley-Interscience.

- CeraRoot. (2006). "Product Catalogue - CeraRoot One piece zirconia dental implant system." Retrieved July 15th, 2007, 2007, from [http://www.ceraroot.com/assets/product\\_cat\\_eng.pdf](http://www.ceraroot.com/assets/product_cat_eng.pdf).
- Coedo, A. G., T. D. López, et al. (1995). "On-line ion-exchange separation and determination of niobium, tantalum, tungsten, zirconium and hafnium in high-purity iron by flow injection inductively coupled plasma mass spectrometry." *Analytica Chimica Acta* **315**: 331-338.
- Coursey, J. S., D. J. Schwab, et al. (2005). Physical reference data: Atomic weights and isotopic compositions with relative atomic masses, NIST.
- Crews, H. M., V. Ducros, et al. (1994). "Mass spectrometric methods for studying nutrient mineral and trace element absorption and metabolism in humans using stable isotopes. A review." *Analyst* **119**(11): 2491-2514.
- Currie, L. A. (1968). "Limits for qualitative detection and quantitative determination." *Analytical Chemistry* **40**: 586-593.
- David, K., J. L. Birck, et al. (1999). "Application of isotope dilution for precise measurement of Zr/Hf and  $^{176}\text{Hf}/^{177}\text{Hf}$  ratios by mass spectrometry (ID-TIMS/ID-ICP-MS)." *Chemical Geology* **157**: 1-12.
- de Bartolo, D., M. C. Cantone, et al. (2000). "Determination of biokinetic parameters for ingestion of radionuclides of zirconium in animals using stable tracers." *Radiation and Environmental Biophysics* **39**: 53-58.
- de Goeij, J. J. M. (2000). "Radiochemical neutron activation analysis of biological materials: Past, present and future." *Journal of Radioanalytical and Nuclear Chemistry* **245**(1): 5-9.
- De Grazia, J. A., P. Ivanovich, et al. (1965). "A double isotope method for measurements of intestinal absorption of calcium in man." *Journal of Laboratory and Clinical Medicine* **66**(5): 822-829.
- Diemer, J. and K. G. Heumann (1999). "Determination of zirconium traces in polymers by ICP-IDMS - a powerful and fast method for routine testing of zirconium residues in polyolefins." *Fresenius Journal of Analytical Chemistry* **364**(5): 421-423.
- Dobrowolski, Z., T. Drewniak, et al. (2002). "Trace elements distribution in renal cell carcinoma depending on stage of disease." *European Urology* **42**: 475-480.
- Duval, V. and M. O. Karlsson (2002). "Impact of Omission or Replacement of Data below the Limit of Quantification on Parameter Estimates in a Two-Compartment Model." *Pharmaceutical Research* **19**(12): 1835-1840.
- Eckerman, K. F. WinChain: Decay Chain Summary Information. Oak Ridge, Oak Ridge National Laboratory.
- Eckerman, K. F. (1993). SEECAL: Program to calculate age-dependent specific effective energies. O. R. N. Laboratory. Oak Ridge.
- Emsley, J. (2001). *Nature's building blocks. An A-Z guide to the elements*. Oxford, Oxford University Press.
- England, T. R. and B. F. Rider (1994). Evaluation and compilation of fission product yields. Los Alamos, NM, Los Alamos National Laboratory.
- Engström, E., A. Stenberg, et al. (2004). "Multi-elemental characterization of soft biological tissues by inductively coupled plasma-sector field mass spectrometry." *Analytica Chimica Acta* **521**: 123-135.
- Erdtmann, G. (1992). *Neutron activation analysis: Techniques and relevant nuclear data*. Jülich, Forschungszentrum Jülich GmbH - KFA - Zentralabteilung für Chemische Analysen.
- Fassett, J. D. and P. J. Paulsen (1989). "Isotope dilution mass spectrometry for accurate elemental analysis." *Analytical Chemistry* **61**(10): 643-649.

- Fletcher, C. R. (1969). "The radiological hazards of zirconium-95 and niobium-95." Health Physics **16**: 209-220.
- Ghosh, S., A. Sharma, et al. (1992). "Zirconium. An abnormal trace element in biology." Biological Trace Element Research **35**: 247-271.
- Giussani, A. M. (1997). Entwicklung von analytischen Methoden für Stoffwechsel- und Biokinetik-Untersuchungen beim Menschen mit Hilfe stabiler Tracer unter besonderer Berücksichtigung von Molybdän, Eberhard-Karls-Universität zu Tübingen, Fakultät für Physik.
- Glascocock, M. (2003, October 1, 2003). "An overview of neutron activation analysis." Retrieved 07.07.2004, 2004, from [http://www.missouri.edu/~glascocock/naa\\_over.htm](http://www.missouri.edu/~glascocock/naa_over.htm).
- Guyton, A. C. and J. E. Hall (2006). Textbook of medical physiology. Philadelphia, Elsevier Saunders.
- Habfast, K. (1998). "Fractionation correction and multiple collectors in thermal ionization isotope ratio mass spectrometry." International Journal of Mass Spectrometry **176**: 133-148.
- Habfast, K. (1998). "Fractionation correction and multiple collectors in thermal ionization isotope ratio mass spectrometry." Int. J. Mass Spectrom. **176**: 133-148.
- Hamilton, E. I., E. Sabbioni, et al. (1994). "Element reference values in tissues from inhabitants of the European community. VI. Review of elements in blood, plasma and urine and a critical evaluation of reference values for the United Kingdom population." The Science of The Total Environment **158**: 165-190.
- Hamilton, J. G. (1947). "The metabolism of the fission products and the heaviest elements." Radiology **43**: 325-343.
- Heatherington, A. C., P. Vicini, et al. (1998). "A Pharmacokinetic/Pharmacodynamic Comparison of SAAM II and PC/WinNonlin Modeling Software." Journal of Pharmaceutical Sciences **87**(10): 1255-1263.
- Heitland, P. and H. D. Köster (2006). "Biomonitoring of 37 trace elements in blood samples from inhabitants of northern Germany by ICP-MS." Journal of Trace Elements in Medicine and Biology **20**: 253-262.
- Heumann, K. G., S. M. Gallus, et al. (1998). "Precision and accuracy in isotope ratio measurements by plasma source mass spectrometry." Journal of Analytical Atomic Spectrometry **13**: 1001-1008.
- Hing, J. P., S. G. Woolfrey, et al. (2001). "Analysis of Toxicokinetic Data using NONMEM: Impact of Quantification Limit and Replacement Strategies for Censored Data." Journal of Pharmacokinetics and Pharmacodynamics **28**(5): 465-479.
- Hirata, T. and T. Yamaguchi (1999). "Isotopic analysis of zirconium using enhanced sensitivity-laser ablation-multiple collector-inductively coupled plasma mass spectrometry." Journal of Analytical Atomic Spectrometry **14**(9): 1455-1459.
- Höllriegel, V., P. Louvat, et al. (2002). "Studies of strontium biokinetics in humans. Part 2: Uptake of strontium from aqueous solutions and labelled foodstuffs." Radiation and Environmental Biophysics **41**: 281-287.
- Höllriegel, V., M. Röhmuß, et al. (2004). "Strontium biokinetics in humans: Influence of alginate on the uptake of ingested strontium." Health Physics **86**(2): 193-196.
- ICRP (1979). Limits for intakes of radionuclides by workers. Part 1. Oxford, UK, Pergamon Press.
- ICRP (1983). Radionuclide transformations: Energy and intensity of emissions. Oxford, UK, Pergamon Press.
- ICRP (1990). Age-dependant doses to members of the public from intake of radionuclides: Part 1: Ingestion dose coefficients. Oxford, UK, Pergamon Press.
- ICRP (1991). 1990 Recommendations of the International Commission on Radiological Protection. Oxford, UK, Pergamon Press.

- ICRP (1993). Age-dependent doses to members of the public from intake of radionuclides. Part 2: Ingestion dose coefficients. Oxford, UK, Pergamon Press.
- ICRP (1994). Human respiratory tract model for radiological protection. Oxford, UK, Pergamon Press.
- ICRP (1995). Age-dependent doses to members of the public from intake of radionuclides: Part 4: Inhalation dose coefficients. Oxford, UK, Pergamon Press.
- ICRP (1995). "Dose coefficients for intakes of radionuclides by workers." ICRP Publication 68.
- ICRP (2002). "Basic Anatomical and Physiological Data for Use in Radiological Protection: Reference Values." ICRP Publication 89.
- ICRP (2006). "ICRP publication 100: Human alimentary tract model for radiological protection." Annals of the ICRP 36(1-2): 1-327.
- Ide, K., Y. Nakamura, et al. (2003). "Determination of trace refractory metal elements in high-purity iron by inductively coupled plasma mass spectrometry." Bunseki Kagaku 52(10): 931-937.
- Ikemoto, T., T. Kunito, et al. (2004). "Comparison of trace element accumulation in Baikal seals (*Pusa sibirica*), Caspian seals (*Pusa caspica*) and northern fur seals (*Callorhinus ursinus*)." Environmental Pollution 127: 83-97.
- Iskander, F. Y. (1996). "Assessment of trace elements in honey produced on uranium mining reclaimed land." The Science of the Total Environment 192: 119-122.
- ISO, BIPM, et al. (1995). Guide to the expression of uncertainty in measurement (GUM). Geneva, International Organization for Standardization.
- Katti, K. S. (2004). "Biomaterials in total joint replacement." Colloids and Surfaces B: Biointerfaces 39(3): 133-142.
- Kienitz, H., Ed. (1968). Massenspektrometrie. Weinheim/Bergstraße, Verlag Chemie GmbH.
- Kunze, J., S. Koelling, et al. (2000). "Use of ultrasonic nebulizer with desolvator membrane for the determination of titanium and zirconium in human serum by means of inductively coupled plasma - mass spectrometry." Fresenius Journal of Analytical Chemistry 366(2): 165-166.
- Kunze, J., M. A. Wimmer, et al. (1998). "Determination of titanium and zirconium wear debris in blood serum by means of HNO<sub>3</sub>/HF pressurized digestion using ICP - optical emission spectrometry." Fresenius Journal of Analytical Chemistry 361(5): 496-499.
- Leggett, R. W. and K. F. Eckerman (1994). "Evolution of the ICRP's biokinetic models." Radiation Protection Dosimetry 53(1-4): 147-155.
- Li, W. B., V. Höllriegl, et al. (2006). "Human biokinetics of strontium. Part I: Intestinal absorption rate and its impact on the dose coefficient of <sup>90</sup>Sr after ingestion." Radiation and Environmental Biophysics 45: 115-124.
- Liang, Q. and D. C. Grégoire (2000). "Determination of trace elements in twenty six Chinese geochemistry reference materials by inductively coupled plasma mass spectrometry." Geostandards Newsletter 24(1): 51-63.
- Lierse v.G., C. and X. Lin (2004). Determination of Zr in blood at concentration of 1ppb: Personal discussion and successive e-mail contact.
- Lindsey, J. K., B. Jones, et al. (2001). "Some statistical issues in modelling pharmacokinetic data." Statistics in Medicine 20(17-18): 2775-2783.
- Link, P., J. Pulz, et al. (2003, 2003/12/02 13:06:42). "FRM-II Technik. Bestrahlungseinrichtungen." Retrieved 27.10.2004, 2004, from <http://www.frm2.tu-muenchen.de/frm2/irradiation/index.shtml>.
- McKelvey, B. A. and K. J. Orians (1998). "The determination of dissolved zirconium and hafnium from seawater using isotope dilution inductively coupled plasma mass spectrometry." Marine Chemistry 60(3-4): 245-255.
- Mealey, J. (1957). "Turn-over of carrier-free zirconium-89 in man." Nature 179: 673-674.

- Mel Chemicals. (2007). "Zirconium Chemicals Introduction." Retrieved July 16th, 2007, 2007, from <http://www.zrchem.com>.
- Merian, E. (1984). Metalle in der Umwelt: Verteilung, Analytik und biologische Relevanz. Weinheim; Deerfield Beach, Florida; Basel, Verlag Chemie.
- Minoia, C., E. Sabbioni, et al. (1994). "Trace element reference values in tissues from inhabitants of the European community. IV. Influence of dietary factors." The Science of The Total Environment **141**(1-3): 181-195.
- Minster, J. F. and L. P. Ricard (1981). "The isotopic composition of zirconium." International Journal of Mass Spectrometry and Ion Physics **37**: 259-272.
- Moje, H. J. (2007). "Moje - Entwicklung und Herstellung von Keramikimplantaten." Retrieved July 15th, 2007, 2007, from <http://www.moje.de/>.
- Morita, H., T. Kita, et al. (1994). "Analysis of serum elements and the contaminations from devices used for serum preparation by inductively coupled plasma mass spectrometry." The Science of The Total Environment **151**(1): 9-17.
- Münker, C., S. Weyer, et al. (2001). "Separation of high field strength elements (Nb, Ta, Zr, Hf) and Lu from rock samples for MC-ICPMS measurements." Geochemistry Geophysics Geosystems **2**(3): 183.
- Munter, A. (1992, November 23rd, 1999). "Neutron scattering lengths and cross sections." Retrieved 18.10.2004, 2004, from <http://www.ncnr.nist.gov/resources/n-lengths/elements/zr.html>.
- National Nuclear Data Center (2007). NuDat 2 database, Brookhaven National Lab.
- NNDC. (2004). "EXFOR Database." 2004, from <http://www.nndc.bnl.gov/exfor/index.html>.
- Nomura, M., K. Kogure, et al. (1983). "Isotopic abundance ratios and atomic weight of zirconium." International Journal of Mass Spectrometry and Ion Physics **50**: 219-227.
- Osborn, T. W., W. B. Broering, et al. (1981). "The determination of zirconium in animal tissues by neutron activation and  $\gamma$ -Spectrometry." Analytica Chimica Acta **128**: 213-219.
- Pitkevich, V. A., V. V. Duba, et al. (1996). "Reconstruction of the composition of the Chernobyl radionuclide fallout and external radiation absorbed doses to the population in areas of Russia." Radiation Protection Dosimetry **64**(1/2): 69-92.
- Ramakumar, K. L. and R. Fiedler (1999). "Calibration procedures for a multicollector mass spectrometer for cup efficiency, detector amplifier linearity, and isotope fractionation to evaluate the accuracy in the total evaporation method." International Journal of Mass Spectrometry **184**: 109-118.
- Rasmussen, G. (2004). Questions regarding TIMS measurement parameters for zirconium.
- Rodushkin, I., E. Engström, et al. (2004). "Determination of low-abundance elements at ultra-trace levels in urine and serum by inductively coupled plasma-sector field mass spectrometry." Analytical and Bioanalytical Chemistry **380**(2): 247-257.
- Rosman, K. J. R. and P. D. P. Taylor (1998). "Isotopic compositions of the elements 1997." Pure and Applied Chemistry **70**(1): 217-235.
- Roth, P., A. Giussani, et al. (1998). "Kinetics of gastrointestinal absorption." Radiation Protection Dosimetry **79**(1-4): 279-282.
- Roth, P. and E. Werner (1985). "Interrelations of radiocalcium absorption tests and their clinical relevance." Mineral and Electrolyte Metabolism **11**: 351-357.
- Saam Institute (1992-2002). SAAM II - Software applications for kinetic analysis University of Washington.
- Sahoo, S. K. and A. Masuda (1997). "Precise measurement of zirconium isotopes by thermal ionization mass spectrometry." Chemical Geology **141**: 117-126.
- Sanchez, G. and J. Lopez-Fidalgo (2003). "Mathematical techniques for solving analytically large compartmental systems." Health Physics **85**(2): 184-193.

- Schönbächler, M., M. Rehkämper, et al. (2004). "Ion exchange chromatography and high precision isotopic measurements of zirconium by MC-ICP-MS." *Analyst* **129**(1): 32-37.
- Schramel, P. (2004). Discussions and test measurements of zirconium with ICP-MS.
- Shiraishi, Y. and R. Ichikawa (1972). "Absorption and Retention of  $^{144}\text{Ce}$  and  $^{95}\text{Zr}$ - $^{95}\text{Nb}$  in Newborn, Juvenile and Adult Rats." *Health Physics* **22**(4): 373-378.
- Smith+Nephew. (2007). "Produktinformation Oxinium." Retrieved July 15th, 2007, 2007, from <http://www.smithnephew.com/Downloads/OXINIUM%20Material%20web.pdf>
- Tolksdorf, E. (1974). "Corrosion behaviour of new Zr alloys." *Journal of Nuclear Materials* **51**: 330-336.
- U.S. National Library of Medicine. (2005). "Hazardous substances data bank (HSDB)." Retrieved July 6th, 2007, 2007, from <http://toxnet.nlm.nih.gov/cgi-bin/sis/htmlgen?HSDB>.
- Verel, I., G. W. M. Visser, et al. (2003). " $^{89}\text{Zr}$  Immuno-PET: Comprehensive procedures for the production of  $^{89}\text{Zr}$ -labeled monoclonal antibodies." *The Journal of Nuclear Medicine* **44**(8): 1271-1281.
- Veronese, I., M. C. Cantone, et al. (2003). "Stable tracer investigations in humans for assessing the biokinetics of ruthenium and zirconium radionuclides." *Radiation Protection Dosimetry* **105**(1-4): 209-212.
- Veronese, I., M. C. Cantone, et al. (2002). The biokinetics of ruthenium and zirconium radionuclides in humans studied with stable tracers. Proceedings of the European IRPA Congress, 8.-11.10.2002, Florence.
- Veronese, I., A. Giussani, et al. (2003). "A re-evaluation of the biokinetics of zirconium in humans." *Applied Radiation and Isotopes* **58**: 431-439.
- Veronese, I., A. Giussani, et al. (2000). Kinetics of Ruthenium in Humans. Proceedings 10th International Congress of the International Radiation Protection Association, Center Hiroshima.
- Walczyk, T. (2004). "TIMS versus multicollector-ICP-MS: coexistence or struggle for survival?" *Analytical and Bioanalytical Chemistry* **378**: 229-231.
- Wayne, D. M., W. Hang, et al. (2001). "A linear time-of-flight mass analyzer for thermal ionization cavity mass spectrometry." *Spectrochimica Acta B* **56**: 1175-1194.
- Werner, E., P. Roth, et al. (2002). "Assessment of intestinal absorption of trace metals in humans by means of stable isotopes." *Isotopes in Environmental and Health Studies* **38**: 7-15.
- Weyer, S., C. Münker, et al. (2002). "Determination of ultra-low Nb, Ta, Zr and Hf concentrations and the chondritic Zr/Hf and Nb/Ta ratios by isotope dilution analyses with multiple collector ICP-MS." *Chemical Geology* **187**: 295-313.
- Xie, Q. and R. Kerrich (1995). "Application of isotope dilution for precise measurement of Zr and Hf in low-abundance samples and international reference materials by inductively coupled plasma mass spectrometry: implications for Zr (Hf)/REE fractionations in komatiites." *Chemical Geology* **123**: 17-27.
- Yang, X. J. and C. Pin (2000). "Determination of trace zirconium and hafnium in basaltic rocks by inductively coupled plasma atomic emission spectrometry after chemical separation: an evaluation of two methods based on extraction chromatography." *Analyst* **125**(3): 453-457.
- Yang, X. J. and C. Pin (2002). "Determination of niobium, tantalum, zirconium and hafnium in geological materials by extraction chromatography and inductively coupled plasma mass spectrometry." *Analytica Chimica Acta* **458**(2): 375-386.
- Yu, L. L., J. D. Fassett, et al. (2002). "Detection limit of isotope dilution mass spectrometry." *Analytical Chemistry* **74**(15): 3887-3891.

- Ziegler, J. F., J. P. Biersack, et al. (2003). SRIM - The Stopping and Range of Ions in Matter: SRIM is a group of programs which calculate the stopping and range of ions (10 eV - 2 GeV /amu) into matter.
- Zweit, J., S. Downey, et al. (1991). "Production of no-carrier-added zirconium-89 for positron emission tomography." Applied Radiation and Isotopes **42**(2): 199-201.



# Annex

## **A. TIMS method development**

This section presents an overview on the experiments performed during the development and optimisation of the TIMS method for tracer measurements of zirconium. The descriptions of the individual experiments and their results are intentionally kept short; any queries on specific topics will be gladly answered by the author.

All measurements were performed with the TRITON instrument installed in spring 2005. For all measurements beyond July 2005, a standard measurement routine with the multi-ion counters of the TRITON, i.e. channeltrons, was used. It was set up according to the suggestions of D. Tuttas (Thermo Fisher Scientific (Bremen) GmbH, Germany) during an onsite training course in July 2005. Details of the routine are described in section 3.2.2.

**Preliminary test of the detection of low amounts of zirconium** (April/May 2005, TRITON measurement performed exclusively by F. Wagner, evaluation by the author)

- Measurement of a standard solution of natural zirconium (PLZR2-2Y; SPEX CertiPrep, Metuchen, NJ, USA), diluted with either Milli-Q water or 3 % HNO<sub>3</sub>
- Samples of 1 µg to 1 ng of zirconium
- Double filament technique (standard for other elements measured in the working group, different temperatures for sample evaporation and ionisation possible)
- The SEM was used as detector.

Results:

- All samples were measurable, but with an unstable beam current and low count rates, resulting in a necessary, large isobaric correction for molybdenum. No ruthenium isobaric interference was observed.
- The measured isotope ratios were in accordance with the expected values of natural zirconium.

**Determination of isotope ratios and concentrations of tracer solutions from the preliminary study in 1998 – 2003** (May 2005, TRITON measurement performed exclusively by F. Wagner, evaluation by the author)

- Isotope ratios were in accordance with the certified values, thereby confirming the accuracy of the instrument.
- Relative standard deviations of isotope ratios were exceeding 20 %. This precision was considered unacceptable for tracer kinetic studies, i.e. the measurement method had to be changed.
- The tracer concentrations measured by IDMS (with natural zirconium as spike) showed that the zirconium tracer solutions were stable over years. Therefore, spare ampoules with injection solution from the preliminary study could be used in the current study.

**Blank measurements** (starting in May 2005)

- Rhenium filaments were found to contain trace amounts of natural zirconium, i.e. the ion production is roughly equivalent to a zirconium sample of 10 – 100 pg, as determined by IDMS.

- The filaments further contain substantial amounts of molybdenum. A comparison of the heating currents in blank samples (both bare filaments and graphite-coated filaments) with natural zirconium samples of variable concentrations and application schemes showed that the molybdenum signal is almost exclusively caused by impurities of the filament material. The isotope ratio 95/90 can be used to qualitatively assess the ion yield of zirconium measurements. A prolonged baking out of the rhenium filaments (4.5 A over 60 min instead of 30 min per filament) prior to sample application does not cause a significant reduction of the molybdenum signal.
- No substantial zirconium, molybdenum, or ruthenium content was found in the solutions used for sample application, i.e. concentrated HNO<sub>3</sub> of sub-boiling distilled grade, or graphite suspension diluted with Milli-Q water.

#### **Tests of the single filament technique with graphite-coated filaments (July/August 2005)**

- Variation of the application scheme (mixing of sample solution and graphite suspension, or application in layers with intermediate drying)
- Variation of the amount of graphite by dilution of the graphite suspension (1:1 to 1:50) with Milli-Q water

#### **Results:**

- No additional interferences from the graphite suspension were found at temperatures suitable for zirconium ionisation.
- The beam stability and ion yield is improved in comparison to the double filament technique. Optimal conditions are a dilution of the ‘Aquadag’ graphite suspension of 1:15, and a layered application scheme of 1 µl diluted suspension, the sample, and another 1 µl of suspension.

#### **Tests of mass fractionation during total sample evaporation**

The results are presented in section 3.2.2 (August 2005).

#### **Test of the effect of centring the sample on the filament during application**

(August 2005)

- The spreading of sample solution on the filament was inhibited by previously applied stripes of molten parafilm.
- Although the ion beam of centred samples was easier to focus, no improvement in beam stability or ion yield was observed; hence, the additional effort in sample preparation was considered unnecessary and all further samples were allowed to distribute over the whole filament surface.

#### **Test of miscibility of two types of zirconium for IDMS during sample application**

(starting in August 2005)

- Low µl amounts of two type solutions (natural zirconium and T-94) were applied to a filament, causing them to form a common droplet, and were subsequently dried together. As a reference, samples of previously mixed larger volumes of the same tracers were also measured.
- The isotope ratios of filament-mixed samples were in accordance with those of the reference samples. The filament-mixing method was thus used as an easy means for the quantitative determination of various zirconium types in further test experiments, e.g. on recovery rates of column chromatography.

### **Reference measurements of natural zirconium as laboratory standard**

(PLZR2-2Y, SPEX CertiPrep, Metuchen, NJ, USA, diluted in 3 % HNO<sub>3</sub>; August/September 2005; these measurements were exclusively performed by F. Wagner)

- 21 samples of 2 ng each of the standard solution were measured with the reference method.
- The mean isotope ratios were in accordance with the expected values of natural zirconium. Their values and uncertainties were used during the study as reference for consecutive control measurements of standard samples to check instrumental accuracy and precision.

### **Tests of sample recovery from the Teflon beakers used during sample preparation**

The recovery was almost complete (~ 1) for concentrated HNO<sub>3</sub>, of the order of 10<sup>-1</sup> for diluted HNO<sub>3</sub>, and poor for H<sub>2</sub>O (September 2005).

### **Chromatography tests of elution profiles and recovery rates – first phase**

(September – November 2005)

- Two-stage column chromatography; one initial column of 2 ml resin volume with Eichrom Ln Resin (cf. section 3.2.1) to remove most elements, and a subsequent column with 0.5 ml anion exchange resin (Dowex 1X8, 200 – 400 mesh size) to remove molybdenum
- 100 ng of natural zirconium either as pure solution, added to urine or added to blood plasma, including digestion of the biological samples; natural zirconium was used since the standard solution had a certified concentration, was cheaper than enriched tracer solutions, and no significant background of zirconium was previously found in measured samples
- 4 elution fractions of 6 ml each for the Ln resin column

Results:

- Recoveries of 75 – 121 % were found for optimally preconditioned Ln resin columns. The recovery of the second column was 13 – 122 %, plus five additional samples in which the loaded amount was exceeded by factors of 6 – 30.
- No significant reduction of molybdenum was obtained with the second column, hence it was decided to abandon this step of sample preparation.

### **Chromatography tests of elution profiles and recovery rates – second phase**

(November/December 2005)

- Single-stage column chromatography with Eichrom Ln resin in columns of either 1 ml or 2 ml resin volume
- 10 ng of natural zirconium as pure solution or added to plasma with subsequent digestion
- 4 elution fractions of 6 ml or 3 ml each for resin volumes of 2 ml or 1 ml, respectively

Results:

- Recoveries of 260 – 430 %, with no clear elution profile, were interpreted as a result of contaminated acids used during the elution step of the chromatography.
- The performance of 1 ml columns was similar to 2 ml columns, but less acid had to be used and later evaporated. Therefore, 1 ml columns were adopted as standard for later experiments.

### **Characterisation of tracer solutions** (starting in October 2005)

- Determination of isotope ratios of the tracer solutions used in the current study; 5 measurements for each tracer, 20 measurements for T-94 as reference for IDMS
- Concentration measurement of T-94 solutions with IDMS, in addition to ICP-OES measurements; 15 measurements

### **Test of the dependence of TIMS results on filament heating control** (December 2005)

- 5 samples, each of 100 ng T-94, were measured, keeping the ion count rates constant by manual regulation of the filament heating current.
- 5 samples were measured at a constant temperature as indicated by the TRITON's pyrometer.
- 5 samples were measured with a constant heating current, allowing a variation of temperature and count rates.

#### Result:

- No significant difference in isotope ratios or their uncertainty was found. Therefore, further samples were measured without manual regulation of the heating current, unless count rates declined fast, or exceeded the operational limit of the channeltron detectors.

### **Chromatography tests of elution profiles and recovery rates – third phase**

(January/February 2006)

- Single-stage column chromatography with Eichrom Ln resin in columns of 1 ml resin volume, with 4 elution fractions of 3 ml each
- 10 ng of T-92 as pure solution or added to plasma or urine with subsequent digestion
- Blind runs without tracer addition

#### Results:

- Elution profiles of T-92 and natural zirconium were found to be different, in that the concentration of natural zirconium rises with ongoing elution, while the concentration of T-92 has a distinct peak in the course of elution.
- Approximately 50 – 100 ng of natural zirconium were found in 8 experiments with 4 pure solutions, 2 plasma, and 2 urine samples.
- The recovery of T-92 was 22 – 34 % in 2 spiked plasma and 2 spiked urine samples.

Subsequent blank measurements of the acidic solutions used during chromatography revealed that some of them contained enough zirconium to contaminate the samples. As a consequence, fresh hydrofluoric acid was obtained, and the suprapure grade hydrochloric acid was purified in the lab by distillation below its boiling point. The background of natural zirconium in experimental samples could typically be reduced to below 10 ng by these efforts, thereby improving the detection limit of zirconium tracers.

### **Test of chromatography columns on memory effects** (January 2006, repeated in May 2006)

A new Ln resin column was loaded and subsequently regenerated 10 times (8 times for the repetition in May), following the scheme in section 3.2.1. The loadings were alternated between 10 ng (100 ng) samples of T-92 and T-94. In both experiments, no indication of memory effects was found, thus each of the Ln resin columns was reused several times during the study.

### **Test of memory effects in Teflon beakers** (starting in April 2006)

In several samples, inexplicably large isotope abundances of  $^{91}\text{Zr}$  and  $^{96}\text{Zr}$  were found. By a systematic revision of all previously measured zirconium samples considering their measured isotope ratios, as well as their preparation and measurement dates, these seemingly erroneous measurements could be attributed to memory effects in certain Teflon beakers which were previously used for the preparation of new, concentrated tracer stock solutions.

This assumption was tested and confirmed by the deposition of  $1\ \mu\text{g}$  of  $^{91}\text{Zr}$  in a Teflon beaker, and subsequent repeated sampling from this beaker after each step of the former standard cleaning procedure. It was shown that the cleaning procedure, although sufficient to remove small sample remnants from typical investigation samples, was not capable of dealing with large remnants from concentrated solutions.

The test was repeated with an altered cleaning procedure, resulting in a new standard procedure which is described in section 3.2.1. The two most important changes were:

- Beakers may not be soaked in a common volume of acid solution because of the risk of cross-contamination.
- Large sample remnants can be removed by placing beakers in an ultrasonic bath over 15 min, filled with concentrated nitric acid to a level which covers a previous sample deposition.

## **B. Algorithm for the calculation of absorption rates**

The algorithm below is a modified excerpt of the source code of ‘volterra.f’ which was programmed by Dr. Paul Roth, GSF, and made available by Dr. Weibo Li, GSF. The original code includes a further program loop (DO...ENDDO) to allow for the calculation of multiple data sets at once. The respective parts of the code have been removed for the sake of clarity.

Input and output variables:

J            running number of time steps (as a default, J = 1 equals t = 0 min)  
QIV(J)    concentration of intravenous tracer in plasma (% of injected tracer per kg plasma) at time step J  
QPO(J)    concentration of oral tracer in plasma (%·kg<sup>-1</sup>) at time step J  
NRINT    number of time steps in input file (default: 301)  
C(J)      (cumulative) absorbed fraction of the oral tracer up to time step J  
F(J)      ratio of QPO(J) over QIV(J)  
R(J)      absorption rate, given as fraction of the initially ingested amount of oral tracer, per time interval (the default time interval is 10 min)  
XA(J)    identical to QIV(J), later used for output  
XB(J)    identical to QPO(J), later used for output  
XC(J)    absorption rate in % of the amount of oral tracer, per time interval  
XD(J)    (cumulative) absorbed fraction of the oral tracer up to time step J, in %  
XE(J)    ratio of QPO(J) over QIV(J), in %  
XF(J)    residual (non-absorbed) fraction of oral tracer in time step J, in %  
XG(J)    absorption rate in % of the residual amount of oral tracer, per time interval

The algorithm calculates the following expressions for C(J) and R(J):

$$C(J) = \frac{1}{2}R(J) + \sum_{i=1}^{J-1} R(i)$$
$$R(J) = \frac{1}{QIV(1)} \left[ QPO(J) - \sum_{i=1}^{J-1} R(i)QIV((J+1)-i) \right]$$

Excerpt of the source code of ‘volterra.f’:

```
R(1) = (QPO(1)/QIV(1))
C(1) = R(1)/2.
F(1) = R(1)
XA(1) = QIV(1)
XB(1) = QPO(1)
XC(1) = R(1)*100.
XD(1) = C(1)*100.
XE(1) = F(1)*100.
DO 80 J=2, NRINT
    K=J-1
    S=0.0
    T=0.0
```

```

DO 70 L=1,K
      M=J+1-L
70      S=R(L)*QIV(M)+S
      R(J)=((QPO(J)-S)/QIV(1))
      T=(R(J)+R(K))/2.
      C(J)=C(K)+T
      F(J)=(QPO(J)/QIV(J))*100.
      XA(J)=QIV(J)
      XB(J)=QPO(J)
      XC(J)=R(J)*100.
      XD(J)=C(J)*100.
80      XE(J)=F(J)
DO 90 YA=1, NRINT
90      XF(YA)=100.-XD(YA)
DO 91 YB=1, NRINT
91      XG(YB)=XC(YB)*100./XF(YB)

```